



Fakultät für Chemie
der Technischen Universität München

Max-Planck-Institut für Biochemie
Abteilung für Molekulare Strukturbioologie

Selective Autophagy Degrades Nuclear Pore Complexes

Chia-Wei Lee

Vollständiger Abdruck der von der Fakultät für Chemie der Technischen Universität München zur Erlangung des akademischen Grades eines **Doktors der Naturwissenschaften (Dr. rer. nat.)** genehmigten Dissertation.

Vorsitzender:

Prof. Dr. Matthias Feige

Prüfer der Dissertation:

1. Hon.-Prof. Dr. Wolfgang Baumeister
2. Prof. Dr. Johannes Buchner
3. Dr. Martin Beck

Die Dissertation wurde am 20.02.2020 an der Technischen Universität München eingereicht und durch die Fakultät für Chemie am 02.11.2020 angenommen.

Contents

List of Publications	1
Summary	2
Zusammenfassung.....	3
1. Introduction	4
1.1 Structural Organization of the Nuclear Pore Complexes (NPCs)	4
Table 1.1: FG-Nups	7
1.2 Biogenesis of the NPCs	8
1.3 Quality Control of the NPCs	10
1.4 Autophagy-mediated Proteolysis.....	12
1.5 Autophagy Receptors	13
1.6 Aim of this Study.....	16
2 Materials and Experimental Methods.....	17
2.1 Escherichia Coli (<i>E. coli</i>) Techniques	17
2.1.1 <i>E. coli</i> Strains for Cloning and Protein Expression	17
Table 2.1: <i>E. coli</i> strains	17
2.1.2 <i>E. coli</i> Plasmids.....	17
2.1.3 <i>E. coli</i> Media.....	18
2.1.4 Cultivation and Storage of <i>E. coli</i>	18
2.1.5 Preparation of Chemically Competent <i>E. coli</i>	18
2.1.6 Transformation of Plasmid DNA into Competent <i>E. coli</i>	19
2.1.7 Expression and Purification of GST-Nup159, GST-Atg8, GST-Atg8 Y49A, L50A and His-Atg8.....	19
2.1.8 Plasmids	20
Table 2.2: Plasmids.....	20
2.2 Saccharomyces cerevisiae (<i>S. cerevisiae</i>) techniques	21
2.2.1 Yeast Strains	21
Table 2.3: Yeast strains.....	21
2.2.2 Media, Buffers and Solutions	24

2.2.3 Yeast Culture, Storage, Starvation, Drug Treatment, and Nup Degradation and EGFP Cleavage Assay.....	25
2.2.4 Competent Yeast Cells and Transformation	26
2.2.5 Genetic Manipulation	26
2.2.6 Mating Type Analysis, Mating, Sporulation, and Tetrad Analysis	27
2.3 Molecular Biological Methods	27
2.3.1 DNA Purification and Analysis	27
2.3.2 Polymerase Chain Reaction (PCR).....	28
2.3.3 Agarose Gel Electrophoresis	29
2.3.4 Cloning.....	29
2.3.5 Site-directed Mutagenesis.....	30
2.4 Biochemical and Cell Biology Methods.....	30
2.4.1 Immunoblot Techniques	30
2.4.2 Co-immunoprecipitation of Nucleoporins	32
2.4.3 Atg8 Interactome and Mass Spectrometry.....	32
2.4.4 Atg8/Nup159 <i>in vitro</i> Binding Assay	33
2.4.5 GST-Atg8 Pulldown with Cell Extract.....	34
2.4.6 Fluorescence Microscopy	34
2.4.7 Microfluidics Experiments	35
2.4.8 Correlative Light and Electron Microscopy (CLEM).....	35
2.4.9 Antibodies	36
2.4.10 Statistics and Reproducibility	36
3 Results	37
3.1 Nucleoporins in <i>S. cerevisiae</i> are Long-lived.....	37
3.2 Identification of Triggers of NPC Degradation.....	38
3.3 Involvement of ESCRT and Proteasome in NPC Degradation	42
3.4 Multiple Pathways are Involved in Starvation-induced NPC Degradation.....	43
3.5 Nuclear Envelope-embedded NPCs are Degraded in the Vacuole via the Core Autophagy Machinery.....	47
3.6 The Core Autophagy Machinery is Crucial for NPC Degradation in Contrast to Other Characterized Selective Autophagy Pathways	52
3.7 Nup159 is a Built-in Autophagy Receptor for NPC Degradation.....	55
3.8 Selective Autophagy is Important for the Clearance of Aberrant NPCs.....	62

4 Conclusions and Discussion.....	68
4.1 Nup159 Specifically Target Membrane-embedded NPCs for Autophagic Turnover	69
4.2 Nup159 Functions Intrinsically as a New Type of Autophagy Receptor.....	69
4.3 The Generation of Nuclear Envelope-derived Vesicles	70
4.4 Cross-regulation between ESCRT, proteasome and autophagy in NPC Degradation	71
References	73
Abbreviations.....	85
Acknowledgments.....	90
Curriculum Vitae	91
Lebenslauf	93

List of Publications

Florian Wilfling^{#*}, **Chia-Wei Lee**[#], Philipp Erdmann^{*}, Yumei Zheng, Dawafuti Sherpa, Stefan Jentsch, Boris Pfander, Brenda Schulman, and Wolfgang Baumeister^{*}

A selective autophagy pathway for phase-separated endocytic protein deposits.

Mol. Cell **80**, 764–778

Shared first authors

Matteo Allegretti^{*}, Christian E. Zimmerli^{*}, Vasileios Rantos, Florian Wilfling, Paolo Ronchi, Herman K.H. Fung, **Chia-Wei Lee**, Wim Hagen, Beata Turonova, Kai Karius, Xiaojie Zhang, Christoph Müller, Yannick Schwab, Julia Mahamid, Boris Pfander[#], Jan Kosinski[#], and Martin Beck[#]

In-cell architecture of the nuclear pore complex and snapshots of its turnover.

Nature **586**, 796–800

Chia-Wei Lee[#], Florian Wilfling[#], Paolo Ronchi, Matteo Allegretti, Shyamal Mosalaganti, Stefan Jentsch, Martin Beck^{*} and Boris Pfander^{*} (2020).

Selective autophagy degrades nuclear pore complexes.

Nat. Cell Biol. **22**, 159–166

Shared first authors

Sahradha Albert, Wojciech Wietrzynski[#], **Chia-Wei Lee**[#], Miroslava Schaffer[#], Florian Beck, Jan M. Schuller, Patrice A. Salomé, Jürgen M. Plitzko, Wolfgang Baumeister^{1*}, and Benjamin D. Engel^{*} (2020).

Direct visualization of degradation microcompartments at the ER membrane.

Proc. Natl. Acad. Sci. USA **117**, 1069–1080.

Equal contribution

Summary

Nucleocytoplasmic transport of molecules and macromolecules across the nuclear envelope (NE) via the membrane-embedded nuclear pore complexes (NPCs) is essential for gene expression, cell growth and cell division in all eukaryotic cells. NPCs are very large proteinaceous assemblies consisting of ~550 individual proteins, termed nucleoporins (Nups) (Beck and Hurt, 2017; Schwartz, 2016). Disruption of NPC integrity has been linked to aging, cancer and neurodegenerative diseases (D'Angelo et al., 2009; Lord et al., 2015; Sakuma and D'Angelo, 2017; Simon and Rout, 2014; Toyama et al., 2013). Nevertheless, the underlying mechanism by which membrane-embedded NPCs are degraded is currently unknown.

Work in this dissertation demonstrates that autophagy, a degradative pathway that eliminates hazardous and unwanted cytosolic content, targets membrane-embedded NPCs for degradation. Upon nitrogen starvation and genetic interference with NPC architecture, Nups are rapidly turned over in budding yeast by the core autophagy machinery as well as vacuolar proteases.

The known set of autophagy receptors involved in nucleophagy is not utilized to degrade NPCs. But autophagic degradation of NPCs is mediated by the cytoplasmically exposed Nup159 that serves as an intrinsic cargo receptor and directly binds to the autophagic marker protein Atg8. Nup159 harbours an Atg8-interacting motif (AIM) in its C-terminus. Mutation of this AIM abolishes its autophagic targeting, thus preventing membrane-embedded NPCs from degradation.

Overall, our findings suggest autophagy serves an inducible and specific process for NPC degradation, offering a possible explanation for NPC longevity under specific conditions.

Zusammenfassung

Der nukleozytoplasmatische Transport von Molekülen und Makromolekülen durch die Kernhülle (NE) über die membraneingebetteten Nuklearporenkomplexe (NPCs) ist für die Genexpression, das Zellwachstum und die Zellteilung in allen eukaryotischen Zellen unerlässlich. NPCs sind sehr große proteinhaltige Zusammenstellungen, die aus ~550 einzelnen Proteinen bestehen, die als Nukleoporine (Nups) bezeichnet werden (Beck and Hurt, 2017; Schwartz, 2016). Eine Störung der NPC-Integrität wurde mit Alterung, Krebs und neurodegenerativen Krankheiten in Verbindung gebracht (D'Angelo et al., 2009; Lord et al., 2015; Sakuma and D'Angelo, 2017; Simon and Rout, 2014; Toyama et al., 2013). Dennoch ist der zugrunde liegende Mechanismus, durch den membraneingebettete NPCs abgebaut werden, derzeit unbekannt.

Diese Studie zeigt, dass Autophagie, welches gefährliche und unerwünschte zytosolische Inhalte eliminiert, Membran eingebetteten NPCs abbaut. Nach Stickstoffmangel und genetischer Beeinträchtigung der NPC-Architektur werden Nups in Hefe schnell durch die Autophagie-Maschine und vakuolare Proteasen abgebaut.

Derzeit bekannte Autophagiorezeptoren spielen für den Abbau keine Rolle. Das cytoplasmatische Protein Nup159 fungiert dabei als intrinsischer Autophagiorezeptor, welcher direkt an das autophagie Markerprotein Atg8 bindet. Nup159 beherbergt in seinem C-Terminus ein Atg8-interagierendes Motiv (AIM). Die Mutation dieses AIM hebt seine autophagosomale-Rekrutierung auf und verhindert so den Abbau von Membran eingebetteten NPCs. Insgesamt deuten unsere Ergebnisse darauf hin, dass die Autophagie einen induzierbaren und spezifischen Prozess für den NPC-Abbau darstellt, der eine mögliche Erklärung für die Langlebigkeit des NPC unter bestimmten Bedingungen bietet.

1. Introduction

1.1 Structural Organization of the Nuclear Pore Complexes (NPCs)

Nuclear pore complexes (NPCs) are giant cylindrical structures embedded into the double lipid bilayer of the nuclear envelope (NE). They facilitate nucleocytoplasmic exchange of macromolecules, such as proteins and mRNA. These aqueous channels are elaborately built from multiple copies of approximately 30 distinct proteins, collectively called nucleoporins (Nups). Most of the Nups are highly conserved among species. According to their localization within the complex, they can be further allocated into different subcomplexes (Figure 1.1) (Beck and Hurt, 2017; Kabachinski and Schwartz, 2015).

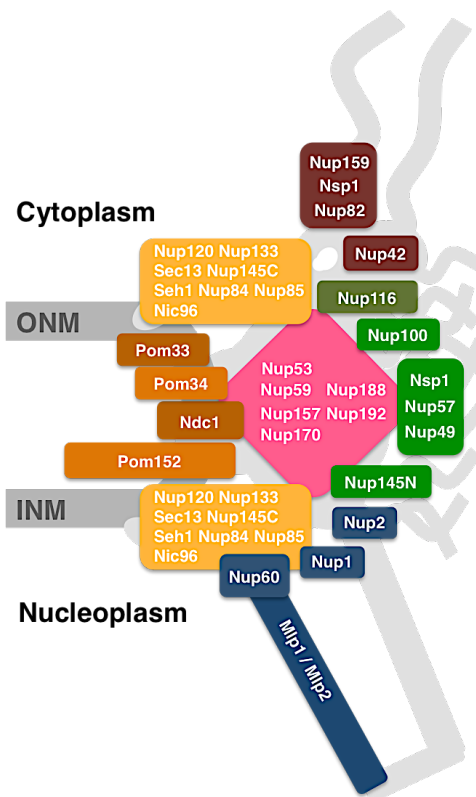


Figure 1.1: Schematic representation of NPC architecture in a cross-section view of the NPC.

The central core of the NPC consists of one inner-ring complex (magenta) flanked on both sides by the outer NPC scaffold (orange, consistent of Y complex and the heteromeric Nic96), together forming the scaffold of NPC. Peripheral nucleoporins constitute cytoplasmic filaments (dark brown) and the nuclear basket (navy blue). The permeability barrier is established by FG-nucleoporins (green). Three pore membrane proteins (Poms) together with Ndc1 (light brown) anchor the NPC scaffold at the outer nuclear membrane (ONM) and inner nuclear membrane (INM) joint.

As revealed by electron microscopy and biochemical approaches, the primary structural components of the pore include: the peripheral cytoplasmic filaments and the nuclear basket, which are placed asymmetrically and perpendicular to the eightfold rotationally symmetric channel body; the transmembrane ring, which anchors the pore

1. INTRODUCTION

directly at the fusion plane of inner and outer nuclear membranes (INM and ONM); the central so-called FG-Nups, which contain multiple phenylalanine-glycine repeats form a hydrogel-like filter to seal the pore, which mainly constitutes the selective transport ability of the pore; the inner ring (IR) are flanked by two outer rings (also called nuclear and cytoplasmic rings (NR and CR), based on their relative positions in NPC), together these three subcomplexes forms the scaffold of the NPC (Figure 1.1).

Besides their localization within the pore, Nup subcomplexes are organized in specific substructures. Among them, the best characterized are the inner ring complex (also denoted as Nup93 subcomplex) and the Y complex (also denoted as Nup107/160 complex in mammals; Nup84 complex in yeast) which is a key scaffolding constituent of the outer ring. The inner ring complex resided at and stabilized the fused inner and outer nuclear membranes. The Y complex on the other hand is distally connected at two sides of the inner ring complex and assembled into a ring with 16 copies of it (in mammals or 8 copies in yeast) in a head-to-tail contact, resulting in both NR and CR (Figure 1.2) (Hampoelz et al., 2019).

Peripheral substructures like the cytoplasmic filaments and the nuclear basket associate with CR and NR, respectively. Eight-projected fibrils from CR are referred to as cytoplasmic filaments that are critical for terminal steps of mRNA export (Hodge et al., 1999). In yeast, each filament in its core consists of two Nup159-Nup82-Nsp1 heterotrimers (Nup82-subcomplex) that dimerize into a P-shaped structure (Fernandez-Martinez et al., 2016; Gaik et al., 2015). DEAD-box RNA helicases such as Dbp5 associate with Nup159 and subsequently removes the shuttling transport receptor Mex67 from the exported mRNP releasing RNA into the cytoplasm (Adams et al., 2014; Weirich et al., 2004).

Opposite to the cytoplasmic filaments are eight-rod shaped extensions from NR constituting a fish-trap-like structure, termed nuclear basket. In yeast, two myosin-like proteins, Mlp1 and Mlp2 (Tpr in vertebrate), form the structural backbone of each basket filament. Additionally, two other basket Nups, Nup1 and Nup60 (vertebrate Nup153), dock the individual filament to CR (Cordes et al., 1997; Meszaros et al., 2015; Strambio-de-Castillia et al., 1999). Recent work implicated that the nuclear basket function as a

1. INTRODUCTION

molecular platform to couple transcriptional regulation and chromatin stability (Strambio-De-Castillia et al., 2010).

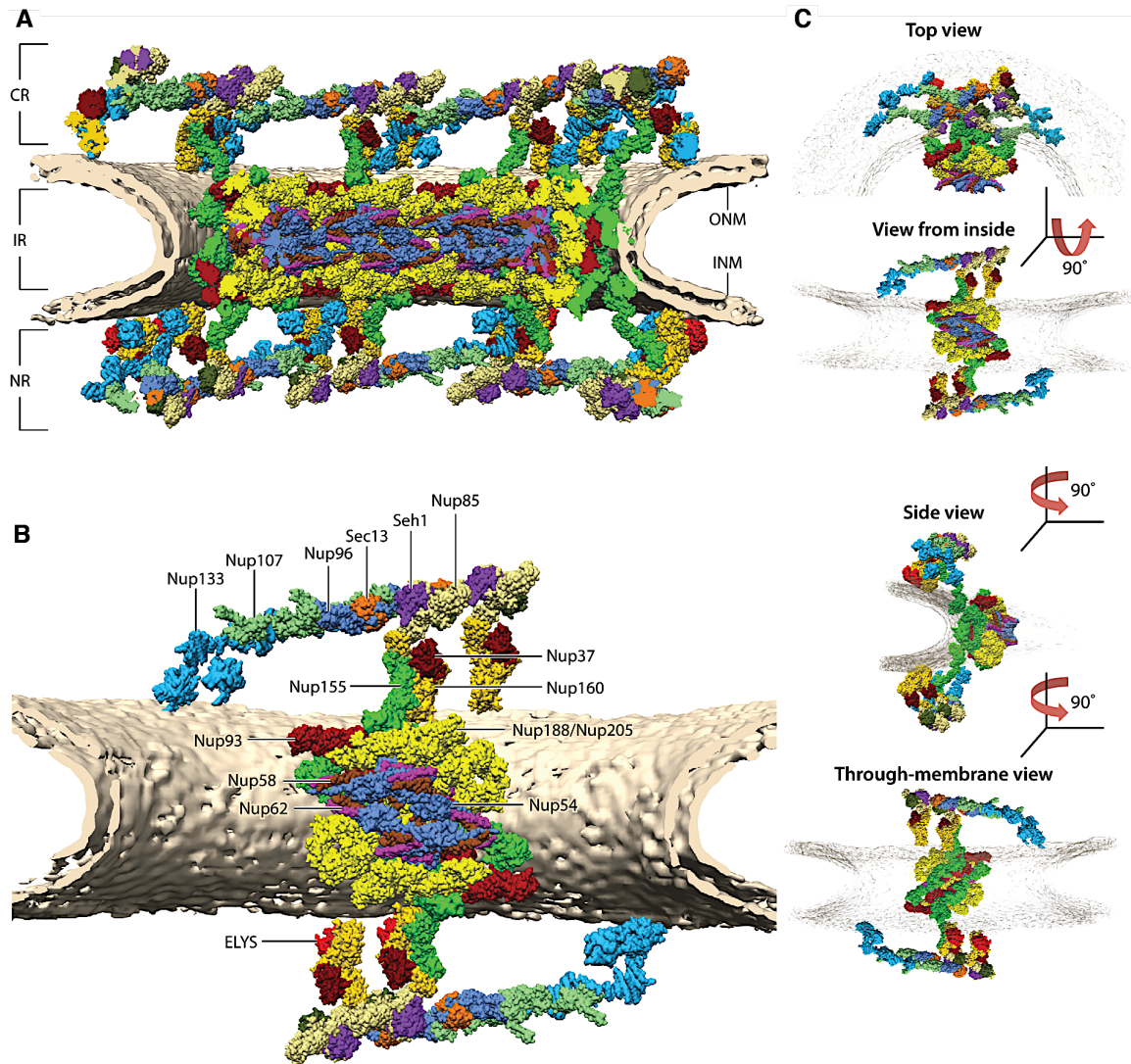


Figure 1.2: The structure of the nuclear pore complex (adapted from Hampaetz et al., 2019).

The scaffold architecture of the human nuclear pore complex is shown (A) in a cut-open view, (B) as a single asymmetric unit, and (C) in different orientations. Individual proteins are color coded; their names and the cytoplasmic ring (CR), inner ring (IR), nuclear ring (NR), outer nuclear membrane (ONM), and inner nuclear membrane (INM) are indicated. Additional abbreviation: ELYS, embryonic large molecule derived from yolk sac.

The central channel is lined with many intrinsically disordered FG-Nups that form the NPC permeability barrier. Molecules greater than ~40 kDa cannot freely cross through

1. INTRODUCTION

the gate but require the interaction with nuclear transport receptors (NTRs) in order to overcome the permeability barrier (Popken et al., 2015; Terry and Wente, 2007; Timney et al., 2016). Although the exact mechanism is not fully understood, it seems FG-domain binding of NTRs allows local melting of the FG-sieve and thus facilitates bidirectional transport of macromolecules (Frey and Gorlich, 2009; Hulsmann et al., 2012; Wente and Rout, 2010). Each FG-Nup has multiple copies of the hydrophobic FG-repeat unit, separated by hydrophilic spacers of variable sequence and length. Based on the primary amino acid sequence, FG-motifs can be classified into 3 major types, including Phe-Gly (FG), Gly-Leu-Phe-Gly (GLFG) and Phe-any-Phe-Gly (FXFG) (Table 1.1) (Patel et al., 2007; Rout et al., 1997).

Table 1.1: FG-Nups

<i>S. cerevisiae</i> Nup	Repeat motif(s)	Localization in NPC	Homologue in Vertebrates
Nup42	FG	Cytoplasmic face	NLP1
Nup159	FG	Cytoplasmic face	Nup214
Nup100	GLFG	Cytoplasmic bias	Nup98
Nup116	GLFG	Cytoplasmic bias	Nup98
Nsp1	FG/FXFG	Cytoplasmic face, central	Nup62
Nup49	GLFG	Central	Nup45, Nup58
Nup57	GLFG	Central	Nup54
Nup145N	GLFG	Nuclear bias	Nup98
Nup1	FXFG	Nuclear face	Nup153
Nup2	FXFG	Nuclear face	Nup50
Nup60	FXF	Nuclear face	Nup153
	FG	Central, integral membrane	Pom121
	FXFG	Cytoplasmic face	Nup358/RanBP2

(For table legend, see next page.)

Table 1.1: FG-Nups.

S. cerevisiae FG-Nups are listed in a table with the contents of its property, relative localization in NPC and homologue in vertebrates. Pom121 and Nup358 are two unique FG-repeat-containing Nups in vertebrates.

In *S. cerevisiae* the FG-repeat proteins, Nup42, Nsp1 and Nup159 are part of the cytoplasmic filaments. Nsp1, Nup49 and Nup57 are distributed centrally in the channel and anchored to Nic96. Together they form the tetrameric Nup57 subcomplex (Nup62 subcomplex in vertebrate). Nup100 and Nup116 are localized biasedly toward the cytoplasmic face of the pore, whereas Nup145N is biased toward the nuclear face of the pore. FXFG repeat-containing Nups are solely belonging to the nuclear basket, including Nup1, Nup2 and FXF repeat-containing Nup60 (Rout et al., 2000; Terry and Wente, 2009). In vertebrates, two unique FG repeat-containing protein Pom121 and FXFG repeat-containing protein Nup358 exist, which are membrane integrated or associated to cytoplasmic fibrils.

Lastly, Pom34, Pom152 and Ndc1, the three innermost integral membrane Nups construct the transmembrane ring and secure the NPC at the NE in budding yeast (Chial et al., 1998; Miao et al., 2006; Rout et al., 2000; Wozniak et al., 1994). A fourth transmembrane nucleoporin is Pom33. In contrast to the others, it localizes to both the NPC as well as the ER. Ndc1 (Lau et al., 2006) is the only conserved nucleoporin whereas the other membrane Nups do not possess any significant sequence similarity but are functionally conserved across species (e.g. gp210 and Pom121). The others are changing from species to species. Additionally, Poms also play an essential role in NPC biogenesis by mediating close apposition of the INM and ONM, which promote the events of membrane fusion (Antonin et al., 2008).

1.2 Biogenesis of the NPCs

In higher eukaryotes, NPC assembly occurs at two distinct stages of the cell cycle: (1) *de novo* synthesized NPCs assemble during interphase, when the number of NPCs is doubling in a given nucleus (Maul et al., 1971), and (2) postmitotic NPC assembly,

1. INTRODUCTION

concomitant with the reassembling of the nuclear envelope (Anderson and Hetzer, 2007, 2008; Dultz et al., 2008).

The first step of *de novo* NPC synthesis is the membrane fusion of INM and ONM. The inside-out evagination occurs at the INM and is mediated by transmembrane Poms (Antonin et al., 2005; Hetzer and Wente, 2009; Lau et al., 2004; Madrid et al., 2006; Miao et al., 2006) as well as the nuclear ring complex of NPC (Vollmer et al., 2012; D'Angelo et al., 2006; Walther et al., 2003a; Walther et al., 2003b). This stabilizes the dome-shaped evagination of INM. On the other hand, the perinuclear ER-resided proteins, reticulon and Yop1 family proteins (Dawson et al., 2009), bend the ONM inward toward INM and promote the event of membrane fusion. In the second step, other scaffold subcomplexes, including inner ring and cytoplasmic ring complexes, join the preexisting Poms and nuclear ring assemblies to complete the scaffold part of NPC. Finally, the assembly of peripheral subcomplexes, such as FG-Nups, nuclear basket and cytoplasmic filaments, finishes the full assembly of the pore (Figure 1.3A) (Otsuka and Ellenberg, 2018).

For postmitotic assembly of NPC, the process starts at mid-anaphase of mitosis when the reformation of nuclear envelope occurs. The recruitment of disassembled NPC components to the chromatin is achieved by embryonic large molecule derived from yolk sac (ELYS/MEL-28), which is crucial for specific targeting of Y-complex to mitotic chromatin (D'Angelo et al., 2006; Ryan et al., 2003; Walther et al., 2003b). Subsequently, the transmembrane Pom121 and Ndc1 join the assembling complex and therefore create a link to the membrane. In contrast to the Y-complex, the inner ring complex assembles gradually and starts with the membrane- and Ndc1-associated Nup53. Nup53 then recruits Nup93 and Nup155, which is in complex with Nup188 and Nup205. The Nup62 complex interacts with Nup93 and other assembly of FG-Nups to establish the permeability barrier. Lastly, the assembly of cytoplasmic filaments and nuclear basket finishes the reassembly (Figure 1.3B) (Otsuka and Ellenberg, 2018).

1. INTRODUCTION

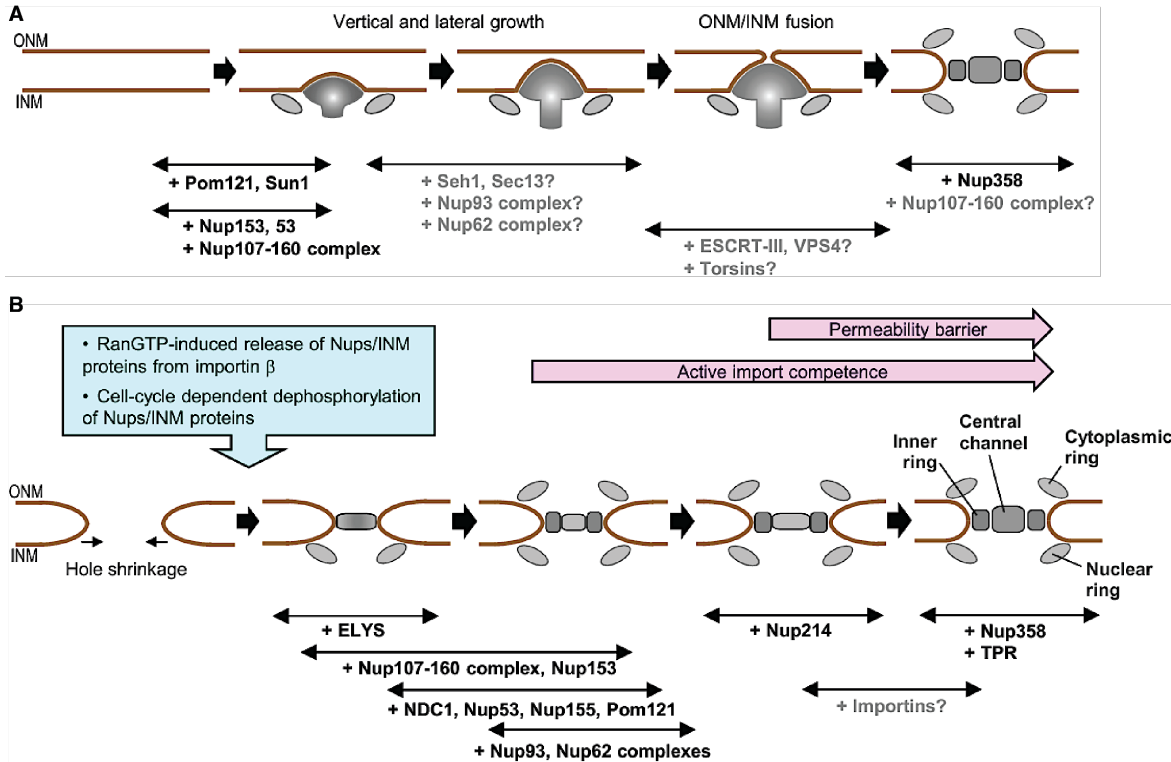


Figure 1.3: Two distinct assembly mechanisms of the NPC (adapted from Otsuka et al., 2018).

(A) Interphase NPC assembly proceeds by an inside-out extrusion of the nuclear membrane. The intermediate is a dome-shaped evagination of the INM, which contains the nuclear ring structure underneath the INM from the beginning and grows in size vertically and laterally until it fuses with the flat ONM.

(B) Postmitotic NPC assembly proceeds by a radial dilation of small membrane openings. The initial prepore contains dense material in the center of the membrane hole as well as the nuclear ring. It dilates radially and obtains active transport competence during IR and CR assembly. The NPC gradually obtains permeability barrier function against small molecules. Proteins involved in individual steps of the assembly are indicated below. Possible molecular requirements are shown in gray.

1.3 Quality Control of the NPCs

Recycling of Nups can be fulfilled during mitosis when the breakdown of NE, simultaneously dismantles the NPCs. Disassembly of NPC and NE is governed by mitotic kinases such as cyclin - dependent kinase 1 (CDK1)/cyclin B and polo-like kinase 1 (PLK1), which phosphorylates Nups, lamins and INM proteins at onset of mitosis, and trigger their dissociation from NE (Laurell et al., 2011; Linder et al., 2017). Specifically,

1. INTRODUCTION

phosphorylation of Nup98 plays a critical role in NPC disassembly, as it is linked to multiple Nups including Ndc1, the Nup93 subcomplex and the Nup62 subcomplex (Otsuka and Ellenberg, 2018).

However, this phenomenon is restricted to non-differentiated, higher eukaryotic cells, since terminally differentiated cells have no cell division, and also fungi such as *S. cerevisiae* undergo a closed mitosis, by which the chromosomes separate within intact nuclei. In fact, the NPC scaffold exhibits an extremely long half-life in postmitotic cells, and its expression is downregulated in terminally differentiated cells such as neurons (D'Angelo et al., 2009; Otsuka and Ellenberg, 2018; Toyama et al., 2013). In aged cells, stable nucleoporins can accumulate damages, resulting in leaky pores (D'Angelo et al., 2009). Moreover, in such cell's protein aggregates, e.g. of β III tubulin, are mis-localized into the nucleus, which is linked to neurodegenerative diseases. Therefore, it is reasonable to speculate that a dedicated mechanism is required to degrade damaged or malfunctioning NPCs, independent of mitosis events.

To ensure the NE integrity, the quality of NPC and its proper assembly are surveilled by the endosomal sorting complexes required for transport (ESCRT) pathway (Thaller et al., 2019; Webster et al., 2014; Webster et al., 2016). The ESCRT pathway mediates membrane fission/bending/scission reactions throughout the cell, and the emerging observations implicate its functions in postmitotic NE sealing, interphase NE lesions repairing, and NPC assembly surveillance (Christ et al., 2016; Stoten and Carlton, 2018). Impairment of ESCRTs lead to accumulation of malformed NPCs in a distinct compartment, the Storage of Improperly assembled NPCs Compartment (SINC). Moreover, sequestration of NPCs into the SINC further prevents nonfunctional NPCs to be inherited by the descendant. This protective mechanism assures that the nuclear compartmentalization is maintained in daughter cells and therefore sustains a notion that defective NPCs might reduce replicative life span (Colombi et al., 2013; Lusk and Colombi, 2014; Makio et al., 2013; Shcheprova et al., 2008).

For specific targeting, ESCRT-III subunits, Chm7 and Snf7, are recruited to NE via the Lap2-emerin-MAN1 (LEM) domain-containing INM proteins, Heh1 and Heh2, upon block of NPC assembly. Direction of the ESCRT-III machinery toward misassembled

NPC intermediates is apparently guided by the interaction between Pom152 and LEM domain-containing proteins at NE (Yewdell et al., 2011), but the mechanistic details of how those proteins collaborate to recognize and clear the defective NPC assemblies remain elusive.

1.4 Autophagy-mediated Proteolysis

The ability to degrade cellular components ranging from proteins to large complexes and organelles is essential for cellular homeostasis. In eukaryotes, this process mainly relies on two major quality control pathways, the ubiquitin-proteasome system (UPS) and autophagy. The UPS is typically responsible for degrading soluble misfolded proteins individually (Finley et al., 2012), whereas the autophagy can remove larger protein complexes, insoluble protein aggregates, and even entire organelles.

Autophagy is an evolutionarily conserved and ubiquitous process that is responsible for the elimination of cytosolic components in response to starvation and cellular stresses through target of rapamycin (TOR) signaling in a degradative compartment, i.e. the lysosome or vacuole. The importance of autophagy is illustrated by its involvement in a wide range of human diseases (Levine and Kroemer, 2008), including infections (Deretic et al., 2013), cancer (Mathew et al., 2007), diabetes (Quan et al., 2012), cardiomyopathy (Mei et al., 2015), and neurodegenerative disorders such as Alzheimer or Parkinson diseases (Nixon, 2013).

The hallmark of macroautophagy (hereafter referred to as autophagy) is the sequestration of cytosolic cargo into a newly synthesized double-membrane organelle, termed autophagosome, that later fuses with the vacuole/lysosome for degradation and recycling (Dikic, 2017; Wen and Klionsky, 2016). This *de novo* biogenesis of autophagosomes in yeast takes place at the phagophore assembly site (PAS, also known as pre-autophagosomal structure) that is proximal to the vacuole, and is characterized by the hierarchical recruitment of conserved proteins to an expanding membrane sac, called isolation membrane or phagophore (Mizushima et al., 2011).

Among these proteins are approximately 19 core proteins encoded by autophagy-related (ATG) genes, which coordinate different steps of autophagy (Figure 1.4) (Levine

1. INTRODUCTION

and Klionsky, 2017). For initiation of autophagy, the Atg1 complex (including the kinase Atg1, the regulatory subunit Atg13, and a ternary subcomplex Atg17-Atg31-Atg29) promote the activity of class III phosphatidylinositol 3-kinase complex I (PtdIns3K-C1, consisting of Vps34, Atg6, Vps15, Atg14 and Atg38) through phosphorylation of Atg14 (Chew et al., 2015; Reggiori and Klionsky, 2013; Yu et al., 2015), which enriches PI3P in the membrane and allows the binding of PI3P-binding proteins to assist phagophore formation. The transmembrane protein Atg9 is trafficked along with the small vesicles to isolation membrane and is thought to serve as lipid donor to the expanding phagophore (Ungermann and Reggiori, 2018). Conjugation of Atg8, an ubiquitin-like protein, to lipid phosphatidylethanolamine (PE) on autophagic membranes using an enzymatic cascade that closely resemble to the reaction of ubiquitination, which further recruits other core machinery proteins and is required for phagophore expansion and autophagosome formation (Kirisako et al., 1999).

1.5 Autophagy Receptors

Contrary to initial views, the purpose of autophagy is not only the non-specific degradation and recycling of cytosolic content, but in fact, cargo is degraded in a highly selective manner (Nakatogawa et al., 2009; Reggiori et al., 2012). A class of specialized proteins, called selective autophagy receptors (autophagy receptors in the following), conveys selectivity. These autophagy receptors recruit their respective cargo and subsequently bind to lipidated Atg8. For the interaction with Atg8 (LC3 in mammals) receptor proteins have a distinct binding site named AIM (Atg8-interacting motif) or LIR (LC3-interacting region), which binds to two hydrophobic pockets (W-site and L-site) on Atg8 (Birgisdottir et al., 2013; Noda et al., 2010). Most AIMs consist of a short conserved sequence (W/F/Y)xx(L/I/V) flanked by at least one proximal acidic residue (Farre and Subramani, 2016; Noda et al., 2010), but also cryptic AIMs have been described that contain not all of the mentioned features (Sawa-Makarska et al., 2014). Besides Atg8, autophagy receptors also interact with the autophagic scaffold protein Atg11, which assists autophagosome assembly directly at the cargo, and further exhibits exquisite substrate specificity of autophagy.

1. INTRODUCTION

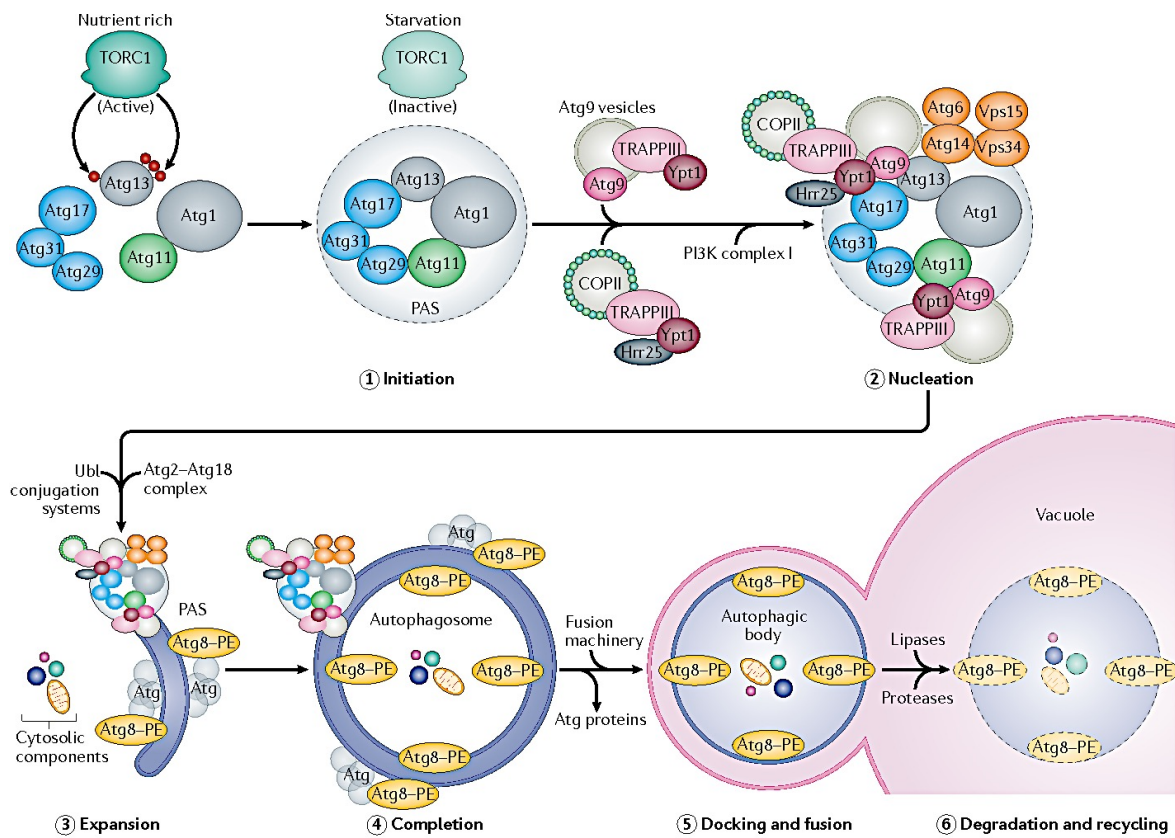


Figure 1.4: Steps in autophagy (adapted from Farré *et al.*, 2017).

Autophagy is inhibited under nutrient-rich conditions via the hyperphosphorylation of Atg13 by target of rapamycin complex 1 (TORC1) kinase; this process prevents a tight interaction between Atg1 kinase and Atg17. Starvation or rapamycin treatment activates autophagy by inhibiting TORC1, leading to the hypophosphorylation of Atg13, which can then interact with Atg1 and Atg17. The first two steps, initiation (step 1) and nucleation (step 2), involve the recruitment of cytosolic components of the core autophagic machinery to the phagophore assembly site (PAS) in yeast (omesomes in mammals). In yeast, the non-selective autophagy-specific PAS is organized partly by the scaffold components Atg11 and Atg17, with Atg17 itself being part of a tripartite Atg17–Atg29–Atg31 subcomplex. Scaffold components then recruit additional proteins, including transport protein particle III (TRAPP III) and Ypt1 (a Rab1 family GTPase), which bring coat protein complex II (COPII) and Atg9 vesicles, to initiate the expansion (step 3) of a double-membrane phagophore. This expansion also involves the activity of phosphoinositide 3-kinase (PI3K) complex I (consisting of Atg6, Atg14, vacuolar protein sorting 34 (Vps34) and Vps15), which generates the phosphatidylinositol 3-phosphate required to recruit other factors involved in phagophore elongation, such as the Atg2–Atg18 complex as well as the ubiquitin-like conjugation systems, Atg8-phosphatidylethanolamine (PE) (Atg8-PE) and Atg5–Atg12–Atg16 (depicted as grey Atg molecules in contact with Atg8-PE).

(Legend continued on next page.)

1. INTRODUCTION

(Figure 1.4, legend continued from last page.)

As a result of this membrane expansion, cargo destined for autophagy is surrounded and engulfed into a double-membrane vesicle called the autophagosome (step 4). Autophagosomes are then transported to lysosomes (or vacuoles in yeast and plants). Docking and fusion (step 5) of the outer autophagosomal membrane with that of the lysosome (vacuole) releases the autophagic body into the lysosomal (vacuolar) lumen, where hydrolases degrade and recycle (step 6) the macromolecular components for cellular use.

Autophagy receptors are further grouped into soluble and membrane-associated receptors. Membrane-associated receptors target damaged or disused organelles into autophagosomes such as mitochondria (Harper et al., 2018), endoplasmic reticulum (ER) (Grumati et al., 2018), or peroxisomes (Sakai et al., 2006). Soluble receptors on the other hand target macromolecular assemblies, which are resistant to proteasomal degradation. Known autophagy cargo targeted by soluble receptors are misfolded or aggregated proteins (Kraft et al., 2008), the cytoplasm-to-vacuole targeting (Cvt) complex (Lynch-Day and Klionsky, 2010), ferritin (Mancias et al., 2014) or ribosomes (Wyant et al., 2018). Importantly, many additional macromolecular assemblies, including the proteasome itself and fatty acid synthase have been described to be degraded by autophagy (Marshall et al., 2016; Shpilka et al., 2015), but have not been linked to a specific autophagy receptor, implying the existence of additional autophagy pathways and receptors. Knowledge of autophagy receptors is crucial to understand the organized degradation of autophagic cargo and will further allow the dissection of the individual autophagic pathways relevant in health and disease.

1.6 Aim of this Study

The NPC is elaborately built from approximately 30 nucleoporins that can be allocated to distinct subcomplexes. Of these subcomplexes only some peripheral components have been shown to be dynamic (Dilworth et al., 2001), while more integral parts of the NPC appear to be remarkably stable. In particular, the scaffold of the NPC exhibits an extremely long half-life in mammals (Savas et al., 2012; Toyama et al., 2013) with notable exceptions (Mathieson et al., 2018) that suggest regulation of NPC turnover by a specific, yet unknown pathway.

Therefore, the central aim of this work is to find out whether and how NPCs are degraded upon NPC damage or other cellular cues. The characterization of NPC quality control pathways might also contribute to our understanding of the underlying principles of neurodegenerative diseases.

2 Materials and Experimental Methods

The subsequent microbiological, biochemical and cloning techniques were based on standard procedures (Ausubel et al, 1994; Green & Sambrook, 2012) or followed the manufacturers' instructions, unless stated specifically. Sterilized flasks, glassware, deionized water and solutions were used for all methods. Unless otherwise mentioned, analytical grade chemicals and reagents were purchased from Agilent, Applied, Avestin, Biosystems, BD, Biomol, Bioneer, Bio-Rad, Chromotek, GE Healthcare, Life Technologies, Merck Millipore, New England Biolabs (NEB), PeqLab, Promega, Qiagen, Roth, Roche, Serva, Sigma-Aldrich, or Thermo Scientific. For database researches (sequence search and comparison, literature research), electronic services were provided by Saccharomyces Genome Database (<http://www.yeastgenome.org/>) and by National Center for Biotechnology Information (<http://www.ncbi.nlm.nih.gov/>).

2.1 Escherichia Coli (*E. coli*) Techniques

2.1.1 *E. coli* Strains for Cloning and Protein Expression

Table 2.1: *E. coli* strains

E. coli strains used in this study

Name	Genotypes
XL1-Blue	<i>recA1 endA1 gyrA96 thi-1 hsdR17 supE44 relA1 lac</i> [F' <i>proAB lacI^q ZΔM15 Tn10 (Tet^r)</i>]
BL21 (DE3)	<i>E. coli F⁻ ompT hsdS_B(r_B⁻, m_B⁻) dcm⁺ Tet^r gal^λ (DE3) EndA Hte [argU ileY LeuW Cam^r]</i>
BL21 (DE3)pLysS	<i>E. coli F⁻ ompT hsdS_B(r_B⁻, m_B⁻) gal dcm (DE3) pLysS(Cam^R)</i>

2.1.2 *E. coli* Plasmids

pGEX-4T1-*NUP159*, pET28a-*ATG8*, pYCplac111-*NUP159-6HA* and pYCplac33-VN-*ATG8* were generated by PCR from yeast genomic DNA extract and subcloning. Other *E.*

2. MATERIALS AND EXPERIMENTAL METHODS

Coli plasmid used was pGAL-Ub-proline- β -galactosidase plasmid (obtained from Kefeng Lu).

2.1.3 *E. coli* Media

LB (Luria-Bertani)-medium/plates:	1% (w/v) Bacto tryptone (Difco)
	0.5% (w/v) Bacto yeast extract (Difco)
	1% (w/v) NaCl
	1.5% (w/v) agar (for plates)
	Sterilized by autoclaving

The respective antibiotic, ampicillin (100 μ g/ml), kanamycin (30 μ g/ml), or chloramphenicol (34 μ g/ml), was added for the selection of plasmids harboring antibiotic resistance genes.

2.1.4 Cultivation and Storage of *E. coli*

Liquid cultures were grown in LB media shaking at 200 rpm at 37 °C except for protein expression (23 °C or 30 °C). Solid cultures on agar plates were incubated at 37 °C. The selection of transformed bacteria was achieved by adding the respective antibiotic to the media. The culture density was determined by measuring the absorbance at a wavelength of 600 nm (OD_{600}). Cultures on solid media were stored at 4 °C up to 7 days. For long-term storages, stationary cultures were frozen in 15% (v/v) glycerol solutions at -80 °C.

2.1.5 Preparation of Chemically Competent *E. coli*

A large batch of *E. Coli* culture was prepared by inoculating the 1 L LB medium with a overnight fresh culture to an OD_{600} of 0.05, and cells were grown at 37 °C with shaking to $OD_{600} \sim 0.5\text{--}0.8$. The culture was then chilled on ice for 20 min and cells were collected by centrifugation (5000 rpm, 15 min, 4 °C). Resuspended the cell pellet in 300 ml Tfb1 solution (30 mM KOAc, 50 mM MnCl₂, 100 mM KCl, 15% (v/v) glycerol, pH adjusted to 5.8 with HOAc) and chilled on ice for 15 min. Cells were pelleted again (2500 rpm, 15

2. MATERIALS AND EXPERIMENTAL METHODS

min, 4 °C) and carefully resuspended in 40 ml Tfb2 solution (10 mM MOPS, 75 mM CaCl₂, 10 mM KCl, 15% (v/v) glycerol, pH adjusted to 7.0 with NaOH). Finally, competent cells were aliquoted on ice and stored at -80 °C.

2.1.6 Transformation of Plasmid DNA into Competent *E. coli*

Shortly before transformed, competent cells were thawed on ice. Mixed the ~20-200 ng plasmid DNA or 5-25 µl of a cloning product with 50-100 µl of competent cells and incubated on ice for 20 min. A heat-shocked was performed at 42 °C for 1 min, followed by a 5 min incubation on ice. For recovery, 1 ml of LB medium without antibiotic was added and shaking at 37 °C for 1 h before plating.

2.1.7 Expression and Purification of GST-Nup159, GST-Atg8, GST-Atg8 Y49A, L50A and His-Atg8

GST-fusion proteins and His-Atg8 were expressed in *E. coli* Rosetta™ 2(DE3) (for GST-fusion proteins) or Rosetta™ 2(DE3)pLysS (for His-Atg8) cells, respectively. Expression was induced with 1mM IPTG in a 1 L culture of LB for 20 h at 22 °C. Cells were harvested by centrifugation and lysed in lysis buffer (GST-fusion proteins: 40 mM Tris pH 7.5, 150 mM NaCl, 5 mM DTT, EDTA-free protease inhibitors cocktail (cComplete Tablets, Roche), 1 mg/ml Pefabloc SC (Roche); His-Atg8: 40 mM Tris pH 7.5, 500 mM NaCl, 5 mM MgCl₂, 5 mM 2-Mercaptoethanol, 20 mM Imidazole, 10% glycerol (w/v), EDTA-free protease inhibitors cocktail (cComplete Tablets, Roche), 1 mg/ml Pefabloc SC (Roche)) using an EmulsiFlex C3 homogenizer (Avestin). DNA was digested using SM DNase (final 75 U/ml, 15 min on ice). Supernatant containing soluble proteins was collected by centrifugation (20000 rpm, 30 min). GST-fusion proteins and His-Atg8 were affinity purified using Glutathione Sepharose 4 Fast Flow (GE Healthcare) or Ni-NTA agarose (Qiagen) respectively (2 h on a rotary wheel at 4 °C). The resins were recovered by gravity-flow chromatography. Resins were subsequently washed 3 times with 25 ml lysis buffer, followed by 3 times with washing buffer (GST-fusion proteins: 40 mM Tris pH 7.5, 450 mM NaCl, 5 mM DTT; His-Atg8: 40 mM Tris pH 7.5, 500 mM NaCl, 5 mM

2. MATERIALS AND EXPERIMENTAL METHODS

MgCl₂, 5 mM 2-Mercaptoethanol, 70 mM Imidazole, 10% glycerol (w/v)). Bound proteins were eluted from the individual resin (GST-fusion proteins: 40 mM Tris pH 7.5, 150 mM NaCl, 5 mM DTT, 50 mM glutathione; His-Atg8: 40 mM Tris pH7.5, 500 mM NaCl, 5 mM MgCl₂, 5 mM 2-Mercaptoethanol, 270 mM Imidazole, 10% glycerol (w/v)). The eluted proteins were collected and dialysed (50 mM Tris pH 7.5, 150 mM NaCl, 20% glycerol (w/v), overnight 4 °C). Purified proteins were directly frozen after dialysis and stored in aliquots at –80 °C until further use. The identity of the different proteins was confirmed by sodium dodecyl sulfate polyacrylamide gel electrophoresis (SDS-PAGE).

2.1.8 Plasmids

Table 2.2: Plasmids

Plasmids used in this study.

E. Coli vectors: pGEX4T-1 (*amp*^R), pGEX4T-3 (*amp*^R) and pET28a (*amp*^R)

Yeast CEN plasmids: pYCplac33 (*URA3*) and pYCplac111 (*LEU2*)

Name	Expression construct
GST-Nup159	<i>pGEX-4T1-Nup159</i>
GST	<i>pGEX4T-3</i>
His-Atg8	<i>pET28a-Atg8</i>
GST-Atg8	<i>pGEX-4T3-Atg8</i>
GST-Atg8 Y49A, L50A	<i>pGEX-4T3-Atg8 Y49A, L50A</i>
Ub-βGal-WT	<i>pGAL-Ub-proline-b-galactosidase::URA3</i>
pYCplac111-Nup159-6HA	<i>pYCplac111-Nup159-6HA::LEU2</i>
pYCplac111-Nup159 ^{AIM1} -6HA	<i>pYCplac111-Nup159 Y1078A, L1081A-6HA::LEU2</i>
pYCplac111-Nup159 ^{AIM2+3} -6HA	<i>pYCplac111-Nup159 F1218A, V1221A, F1225A, L1228A-6HA::LEU2</i>
pYCplac111-Nup159 ^{AIM4} -6HA	<i>pYCplac111-Nup159 Y1317A, L1320A-6HA::LEU2</i>
pYCplac111-Nup159 ^{AIM5} -6HA	<i>pYCplac111-Nup159 F1434A, V1437A-6HA::LEU2</i>
VN-Atg8	<i>pYCplac33-VN-Atg8::URA3</i>
VN-Atg8 Y49A, L50A	<i>pYCplac33-VN-Atg8 Y49A, L50A::URA3</i>

2.2 *Saccharomyces cerevisiae* (*S. cerevisiae*) techniques

2.2.1 Yeast Strains

Table 2.3: Yeast strains

Yeast strains used in this study. All strains are isogenic to DF5 (Finley et al., 1987).

Name	Relevant genotypes
DF5	<i>trp1-1 ura3-52 his3 200 leu2-3,11 lys2-801 CAN1 BARI</i>
CW066	<i>NIC96^{EGFP}::klTRP1</i>
CW134	<i>POM152^{EGFP}::klTRP1</i>
CW149	<i>NUP188^{EGFP}::klTRP1</i>
CW185	<i>atg8::kanMX6 POM152^{EGFP}::klTRP1</i>
CW191	<i>atg3::HIS3MX6 NUP192^{EGFP}::klTRP1</i>
CW192	<i>atg4::HIS3MX6 NUP192^{EGFP}::klTRP1</i>
CW193	<i>atg6::HIS3MX6 NUP192^{EGFP}::klTRP1</i>
CW196	<i>atg7::kanMX6 NUP192^{EGFP}::klTRP1</i>
CW198	<i>atg8::kanMX6 NUP192^{EGFP}::klTRP1</i>
CW205	<i>nvj1::hphNT1 NUP192^{EGFP}::klTRP1</i>
CW243	<i>nup133::hphNT1 NUP192^{EGFP}::klTRP1</i>
CW244	<i>nup120::hphNT1 NIC96^{EGFP}::klTRP1</i>
CW264	<i>NUP159^{EGFP}::klTRP1</i>
CW264	<i>NUP133^{EGFP}::klTRP1</i>
CW276	<i>NUP192^{EGFP}::klTRP1</i>
CW284	<i>nup120::hphNT1 NUP192^{EGFP}::klTRP1</i>
CW346	<i>dsk2::kanMX6 NUP192^{EGFP}::klTRP1</i>
CW356	<i>atg8::kanMX6 NUP133^{EGFP}::klTRP1</i>
CW363	<i>atg8::kanMX6 NUP159^{EGFP}::klTRP1</i>
CW382	<i>cue5::HIS3MX6 NUP192^{EGFP}::klTRP1</i>
CW470	<i>atg19::kanMX6 NUP192^{EGFP}::klTRP1</i>
CW474	<i>atg11::kanMX6 NUP159^{EGFP}::klTRP1</i>
CW481	<i>atg11::kanMX6 NUP192^{EGFP}::klTRP1</i>
CW566	<i>nup120::hphNT1 EGFP-ATG8::natNT2</i>
CW571	<i>EGFP-ATG8::natNT2</i>
CW575	<i>atg1::kanMX6 NUP192^{EGFP}::klTRP1</i>

2. MATERIALS AND EXPERIMENTAL METHODS

Name	Relevant genotypes
CW654	<i>prb1::natNT2 pep4::HIS3MX6 NUP192^{EGFP}::klTRP1</i>
CW723	<i>atg40::kanMX6 NUP192^{EGFP}::klTRP1</i>
CW725	<i>atg39::HIS3MX6 NUP192^{EGFP}::klTRP1</i>
CW791	<i>atg39::HIS3MX6 atg40::kanMX6 NUP192^{EGFP}::klTRP1</i>
CW1106	<i>POM152^{6HA}::kanMX6</i>
CW1108	<i>NUP159^{6HA}::kanMX6</i>
CW1110	<i>NUP192^{6HA}::kanMX6</i>
CW1156	<i>vps4::natNT2 NUP192^{EGFP}::klTRP1</i>
CW1432	<i>pADH-EGFP-ATG8::natNT2 NUP159^{6HA}::kanMX6</i>
CW1431	<i>cim3-1 pADH-EGFP-ATG8::natNT2</i>
CW1434	<i>pADH-EGFP-ATG8::natNT2 NUP192^{6HA}::kanMX6</i>
CW1442	<i>pADH-EGFP-ATG8::natNT2 POM152^{6HA}::kanMX6</i>
CW2708	<i>pep4::HIS3MX6 NUP159^{6HA}::kanMX6</i>
CW2709	<i>pep4::HIS3MX6 NUP159^{6HA}::kanMX6 EGFP-ATG8::natNT2</i>
CW2710	<i>pep4::HIS3MX6 NUP192^{6HA}::kanMX6 EGFP-ATG8::natNT2</i>
CW2711	<i>pep4::HIS3MX6 NUP192^{6HA}::kanMX6</i>
CW2792	<i>cim3-1 NUP192^{EGFP}::klTRP1</i>
CW2951	<i>atg15::HIS3MX6 nvj1::hphNT1 NUP192^{EGFP}::kanMX6 VPH1^{mars}::natNT2</i>
CW2952	<i>atg15::HIS3MX6 NUP192^{EGFP}::kanMX6 VPH1^{mars}::natNT2</i>
CW2953	<i>atg15::HIS3MX6 atg8::kanMX6 NUP192^{EGFP}::kanMX6 VPH1^{mars}::natNT2</i>
CW3001	<i>pADH-VN-ATG8::natNT2 NUP159^{VC}::HIS3MX6 NUP170^{mars}::kanMX6</i>
CW3002	<i>nup120::hphNT1 pADH-VN-ATG8::natNT2 NUP159^{VC}::HIS3MX6 NUP170^{mars}::kanMX6</i>
CW3006	<i>vps4::hphNT1 pADH-EGFP-ATG8::natNT2</i>
CW3017	<i>pADH-VN-ATG8::natNT2 NUP192^{VC}::HIS3MX6 NUP170^{mars}::kanMX6</i>
CW3018	<i>pADH-VN-ATG8::natNT2 MLP1^{VC}::HIS3MX6 NUP170^{mars}::kanMX6</i>
CW3019	<i>atg15::HIS3MX6 NUP192^{EGFP}::kanMX6 NUP84^{mars}::natNT2</i>
CW3020	<i>atg15::HIS3MX6 NUP192^{EGFP}::kanMX6 NUP159^{mars}::natNT2</i>
CW3025	<i>pep4::HIS3MX6 pADH-EGFP-ATG8::natNT2 POM152^{6HA}::kanMX6</i>
CW3026	<i>pep4::HIS3MX6 POM152^{6HA}::kanMX6</i>
CW3027	<i>atg15::HIS3MX6 NUP192^{EGFP}::kanMX6 NDC1^{mars}::natNT2</i>
CW3072	<i>atg15::HIS3MX6 atg1::hphNT1 NUP192^{EGFP}::kanMX6 VPH1^{mars}::natNT2</i>
CW3073	<i>atg15::HIS3MX6 atg7::hphNT1 NUP192^{EGFP}::kanMX6 VPH1^{mars}::natNT2</i>
CW3101	<i>rad23::kanMX6 dsk2::kanMX6 NUP192^{EGFP}::klTRP1</i>
CW3107	<i>rpn13::kanMX6 NUP192^{EGFP}::klTRP1</i>

2. MATERIALS AND EXPERIMENTAL METHODS

Name	<i>Relevant genotypes</i>
CW3110	<i>rad23::kanMX6 NUP192^{EGFP}::klTRP1</i>
CW3114	<i>rpn10::HIS3MX6 atg8::kanMX6 NUP192^{EGFP}::klTRP1</i>
CW3116	<i>rpn10::HIS3MX6 NUP192^{EGFP}::klTRP1</i>
CW3128	<i>pADH-EGFP-ATG8::natNT2 nup159::hphNT1 pYCplac111-Nup159-6HA::LEU2</i>
CW3129	<i>pADH-EGFP-ATG8::natNT2 nup159::hphNT1 pYCplac111-Nup159^{AIM4}-6HA::LEU2</i>
CW3130	<i>NUP192^{EGFP}::klTRP1 nup159::hphNT1 pYCplac111-Nup159-6HA::LEU2</i>
CW3140	<i>pADH-EGFP-ATG8::natNT2 nup159::hphNT1 pYCplac111-Nup159^{AIM1}-6HA::LEU2</i>
CW3141	<i>NUP192^{EGFP}::klTRP1 nup159::hphNT1 pYCplac111-Nup159^{AIM1}-6HA::LEU2</i>
CW3149	<i>pADH-EGFP-ATG8::natNT2 nup159::hphNT1 pYCplac111-Nup159^{AIM5}-6HA::LEU2</i>
CW3150	<i>pADH-EGFP-ATG8::natNT2 nup159::hphNT1 pYCplac111-Nup159^{AIM2+3}-6HA::LEU2</i>
CW3161	<i>NUP133^{EGFP}::klTRP1 nup159::hphNT1 pYCplac111-Nup159-6HA::LEU2</i>
CW3162	<i>NUP133^{EGFP}::klTRP1 nup159::hphNT1 pYCplac111-Nup159^{AIM1}-6HA::LEU2</i>
CW3184	<i>nup120::hphNT1 NIC96^{EGFP}::klTRP1 nup159::natNT2 pYCplac111-Nup159-6HA::LEU2</i>
CW3185	<i>nup120::hphNT1 NIC96^{EGFP}::klTRP1 nup159::natNT2 pYCplac111-Nup159^{AIM1}-6HA::LEU2</i>
CW3186	<i>nup120::hphNT1 NUP192^{EGFP}::klTRP1 nup159::natNT2 pYCplac111-Nup159-6HA::LEU2</i>
CW3187	<i>nup120::hphNT1 NUP192^{EGFP}::klTRP1 nup159::natNT2 pYCplac111-Nup159^{AIM1}-6HA::LEU2</i>
CW3224	<i>NUP159^{6HA}::kanMX6 pADH-EGFP-ATG11::natNT2</i>
CW3246	<i>nup116::natNT2 NUP188^{EGFP}::klTRP1</i>
CW3249	<i>NUP192^{EGFP}::klTRP1 nup159::hphNT1 pYCplac111-Nup159-6HA::LEU2 atg15::natNT2</i>
CW3250	<i>NUP192^{EGFP}::klTRP1 nup159::hphNT1 pYCplac111-Nup159^{AIM1}-6HA::LEU2 atg15::natNT2</i>
CW3254	<i>nup116::HIS3MX6 pADH-EGFP-ATG8::natNT2 NUP159^{6HA}::kanMX6</i>
CW3270	<i>nup116::natNT2 NUP84^{EGFP}::klTRP1 NUP159^{6HA}::kanMX6</i>
CW3271	<i>NUP84^{EGFP}::klTRP1 NUP159^{6HA}::kanMX6</i>
CW3272	<i>nup116::natNT2 NUP133^{EGFP}::klTRP1</i>
CW3352	<i>NUP159^{VC}::HIS3MX6 NUP170^{mars}::natNT2 atg8::kanMX6 pYCplac33-VN-Atg8::URA3</i>
CW3353	<i>NUP159^{VC}::HIS3MX6 NUP170^{mars}::natNT2 atg8::kanMX6 pYCplac33-VN-Atg8 Y49A, L50A::URA3</i>
FW_Y134	<i>pep4::hphNT1 pADH-EGFP-ATG8::natNT2</i>

2. MATERIALS AND EXPERIMENTAL METHODS

2.2.2 Media, Buffers and Solutions

YP-media/plates:	1% (w/v) Bacto yeast extract (Difco) 2% (w/v) Bacto peptone (Difco) 2% (w/v) carbon source (glucose (D), galactose (Gal), raffinose (Raf)) 2% (w/v) agar (only for plates) Sterilized by autoclaving
YPD G418/NAT/Hph plates:	After autoclaving, YPD medium with 2% (w/v) agar was cooled to 50 °C, and 200 mg/l G418 (geneticin disulphate, PAA Laboratories), 100 mg/l NAT (nourseothricin, HKI Jena) or 500 mg/l Hph (hygromycin B, PAA Laboratories) were added.
Synthetic drop-out media/plates:	0.67% (w/v) yeast nitrogen base (Difco) 0.133% (w/v) amino acid master mix -8 + amino acid supplements (omitting individual ones according to the requirements) 2% (w/v) carbon source (glucose (D), galactose (Gal), raffinose (Raf)) 2% (w/v) agar (only for plates) Sterilized by autoclaving
Amino acid master mix -8 stock:	25 g each: Ala, Asn, Asp, Cys, Gln, Glu, Gly, Ile, Phe, Pro, Ser, Thr, Tyr, Val, myo-Inositol 2.5 g para-Aminobenzoic acid
Amino acid supplements:	0.0175% (w/v) final: Leu 0.00875% (w/v) final: His, Met, Arg, Trp, Ura, Lys-monohydrate 0.00225% (w/v) final: Adenine hemisulfate salt
Sporulation medium:	2% (w/v) KAc Sterilized by autoclaving
SORB buffer:	100 mM LiOAc 10 mM Tris-HCl, pH 8.0 1 mM EDTA, pH 8.0 1 M sorbitol

2. MATERIALS AND EXPERIMENTAL METHODS

Sterilized by filtration	
PEG Solution:	100 mM LiOAc 10 mM Tris-HCl, pH 8.0 1 mM EDTA, pH 8.0 40% (w/v) PEG-3350 Sterilized by filtration and stored at 4 °C
Zymolase 20T solution:	900 mM sorbitol 100 mM Tris-HCl, pH 8.0 100 mM EDTA, pH 8.0 50 mM DTT (add freshly) 0.5 mg/ml zymolase 20T (ICN Biochemicals) Sterilized by filtration and stored at -20 °C

2.2.3 Yeast Culture, Storage, Starvation, Drug Treatment, and Nup Degradation and EGFP Cleavage Assay

Yeast cells were streaked freshly from glycerol stocks (saturated yeast culture with 15% (v/v) glycerol, stored at -80 °C) on YPD or selective plates and grown for 1 to 3 days at 30 °C, or 25 °C for temperature-sensitive (*ts*) mutants. Usually, cells were cultured overnight in YPD- or SC-medium with a shaking incubator (150-200 rpm) at 30 °C. For Nup degradation and EGFP cleavage assay, cells were grown to mid-log phase (OD₆₀₀ 1.0, corresponds to ~2×10⁷ cells/ml) then switched into SD-N medium (synthetic minimal medium lacking nitrogen; 0.17% YNB without amino acids and ammonium sulfate, supplemented with 2% glucose) and incubated for the indicated time. Alternatively, cells were treated with 80 µg/ml cyclohexamide (CHX), 12 nM rapamycin, 0.05% methyl methanesulfonate (MMS), 0.5 µM tunicamycin (Tm), 30 µM cadmium chloride (CdCl₂), 2 mM hydrogen peroxide (H₂O₂), 5 µg/ml canavanine (Can) or 15 µg/ml nocodazole (NOC) for the indicated times. Autophagy substrates were tagged at the endogenous, chromosomal location with EGFP and their vacuolar degradation following starvation

2. MATERIALS AND EXPERIMENTAL METHODS

was monitored by accumulation of the released EGFP moiety, which is largely resistant to vacuolar degradation.

2.2.4 Competent Yeast Cells and Transformation

50 ml mid-log phase yeast cultures were harvested (500 g, 5 min, 25 °C) and washed 1 time with 25 ml sterilized water, followed by 1 time with 5 ml SORB buffer. The cells were resuspended in 360 µl SORB buffer and 50 µl carrier DNA (10 mg/ml herring sperm DNA, Invitrogen) and then stored at –80 °C.

For transformation, PCR products or 0.2 µg of circular or 1-2 µg linearized plasmid DNA was mixed with 15-50 µl of competent cells, respectively. 6 volumes of PEG solution was added and the cell suspension was incubated at 30 °C for 30 min, followed by a 42 °C heat-shocked for 10-15 min. After 1 volume of DMSO was added, cells were heat-shocked (42 °C) for 10–15 min and chilled on ice. Cells were pelleted (500 g, 3 min, 25 °C) and plated on selective media plates, or allowed recovery in 1 ml YPD for 1.5-2 h before plating when antibiotic resistance cassettes were used (natNT2, hphNT1 or kanMX4). Plates were incubated at 25 °C or 30 °C until single colonies appeared, or replica plated using sterile velvet if necessary.

2.2.5 Genetic Manipulation

Chromosomal gene deletion or tagging was performed according to the standard protocols by a PCR strategy (Janke et al., 2004; Knop et al., 1999). To design the primers, the oligonucleotides contained the flanking sequences of the target gene (50 bp overhangs) were fused at its 3' end with additional primer sequences that provided to amplify the marker cassettes (optionally with epitope tags). Cells were transformed with PCR-amplified cassettes from a series of pYM vectors and selection based on the marker of used cassette. Homologous recombination initiated by the 50 bp overhangs directed cassette integration and then correct insertion was checked by yeast colony PCR or immunoblot (to test for absence of a deleted ORF or proper epitope-tagging).

2. MATERIALS AND EXPERIMENTAL METHODS

2.2.6 Mating Type Analysis, Mating, Sporulation, and Tetrad Analysis

Mating type of haploid yeast was determined by using the pheromone-hypersensitive tester strains, RC634a and RC75-7 α . 20 μ l of an aqueous cell suspension of each tester strain was mixed with 10 ml molten 1% (w/v) agar solution (precooled to ~45 °C before adding cells). A layer of mixture was poured on top of regular YPD plates. Strains to be analyzed were replica plated on the a- and α -tester top agar plates. The tester cells cannot grow in proximity of cells of different mating type. Consequently, a halo of clear agar appears around the colony after 1-2 days of incubation, indicating this colony harbors the opposite mating type to the tester strain.

To mate yeast cells, similar amount of haploid strains of opposite mating types (MAT a and MAT α) were mixed on a pre-warmed YPD plate and grown overnight. Cells were then restreaked or replica plated on selective media plates to select diploid cells.

For sporulation, 500 μ l of diploid cultures were pelleted and washed 3 times with water. Cell pellets were resuspended in 5 ml 2% KAc and incubated at 25 °C for 3-5 days with shaking (220 rpm). 10 μ l of sporulation culture was mixed with an equal amount of zymolase 20T solution (see section “2.2.2”) and incubated at 25 °C for 6 min to remove cell wall. The spores were dissected in tetrads with a micromanipulator (Singer MSM Systems). Germination usually took 3-5 days on non-selective YPD plates and genotypes were determined by replica plating on selective plates and mating type tester plates.

2.3 Molecular Biological Methods

2.3.1 DNA Purification and Analysis

Plasmid DNA was isolated by alkaline lysis and binding to anion-exchange matrices using AccuPrep® Plasmid Mini Extraction Kit (Bioneer) and followed the manufacturers' instructions. Genomic DNA was extracted from *S. cerevisiae* cells using the MasterPure™ Yeast DNA Purification kit (Epicentre®). DNA fragments from gel slices and PCR products were purified using AccuPrep® PCR and Gel Purification Kit

2. MATERIALS AND EXPERIMENTAL METHODS

(Bioneer). DNA concentrations were measured using a NanoDrop ND-1000 instrument (PeqLab). DNA sequencing services were provided from Eurofins.

2.3.2 Polymerase Chain Reaction (PCR)

PCR was performed according to standard protocols. PCR technique was used for cloning (Phusion PCR; NEB), for site-directed mutagenesis (Pfu Turbo PCR; Stratagene), for genetic manipulation (Vent/ Knop PCR or *Knop* PCR; NEB) (Janke et al., 2004) or to test genetic modifications (yeast colony PCR and Taq polymerase PCR; MPI Biochemistry Core Facility). PCR reactions were performed in a thermal cycler (Applied Biosystems) in a total volume of 50 µl.

PCR reaction setups

Reagent	Taq PCR	Phusion PCR
DNA template:	10 ng plasmid or 200 ng genomic DNA or yeast colony	
dNTP (10 mM each):		1 µl
Primer for. (10 µM):	1.5 µl	2.5 µl
Primer rev. (10 µM):	1.5 µl	2.5 µl
Polymerase buffer:	2.5 µl*	10 µl**
Polymerase:	0.25 µl	0.5 µl
Total with H ₂ O:	to 25 µl	to 50 µl

* 10× ThermoPol reaction buffer (Thermo); ** 5× Phusion HF or GC buffer (NEB)

PCR amplification protocols

	Taq PCR		Phusion PCR	
Step	Temperature	Duration	Temperature	Duration
Initial denaturation:	94 °C	5 min	98 °C	2 min
Denaturation:	94 °C	30 sec	98 °C	20 sec
Annealing:	55 °C*	30 sec	55 °C*	30 sec
Elongation:	72 °C	1 kb/min	72 °C	1 kb/30 sec
Final extension:	72 °C	5 min	72 °C	7 min

2. MATERIALS AND EXPERIMENTAL METHODS

Cooling:	4 °C	hold	4 °C	hold
----------	------	------	------	------

* Variable (depends on primer Tm (melting temperature)); shaded parts were cycled for 30-35 times.

The elongation time for Phusion PCR of *NUP159* is 6 min and of *ATG8* is 45 sec.

2.3.3 Agarose Gel Electrophoresis

Low-melt agarose ((w/v) 0.7–2%) (Invitrogen) was dissolved in 1× TBE buffer (Tris-borate buffer; 189 mM Tris, 89 mM boric acid, 2 mM EDTA) and melted by boiling. 5 µg/ml of ethidium bromide (EtBr) was added before gel casting. DNA was mixed with 5× DNA loading dye (0.25% SDS, 25 mM EDTA pH 8.0, 25% glycerol, Orange G in H₂O) and gels were run at 80-120 V in 1x TBE buffer. The 1 kb plus DNA ladder (Invitrogen) was used as size marker and DNA bands were visualized using a UV transilluminator (324 nm, VWR GenoSmart).

2.3.4 Cloning

Briefly, the primers contain restriction enzyme-digested site were used for PCR from genomic DNA templates (see section “2.3.2”). Separated the PCR products by gel electrophoresis (see section “2.3.3”) and were subsequently purified by gel purification kit (see section “2.3.1”). Purified insert DNA and ~2.5 µg vectors were subjected to restriction enzyme digestion (NEB) according to the manufacturer’s instructions. To prevent vector self-ligation, vectors were dephosphorylated by addition of 1 µl FastAP phosphatase (Thermo; 1 h at 37 °C) into the digestion mixture and purified using PCR purification kit (see section “2.3.1”). Digested insert DNA were purified again with PCR purification kit. ~50–150 ng vector DNA with a 3-10 fold excess molar of insert DNA were mixed together and ligated in a 15 µl reaction using T4 ligase (NEB) for 30 min at room temperature according to the manufacturer’s instructions. Finally, the ligation mixture was used for transformation of 100 µl competent XL1-Blue *E. coli* cells and recovered the cells with 1 ml LB for 1.5 h at 37 °C before plating.

2. MATERIALS AND EXPERIMENTAL METHODS

2.3.5 Site-directed Mutagenesis

PCR-based strategy was applied using the Pfu Turbo polymerase (Stratagene) and QuikChange Site-Directed Mutagenesis Kit (Stratagene) and followed the manufacturer's instructions (including the optimal primer design). PCR products were digested by methylation specific restriction enzyme DpnI (NEB; 1 µl, 4 h at 37 °C) and 20 µl out of 50 µl reaction mixture was used for transformation of 100 µl competent XL1-Blue *E. coli* cells. Cells were recovered with 1 ml LB for 1.5 h at 37 °C before plating.

Pfu Turbo PCR protocol

Step	Temperature	Duration
Initial denaturation:	95 °C	2 min
Denaturation:	95 °C	30 sec
Annealing:	50 °C*	30 sec
Elongation:	68 °C	1 kb/min
Final extension:	68 °C	15 min
Cooling:	4 °C	hold

* Variable (depends on primer Tm (melting temperature)); shaded parts were cycled for 20 times.

The elongation time for site-directed mutagenesis of pYCplac111-*NUP159-6HA* is 25 min, of pGEX-4T3-*ATG8* is 12 min, and of pYCplac33-VN-*ATG8* is 16 min.

2.4 Biochemical and Cell Biology Methods

2.4.1 Immunoblot Techniques

HU loading buffer:	8 M Urea 5% (w/v) SDS 200 mM Tris, pH 6.8 20 mM dithiothreitol (DTT) 1.5 mM Bromophenol blue
--------------------	--

2. MATERIALS AND EXPERIMENTAL METHODS

MOPS buffer:	50 mM MOPS 50 mM Tris base 3.5 mM SDS 1 mM EDTA
Blotting buffer:	250 mM Tris base 1.92 M glycine 0.1% (w/v) SDS 20% (v/v) methanol
TBS-T solution:	25 mM Tris, pH 7.5 137 mM NaCl 2.6 mM KCl 0.1% (v/v) Tween 20

3×10^7 cells (OD₆₀₀ 1.5) were harvested for the indicated time points and total cell protein extracts were obtained by alkaline lysis (2 M NaOH and 7.5% (v/v) 2- Mercaptoethanol for 15 min on ice) followed by TCA precipitation (Trichloroacetic acid; to a final concentration of 22% for 10 min on ice). Proteins pellets were collected by centrifugation (14000 rpm, 20 min) and solubilized in HU loading buffer and disrupted by vortexing with an equal volume of acid-washed glass beads for 6 min. Followed by an incubation at 65 °C (1400 rpm) for 10 min. The pre-cast NuPAGE 4%–12% gradient gels (Invitrogen) were used. Protein samples were loaded, and gels were run in MOPS buffer at constant voltage of 80-200V. For estimation of protein molecular weight, the Precision Plus All Blue Standard (Bio-Rad) was used.

For western blot analysis, proteins separated by SDS-PAGE were transferred onto methanol-activated polyvinylidene difluoride (PVDF) membranes (Immobilon®-P) using a wet transfer protocol. Blots were assembled in a cassette and blotting was performed in Amersham Biosciences blot chambers at 75 V constant voltage at 4 °C for 2 h. Membrane then blocked in 5% (w/v) skim milk powder in TBS-T solution for 30 min at 25 °C and subsequently incubated overnight with primary antibody dissolved in 5% milk/TBS-T (with 0.02% sodium azide). Next, the membrane was washed 3 times with TBS-T and incubated with secondary antibody coupled to horseradish peroxidase in 5%

2. MATERIALS AND EXPERIMENTAL METHODS

milk/TBS-T for 1-3 h (see section “2.4.9” for specific secondary antibodies). Lastly, the membrane was washed 3 times for 15 min in TBS-T. Detection of proteins was performed using chemiluminescence reagents (ECL or ECL plus, Thermo Scientific). Signals were detected using Amersham Hyperfilm ECL (GE Healthcare) and further processed in Adobe Photoshop.

2.4.2 Co-immunoprecipitation of Nucleoporins

200 OD₆₀₀ yeast lysates were prepared by cell disruption on a multitube bead-beater (MM301 from Retsch GmbH) in lysis buffer (100 mM Hepes pH 7.4, 150 mM NaCl, 1% NP-40, 10% glycerol, 50 mM NaF, 2 mM phenylmethylsulfonyl fluoride (PMSF), and EDTA-free protease inhibitor cocktail (cComplete Tablets, Roche)) with zirconia/silica beads. The extracts were cleared by centrifugation at 8000 g for 10 min and supernatants were incubated with EGFP-Trap_A matrix (ChromoTek) or Ni-NTA agarose beads (Qiagen) for 2 h with head-over-tail rotation at 4 °C and followed by 5 times washing steps with lysis buffer to remove nonspecific background binding. Bound proteins were eluted by adding HU loading buffer and incubated at 65 °C for 10 min.

2.4.3 Atg8 Interactome and Mass Spectrometry

To analyse the Atg8 interactome upon nitrogen starvation, yeast cells were grown in 200 ml YPD medium. At OD₆₀₀ 1 cells were shifted to SD-N medium and incubated for 16 h at 30 °C. Yeast cells were collected by centrifugation and yeast lysates were prepared by cell disruption on a multitube bead-beater (MM301 from Retsch GmbH) in yeast lysis buffer (20 mM Hepes pH 7.5, 150 mM KOAc, 1% NP-40, 5% glycerol, 10 mM N-Ethylmaleimide, 1 mg/ml Pefabloc SC (Roche), and EDTA-free protease inhibitor cocktail (cComplete Tablets, Roche)) with zirconia/silica beads. The extracts were cleared by centrifugation at 2000 g for 10 min. Supernatants were incubated with EGFP-Trap_M matrix (ChromoTek GmbH) for 1 h on a rotary wheel at 4 °C. Magnetic beads were washed 2 times with yeast lysis buffer and 4 times with washing buffer (50 mM Tris pH 7.5, 150 mM NaCl, 1 mg/ml Pefabloc SC (Roche), and EDTA-free protease inhibitor cocktail (cComplete Tablets, Roche)) to remove any residual detergent. The supernatants

2. MATERIALS AND EXPERIMENTAL METHODS

from the beads were removed and the beads were incubated with a buffer containing 4 M urea and 20 mM DTT in 25 mM Tris pH 8.0 buffer for 10 minutes followed by incubation with 40 mM chloroacetamide for 20 minutes for alkylation of cysteines. The sample was diluted to final concentration of 1 M urea with digestion buffer (25 mM Tris pH 8.0) and vortexed. The sample was digested for 2 h with 0.5 µg of endoproteinase lysine-C (Wako chemicals) and then digested with 0.5 µg of trypsin (Promega) overnight. The digested peptides were purified using StageTip (Rappsilber et al., 2003). Peptides were loaded on a 15 cm column (inner diameter = 75 microns) packed with C18 reprosil 3 micron beads (Dr Maisch GmbH) and directly sprayed into a LTQ-Orbitrap XL instrument operated in a data-dependent fashion. Up to top 5 precursors were selected for fragmentation by CID and analysed in the iontrap. The raw data were processed using MaxQuant (Cox and Mann, 2008) version 1.6.0.15. Peak lists generated were searched against a yeast ORF database using Andromeda search engine built into Maxquant. Proteins were quantified using the MaxLFQ algorithm (Cox et al., 2014). Analysis was performed using Perseus (Tyanova et al., 2016) version 1.5.2.4. Raw data are uploaded at EBI PRIDE.

2.4.4 Atg8/Nup159 *in vitro* Binding Assay

The *in vitro* binding assay was performed by incubation of the indicated protein combinations in 1 ml assay buffer (50 mM Tris pH 7.5, 150 mM NaCl, 5% glycerol (w/v), 20 mM Imidazol, 0.1% Triton X-100) for 1h at room temperature. 50 µl were used as input control and mixed with an equal amount of HU loading buffer. The rest of the supernatant was added to 100 µl Ni-NTA agarose (Qiagen) slurry and incubated for 2.5 h at 4 °C on a rotary wheel. The resin was collected by centrifugation (800 rpm, 1 min) and washed 6 times with 1 ml washing buffer (50 mM Tris pH 7.5, 150 mM NaCl, 5% glycerol (w/v), 20 mM Imidazol, 1% Triton X-100). After the last washing step, the supernatant was removed (27g needle) and the proteins were eluted with 50 µl of elution buffer (50 mM Tris pH 7.5, 150 mM NaCl, 5% glycerol (w/v), 270 mM Imidazol, 1% Triton X-100). The eluate was transferred into a new tube (27g needle), mixed with an equal amount of HU loading buffer and analyzed by SDS-PAGE. Proteins separated by SDS-PAGE were stained with PageBlue Protein Staining Solution (Thermo Scientific).

2. MATERIALS AND EXPERIMENTAL METHODS

2.4.5 GST-Atg8 Pulldown with Cell Extract

The indicated GST-fusion proteins were incubated (125 µg) diluted in 1ml assay buffer (50 mM Tris pH 7.5, 150 mM NaCl, 5% glycerol (w/v, 0.1% Triton X-100) and mixed with 50 µl Glutathione Sepharose 4 Fast Flow (GE Healthcare) slurry. The mixture was incubated for 2 h at 4 °C on a rotary wheel. Meanwhile the yeast lysate was prepared as described above (mass spectrometry, 20µl were kept as input control and mixed with 200 µl HU loading buffer). The Glutathione Sepharose was collected by centrifugation (800 rpm, 1 min) and washed one time with washing buffer (50 mM Tris pH 7.5, 150 mM NaCl, 5% glycerol (w/v), 1% Triton X-100) followed by one time with the yeast lysis buffer (20 mM Hepes pH 7.5, 150 mM KOAc, 1% NP-40, 5% glycerol, 1 mg/ml Pefabloc SC (Roche), and EDTA-free protease inhibitor cocktail (cOmplete Tablets, Roche)). Subsequently, 300 µl of the yeast lysate containing Nup159-6HA was mixed with 700 µl yeast lysis buffer and added to the resin (2.5 h, 4 °C rotary wheel). The resin was washed three times with yeast lysis buffer and the supernatant was in the final step removed with a 27g needle. The bound proteins were denatured by addition of 50 µl HU loading buffer and incubation at 65 °C for 10 min.

2.4.6 Fluorescence Microscopy

For fluorescence microscopy yeast cells were grown in SC-medium supplemented with all essential amino acids and 2% glucose. The next day cells were diluted to OD₆₀₀ 0.1 and grown till mid-log phase (0.5-0.8 OD₆₀₀) before imaged. Microscopy slides were pre-treated with 1 mg/ml Concanavalin A (ConA) solution. The widefield imaging was performed at the Imaging Facility of the Max Planck Institute of Biochemistry (MPIB-IF) on a GE DeltaVision Elite system based on an OLYMPUS IX-71 inverted microscope, an OLYMPUS (100X/1.40 UPLSAPO and 60X/1.42 PLAPON) objective and a PCO sCMOS 5.5 camera. Images were deconvolved using the softWoRx® Software (methode: additive enhanced, 20 iterations). Image analysis was performed using ImageJ (<https://imagej.nih.gov/ij/>).

2. MATERIALS AND EXPERIMENTAL METHODS

2.4.7 Microfluidics Experiments

Microfluidics experiments were performed on a CellASIC® ONIX microfluidic platform (Merck) with the CellASIC® ONIX microfluidic plates for haploid yeast cells. Cells were loaded from a logarithmic growing culture (OD_{600} 0.5-0.8) according to manufacturer's manual and imaged in 1 h intervals over a time course of 24 h. At each position for each time point a z-stack was recorded (300 nm). Imaging was performed with a constant media flow rate of 1 psi. To rapidly switch media, flow rate was set to 5 psi for 5 min and then switched back to a flow rate of 1 psi. Cells were initially cultured for 2 h in low fluorescence synthetic growth medium and then switch to SD-N medium for 24 h. The microscope used was the same as described in the Fluorescence microscopy section. Quantification of nuclear signal was performed using the software ImageJ (<https://imagej.nih.gov/ij/>), complemented with all the default plugins provided by FIJI (<https://fiji.sc>) and the additional ones provided by the ImageScience update site. Each frame in the time-lapse movies following the variation of the signal over time was preprocessed independently to determine the location and size of nuclei in the field of view. Their segmentation was achieved by first applying a Laplacian of Gaussian filter, then using the Otsu threshold method to transform the images in binary maps. Finally, nuclei boundaries were rounded by morphological opening. Once the location and the extension of nuclei were determined, an interactive script allowed the user to select the same nuclei at different time frames and to extract the corresponding average intensity and volume.

2.4.8 Correlative Light and Electron Microscopy (CLEM)

CLEM analysis was conducted as previously described (Kukulski et al., 2011). *S. cerevisiae* cells were grown in YPD to OD_{600} 1.0, washed two times with SD-N medium and subsequently resuspended in SD-N medium. After incubation in SD-N medium for 24 h the strain was high pressure frozen (HPM010, AbraFluid) and freeze substituted (EM-AFS2, Leica) with 0.1% uranyl acetate in acetone for 72 h at -90 °C. The temperature was then raised to -45 °C at 3 °C /h and samples were further incubated for 5 h. After rinsing in acetone, the samples were infiltrated in Lowicryl HM20 and the resin was polymerized under UV light. 300 nm sections were cut with a microtome (EM UC7,

2. MATERIALS AND EXPERIMENTAL METHODS

Leica) and placed on carbon coated 200 mesh copper grids (S160, Plano). The fluorescence microscopy (FM) imaging of the sections was carried out as previously described using a widefield fluorescence microscope (Olympus IX81) equipped with an Olympus PlanApo 100X 1.40 NA oil immersion objective and a CCD camera (Orca-ER; Hamamatsu Photonics). After fluorescence imaging, grids were post-stained with uranyl acetate and lead citrate. Tilt series of the cells of interest were acquired semi-automatically on a Tecnai F30 (Thermofisher, FEI) at 300 kV using Serial-EM (Mastronarde, 2005). Tomograms were reconstructed and manually segmented using IMOD (Kremer et al., 1996). Overlays of fluorescence spots and tomograms were performed with ec-CLEM Plugin (Paul-Gilloteaux et al., 2017) in ICY (de Chaumont et al., 2012) by clicking manually on corresponding pairs of notable features in the two imaging modalities.

2.4.9 Antibodies

Monoclonal antibodies against HA-epitope (clone F-7) and EGFP (clone B-2) were purchased from Santa Cruz Biotechnology, Dpm1 (clone 5C5A7) and Pgk1 antibodies (clone 22C5D8) were from Invitrogen, Nsp1 antibody (32D6 catalogue ab4641) was from Abcam, and Nup98 antibody (2H10) was from BioAcademia. Polyclonal antibody against Nup84 (SAB2501815) was from Sigma. Mouse monoclonal anti- β -galactosidase antibody (Z378A) was purchased from Promega.

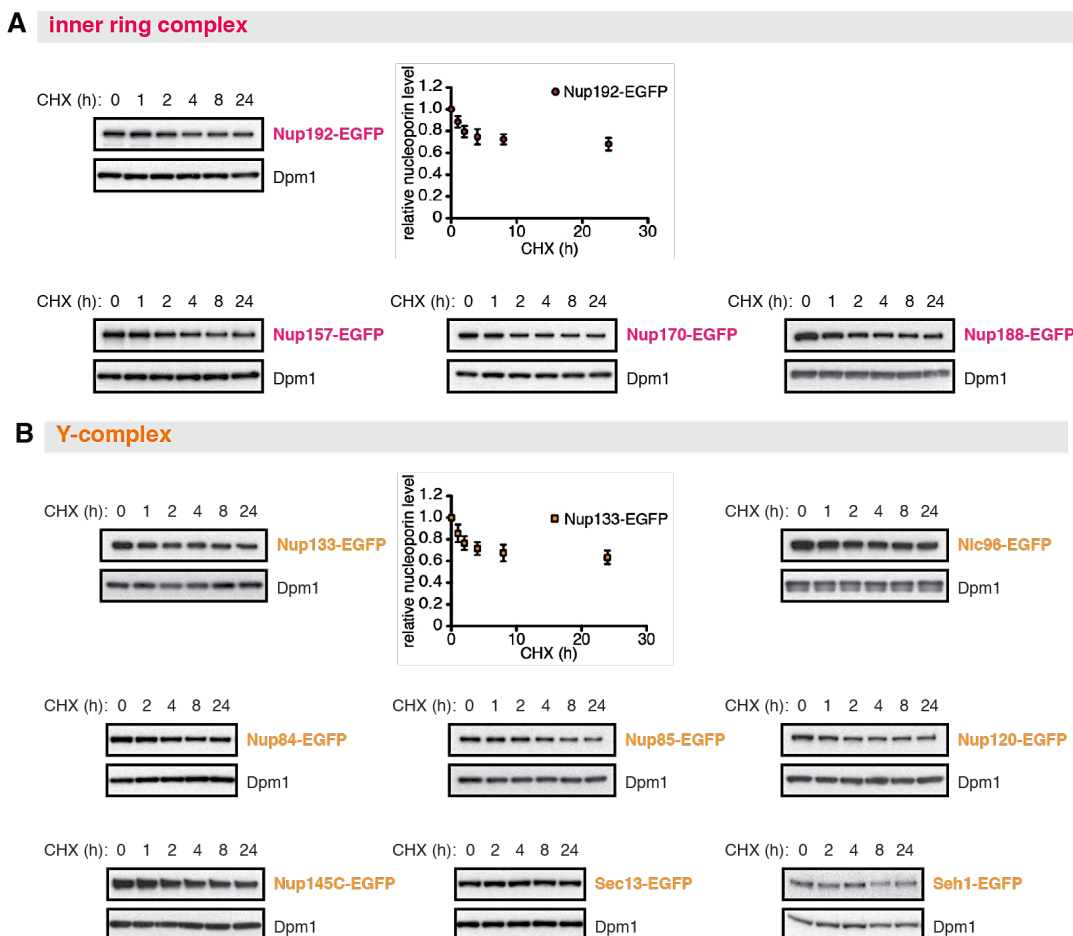
2.4.10 Statistics and Reproducibility

Representative results of at least two independent experiments were presented in all figure panels. P-value for all graphs were generated with the two-tailed Student's t test as indicated in the figure legends and as followed: NS: $P \geq 0.05$; *: $P \leq 0.05$; **: $P \leq 0.005$; ***: $P \leq 0.001$. All error bars represent standard deviation form mean.

3 Results

3.1 Nucleoporins in *S. cerevisiae* are Long-lived

In this study the budding yeast *Saccharomyces cerevisiae* was used as a simple and genetically tractable eukaryotic model organism to study mechanisms of NPC turnover. Since previous reports demonstrated in mouse brains that the integral parts of the NPC exhibit an extremely long half-life (Savas et al., 2012; Toyama et al., 2013), it was unknown if yeast NPCs are also stable. To determine Nups stability, cells expressing the yeast homologues of both mammalian IR and Y-complexes were endogenously tagged with EGFP and subsequently treated with cycloheximide, which prevents protein biosynthesis by blocking translation elongation. Indeed, the integral parts of the yeast NPC are long-lived with half-lives exceeding the generation time by several fold (Figures 3.1A and 3.1B).



(For figure legend, see next page.)

3. RESULTS

Figure 3.1: The integral parts of yeast NPC are stable.

(A and B) Degradation of inner-ring nucleoporins (Nup157-EGFP, Nup170-EGFP, Nup188-EGFP and Nup192-EGFP (A)) and outer-ring nucleoporins (Nic96-EGFP, Nup84-GFP, Nup85-EGFP, Nup120-EGFP, Nup133-EGFP, Nup145C-EGFP, Sec13-EGFP and Seh1-EGFP (B)) was measured after cycloheximide-block (CHX; 80 µg/ml) of translation by anti-GFP immunoblotting. Dpm1 serves as control. Quantification from (n=3) experiments are shown as mean ± s.d..

3.2 Identification of Triggers of NPC Degradation

Given that the scaffold of NPC is extremely stable with limited turnover over the lifespan of budding yeast (Figures 3.1A and 3.1B), a drug screen was embarked for conditions that convert the scaffold Nups from long-lived to short-lived. Under both nitrogen deprivation and canavanine treatment, the degradation of Nup192, a core-scaffolding component of the NPC inner ring, could be triggered (Figure 3.2). Nevertheless, canavanine, an arginine analogue incorporated into every arginine residue of proteins, is lacking specificity and results in misfolding of a broad range of proteins. This can lead to pleiotropic effects that are hard to interpret such as misfolding of Nups and therefore reduced incorporation. In contrast, nitrogen starvation triggers accelerated protein turnover in order to restore intracellular amino acid homeostasis, mainly by up-regulation of autophagy (Mizushima et al., 2011; Wen and Klionsky, 2016). Therefore, I decided to investigate the degradation of Nups under nitrogen starvation.

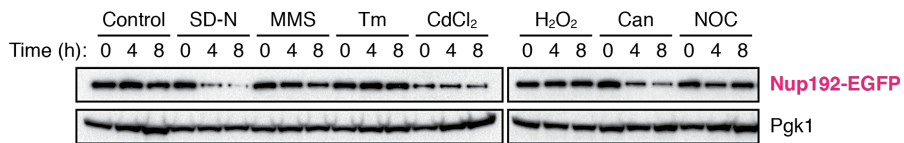


Figure 3.2: Nitrogen starvation and canavanine treatment trigger NPC scaffold proteins degradation.
Nup192-EGFP-tagged cells were treated with nitrogen starvation medium (SD-N), methyl methanesulfonate (MMS, DNA damage inducer, 0.05 %), tunicamycin (Tm, ER-stress inducer, 0.5 µM), cadmium chloride (CdCl₂, oxidative stress inducer, 30 µM), hydrogen peroxide (H₂O₂, oxidative stress inducer, 2 mM), canavanine (Can, unfolded protein response, 5 µg/ml) or nocodazole (NOC, cell cycle arrest, 15 µg/ml) for indicated times. Pgk1 serves as control.

3. RESULTS

To test if other Nups of the NPC are also degraded, different members of the NPC scaffold were tagged endogenously with EGFP and their degradation was monitored specifically under conditions of nitrogen starvation. Notably, the protein levels of individual scaffold Nups were markedly decreased after nitrogen deprivation and concomitantly an accumulation of stable EGFP fragments, released from full-length EGFP-tagged scaffold Nup, was detected (Figures 3.3A and 3.3B). This appearance of free EGFP indicates degradation of these proteins inside the vacuole, since the compact fold of EGFP renders it resistant towards the degradation by vacuolar hydrolases (Cheong et al., 2008).

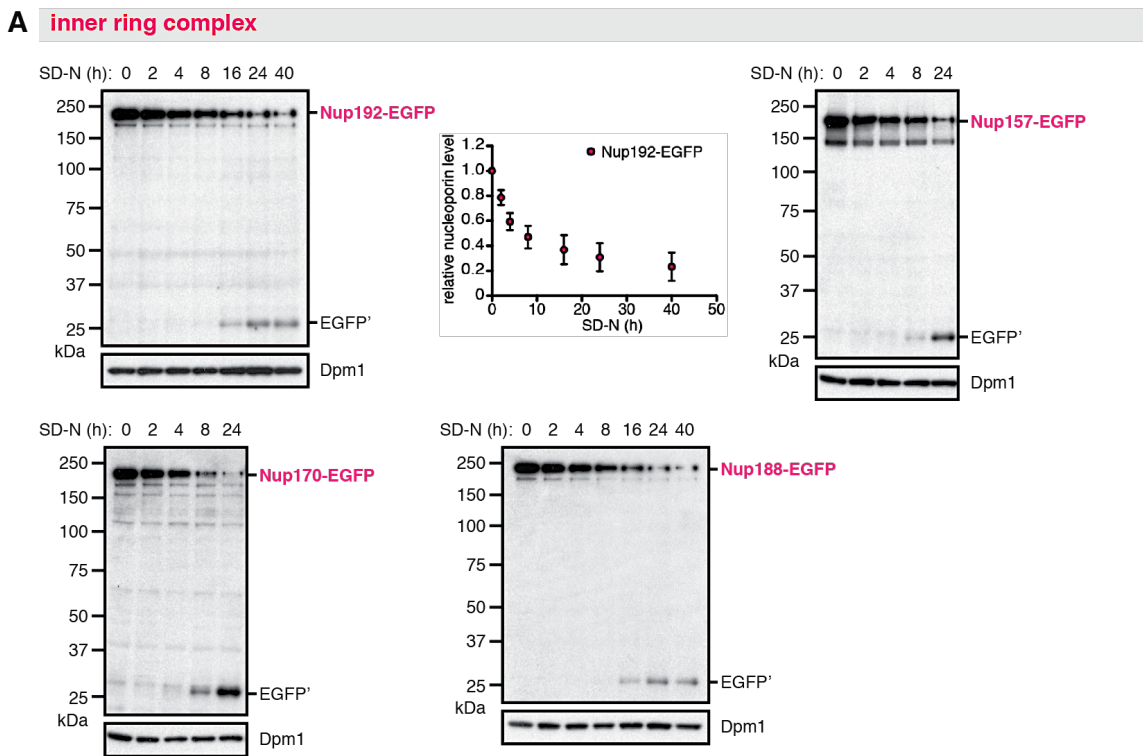


Figure 3.3: Nitrogen starvation and canavanine treatment trigger NPC scaffold proteins degradation.
 (A) Degradation of inner-ring nucleoporins (Nup157-EGFP, Nup170-EGFP, Nup188-EGFP and Nup192-EGFP) was measured upon nitrogen starvation (SD-N) by anti-EGFP immunoblotting. EGFP' denotes vacuolar EGFP remnant. Dpm1 serves as loading control. Right: quantification from (n=3) experiments is shown as mean \pm s.d.

In accordance, simultaneous deletion of *PEP4* and *PRB1*, two genes encoding critical vacuolar resident proteases, attenuated the production of free EGFP and stabilized the

3. RESULTS

full-length EGFP-tagged Nups (Figure 3.4), suggesting that NPC are partially degraded within the vacuole.

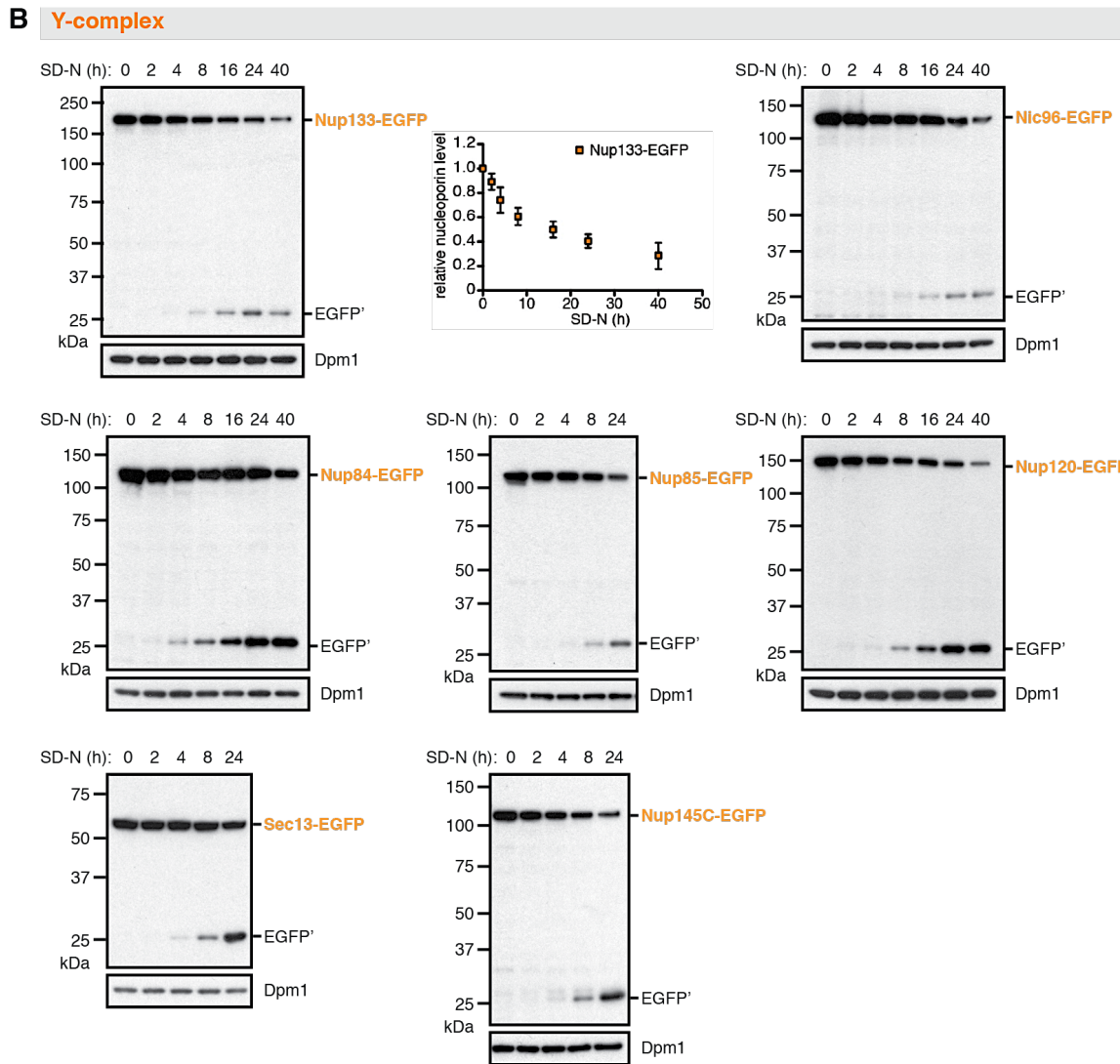


Figure 3.3: Nitrogen starvation and canavanine treatment trigger NPC scaffold proteins degradation.
(B) Degradation of outer-ring nucleoporins (Nic96-EGFP, Nup84-GFP, Nup85-EGFP, Nup120-EGFP, Nup133-EGFP, Nup145C-EGFP and Sec13-EGFP) was measured upon nitrogen starvation (SD-N) by anti-EGFP immunoblotting. EGFP' denotes vacuolar EGFP remnant. Dpm1 serves as loading control. Right: quantification from (n=3) experiments is shown as mean ± s.d.

Nitrogen starvation is a physiological condition under which protein turnover is strongly accelerated to restore intracellular amino acid homeostasis by inhibition of the

3. RESULTS

TORC1 complex. Consistent with this, NPC turnover was also observed when cells were treated with rapamycin, an inhibitor of the TORC1 complex. In contrast, glucose starvation does not (Figures 3.5A and 3.5B) lead to NPC degradation. Taken together, these data demonstrate that NPC turnover is activated upon nutrient restriction.

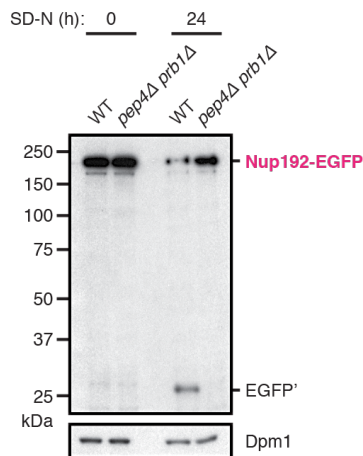


Figure 3.4: Vacuolar turnover of NPC scaffold proteins upon nitrogen starvation.

Analysis of Nup192-EGFP degradation in nitrogen-starved *wildtype* and vacuolar proteases-deficient (*pep4Δ prb1Δ*) cells by anti-EGFP immunoblotting. Dpm1 was used as loading control.

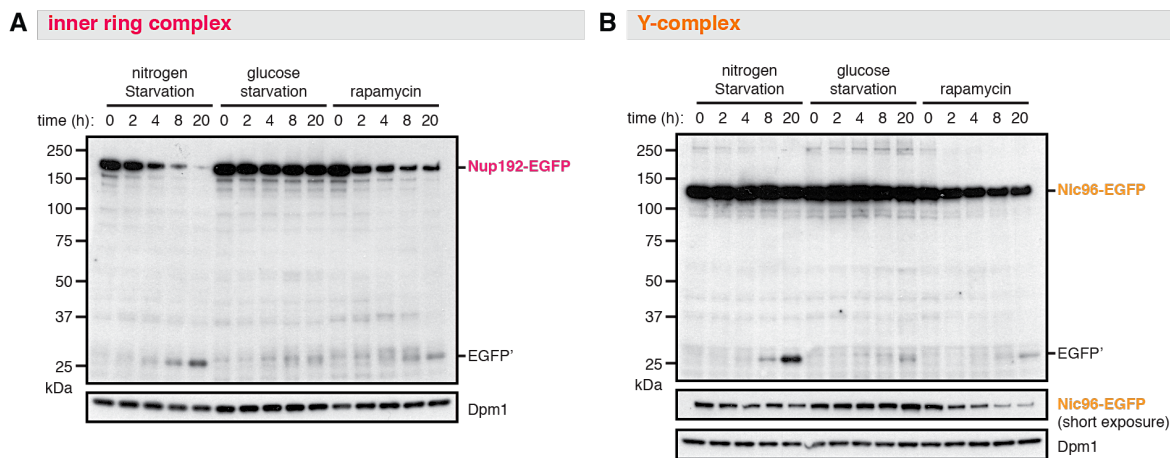


Figure 3.5: NPC scaffold proteins are degraded upon nitrogen starvation and mTOR inhibition.

(A and B) Nup192-EGFP-tagged (A) and Nic96-EGFP-tagged (B) cells were subjected to nitrogen starvation (SD-N), glucose starvation (YPD medium lacking glucose), or rapamycin treatment (12 nM) for indicated times. The Nup192-EGFP and Nic96-EGFP western blots illustrate that nitrogen starvation or rapamycin treatment, but not glucose starvation induces a drop in Nup192-EGFP and Nic96-EGFP levels. Dpm1 serves as control.

3. RESULTS

3.3 Involvement of ESCRT and Proteasome in NPC Degradation

Previous work has shown that NPC assembly is under surveillance by the ESCRT–III/Vps4 complex and that defective assembly intermediates are eliminated in a proteasome-dependent manner (Webster et al., 2014). Indeed, nucleoporins are stabilized upon nitrogen starvation when ESCRT function is impaired by a *VPS4* deletion (Figure 3.6, see also Figure 3.7 for more ESCRT mutants) or when proteasome function is impaired by deletion of the proteasomal ubiquitin receptor *RPN10* (Figure 3.6, the stabilization of proteasome model substrate Ub- β gal in *rpn10* Δ cells was provided as a control of impaired proteasome activity). This stabilization was specific for deletion of *RPN10* since genetic ablation of other ubiquitin-proteasome receptors exhibited no stabilization of Nup192-EGFP levels (Figure 3.8). Notably, in the *rpn10* Δ strain a considerable fraction of Nup192-EGFP was still degraded upon starvation and the appearance of free EGFP indicated an additional degradation pathway via the vacuole (Figure 3.6).

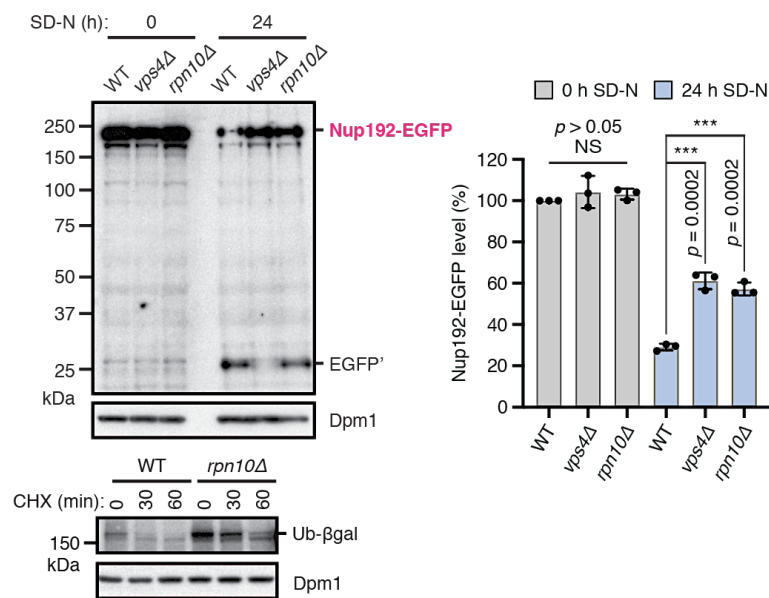


Figure 3.6: Involvement of ESCRT-III/Vps4 and proteasome in the degradation of nucleoporins.

Degradation of Nup192-EGFP in wildtype, ESCRT-deficient (*vps4* Δ) and proteasome mutants (*rpn10* Δ) with quantification (shown as mean \pm s.d. (n=3), ***p \leq 0.005, two-tailed Student's t-Test) of Nup192-EGFP levels before and after 24h of nitrogen starvation. The Ub- β gal proteasome model substrate is stabilized in *rpn10* Δ cells upon cyclohexamide treatment (80 μ g/ml). Dpm1 serves as loading control.

3. RESULTS

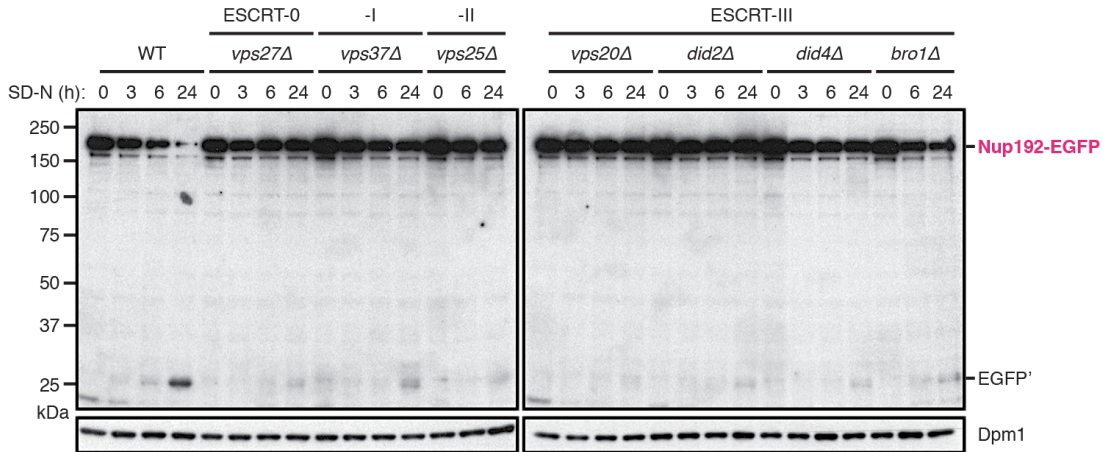


Figure 3.7: ESCRT machinery is required for starvation-induced nucleoporins turnover.

Starvation-induced Nup192-EGFP degradation was measured by immunoblotting for indicated time in *wildtype* and mutants cells, deficient in ESCRT-0 (*vps27Δ*), ESCRT-I (*vps37Δ*), ESCRT-II (*vps25Δ*), or ESCRT-III (*vps20Δ, did2Δ, did4Δ* and *bro1Δ*) modules. Dpm1 serves as loading control.

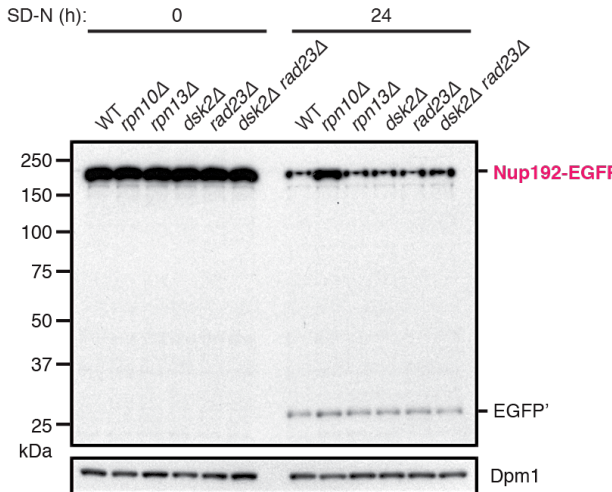


Figure 3.8: Rpn10 functions as a specific receptor for degradation of the nucleoporins under nutrient starvation.

Degradation of Nup192-EGFP upon nitrogen starvation as in Figure 3.6, but in different proteasomal ubiquitin receptor mutants (*rpn10Δ, rpn13Δ, rad23Δ, dsk2Δ, rad23Δ dsk2Δ*). Dpm1 was used as loading control.

3.4 Multiple Pathways are Involved in Starvation-induced NPC Degradation

Since nitrogen deprivation leads to rapid activation of the autophagy machinery, it is reasonable to hypothesize that autophagy could be a mechanism for NPC degradation. To address this, a deletion of the core autophagy protein Atg8 was introduced and the degradation of Nup192-EGFP upon nitrogen starvation was compared to the degradation

3. RESULTS

in the *rpn10Δ* strain. Notably, a comparable level of stabilized Nup192-EGFP after starvation was observed in both *atg8Δ* and *rpn10Δ* strains, albeit a significant amount of Nup192-EGFP was still degraded (Figure 3.9). Concurrently, the appearance of free EGFP was entirely blocked in the *ATG8* deletion mutant, suggesting that the pool of Nup192-EGFP degraded in the vacuole was dependent on the autophagy machinery. Similar results were obtained for the deletion of other core autophagy genes (*ATG1*, *ATG3*, *ATG4*, *ATG5*, *ATG6*, and *ATG7*) (Figure 3.10). Only when both degradative pathways were impaired in a *rpn10Δ atg8Δ* double mutant, the levels of Nup192-EGFP were completely stabilized (Figure 3.9).

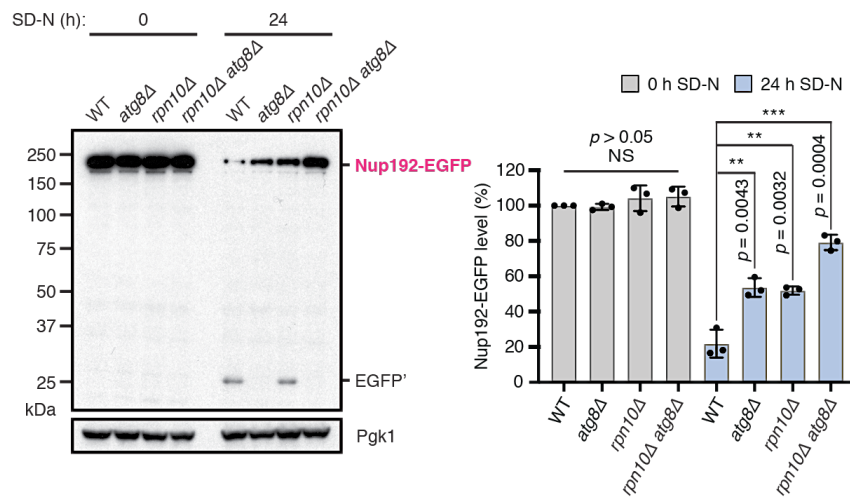


Figure 3.9: Scaffold Nups are degraded upon nitrogen starvation by both autophagy and proteasome. Degradation of Nup192-EGFP in *wildtype*, autophagy-deficient (*atg8Δ*) and proteasome mutants (*rpn10Δ*) as well as in *atg8Δ rpn10Δ* double mutants with quantification (shown as mean \pm s.d. (n=3), *** $p \leq 0.005$, two-tailed Student's t-Test) of Nup192-EGFP levels before and after 24h of nitrogen starvation. Pgk1 serves as loading control.

However, when proteasome function was impaired by other means either by using a temperature sensitive mutant *cim3-1* or by chemical inhibition with MG132, I found that after starvation not only the levels of Nup192-EGFP were preserved but also the accumulation of cleaved EGFP was strongly decreased (Figures 3.11A and 3.11B). Similar results were also obtained for the *yps4Δ* mutant as well as other ESCRT mutants (Figures 3.6 and 3.7). This suggested to me that autophagy might be impaired under these

3. RESULTS

conditions. In accordance, both *cim3-1* as well as *vps4Δ* mutant cells showed a strong impairment of autophagy flux, as judged by the reduced degradation of EGFP-Atg8 and the appearance of free EGFP (Figure 3.12). It is likely that cross-regulation between these degradative pathways exists which has secondary effects on autophagy. This is interesting and warrants further examination. From those findings, I conclude that the turnover of the scaffold Nup192 is dependent on at least two pathways, which involve degradation by the proteasome and autophagy, respectively.

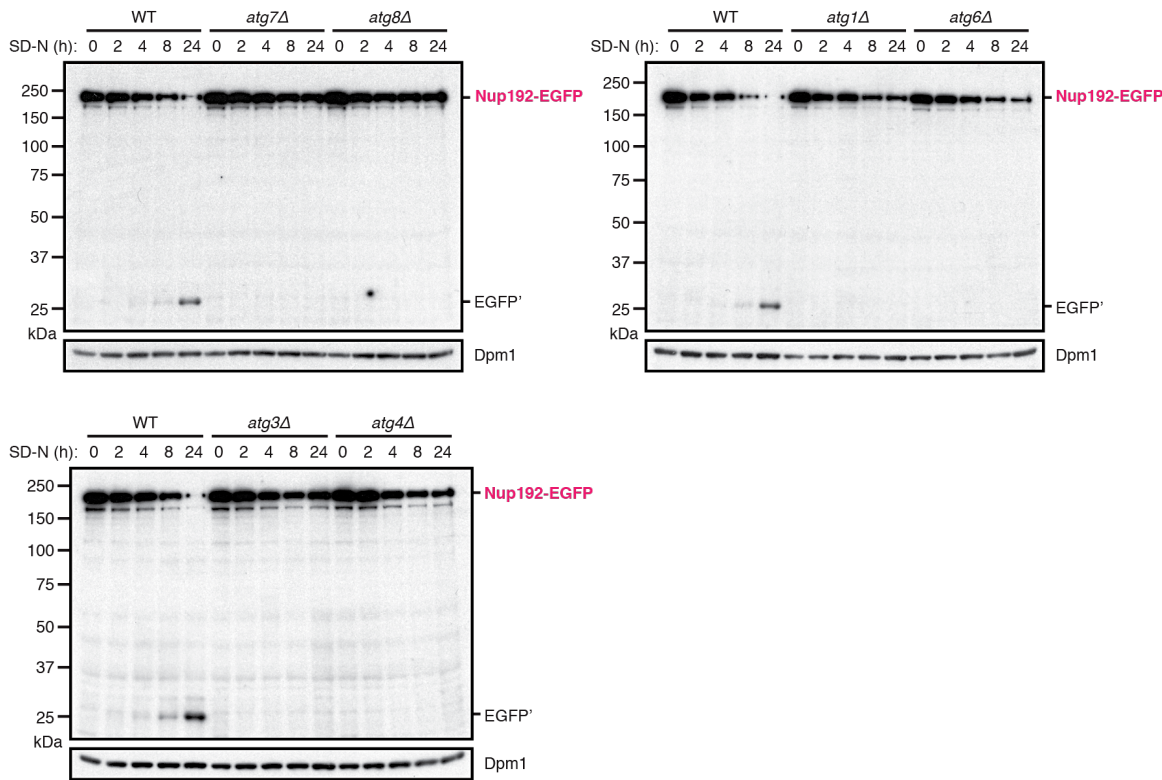


Figure 3.10: Genetic links between NPC degradation and the core autophagy machinery.

Starvation-induced Nup192-EGFP degradation was measured as in Figure 3.7, but in *atg7Δ*, *atg8Δ*, *atg1Δ*, *atg6Δ*, *atg3Δ* and *atg4Δ* cells deficient in the core autophagy machinery. Autophagy-deficient cells do not show appearance of the free EGFP band and lead to stabilization of Nup192-EGFP. Dpm1 serves as loading control.

3. RESULTS

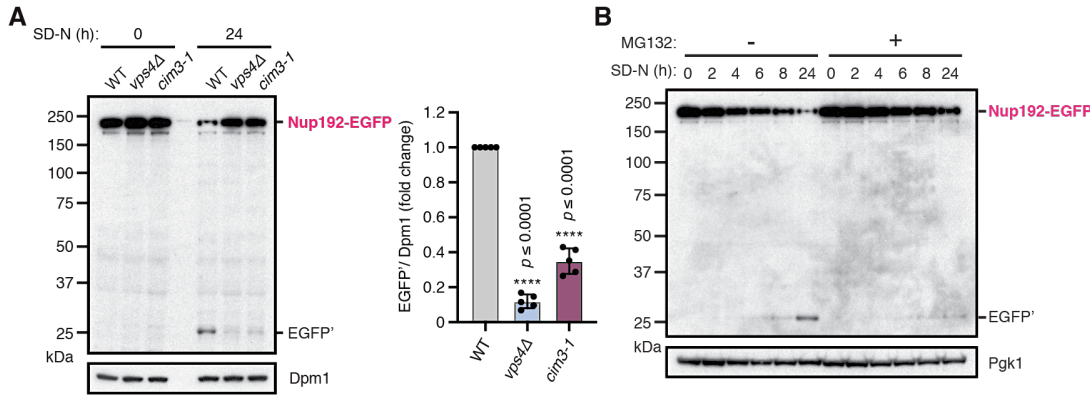


Figure 3.11: Functional impairment of proteasome or ESCRT affects autophagy-mediated NPC degradation.

(A) Degradation of Nup192-EGFP upon nitrogen starvation was measured in *wildtype* and mutants cells, deficient in ESCRT (*vps4Δ*) or proteasome (*cim3-1*) as in Figure 3.6. Quantification from (n=3) experiments are shown as mean \pm s.d.. Dpm1 serves as loading control.

(B) Starvation-induced Nup192-EGFP degradation in *pdr5Δ* cells, which were treated with or without proteasome inhibitor MG132 (100 μ M), was measured as in Figure 3.7. Pdr5, a multi-drug transporter constituent, was deleted to enhance efficacy of MG132.

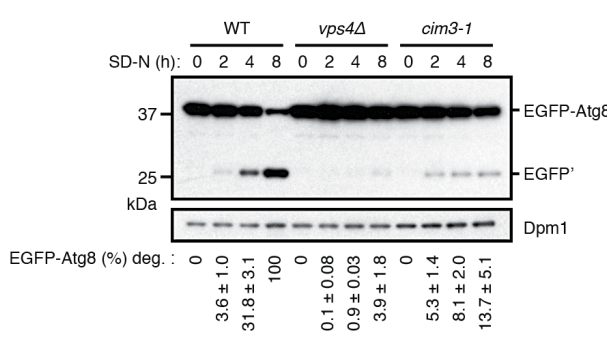


Figure 3.12: Monitoring of autophagy flux in both proteasome and ESCRT mutants.

Atg8-degradation and vacuolar cleavage of EGFP-Atg8 was measured by immunoblotting in *wildtype*, *vps4Δ*, and *cim3-1* mutant cells before and after induction of autophagy by nitrogen starvation. Quantification from (n=3) experiments are shown as mean \pm s.d.. Dpm1 serves as loading control.

3. RESULTS

3.5 Nuclear Envelope-embedded NPCs are Degraded in the Vacuole via the Core Autophagy Machinery

The results that all scaffold Nups are degraded via autophagy suggests degradation of membrane-embedded NPCs rather than single Nups. To test this idea, other Nups from different subcomplexes were tagged endogenously with EGFP and their degradation was monitored upon nitrogen starvation. Remarkably, all tested Nups, including the membrane-embedded Pom152, were subjected to autophagosomal turnover, as judged by stabilization of individual Nup-EGFP fusion proteins in the *ATG8* deletion background (Figure 3.13).

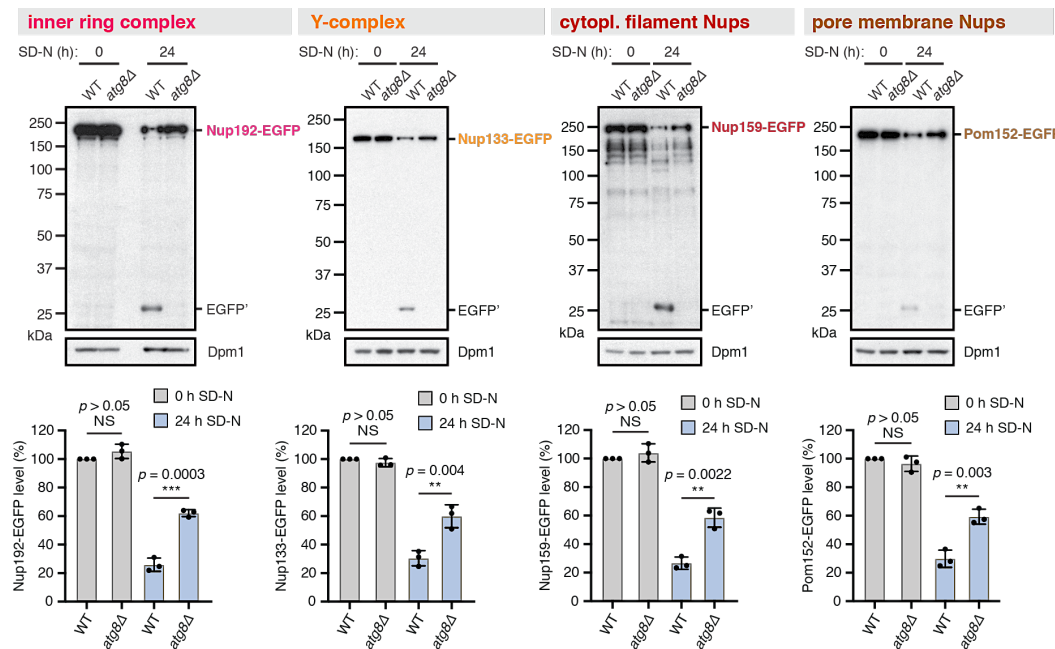


Figure 3.13: Nups from different subcomplexes are degraded upon nitrogen starvation via autophagy. Degradation of different Nup-EGFP fusion proteins from different subcomplexes in *wildtype* and mutant cells deficient in the core autophagy machinery (*atg8Δ*) upon starvation measured as in Figure 3.6. Dpm1 serves as loading control.

Moreover, examining the fluorescence signal of scaffold Nup-EGFP tagged cells in the absence of the core autophagy machinery revealed a strong displacement of both Nup192 and Nup120 on the nuclear envelope when cells were starved of nitrogen (Figures 3.14A and 3.14B). Specifically, Nup192 stained the entire nuclear envelope, giving it a shrivelled appearance, which could be clearly observed in more than 60% of

3. RESULTS

the cells starved for 24 h. However, such a phenotype renders the quantification of Nup levels at the NE more difficult. Therefore, a trackable system should be applied for measuring the nuclear volume and the fluorescence signal simultaneously over time.

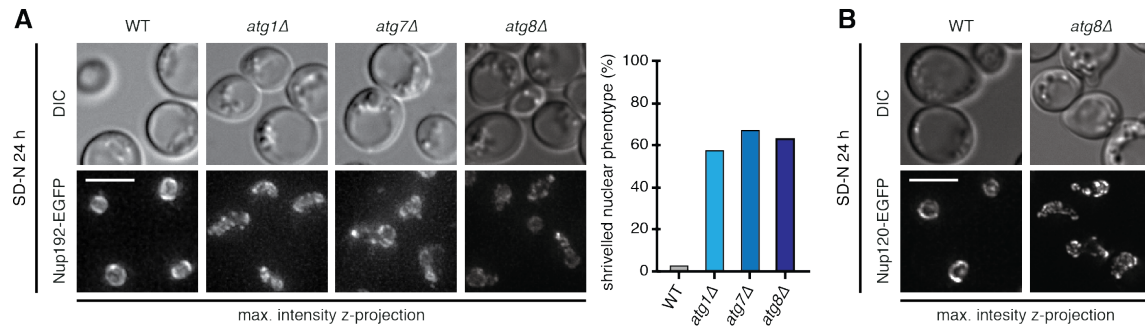


Figure 3.14: Autophagy deficiency leads NPCs displacement on nuclear envelope upon nitrogen deprivation.

(A and B) Fluorescence microscopy images of EGFP-tagged Nup192 (A) and Nup120 (B) cells compared to different mutant strains (*atg1Δ*, *atg7Δ* and *atg8Δ*) after 24h of nitrogen deprivation (representative of at least 300 cells). Quantification of cells with “shriveled” Nup192-EGFP appearance (300 cells were quantified per condition), scale bar, 5 μ m.

In order to quantify Nup levels, especially for the nuclear membrane-associated pool, cells were trapped in a microfluidics device and fluorescence signal of Nup192-EGFP at the nuclear envelope was monitored in single cells before and after starvation. The volume of the nucleus largely increased in cells deficient for Atg8 (*atg8Δ*) as compared to *wildtype* cells when switched to media lacking nitrogen (Figure 3.15). Conversely, the overall levels of membrane-associated Nup192-EGFP decreased during starvation, but remained constant in *atg8Δ* cells (Figure 3.15).

Recruitment of autophagic substrates is mainly mediated by the interaction with the ubiquitin-like protein Atg8, which is anchored to the autophagosomal membrane by conjugation to the lipid phosphatidylethanolamine. To foster the idea of autophagic turnover of membrane-embedded NPCs, the interactome of Atg8 was determined by immunoprecipitation of EGFP-Atg8 followed by quantitative mass spectrometry (qMS) from nitrogen starved *pep4Δ* cells. Among the statistically significant enriched proteins, various Nups, including all scaffold components of the inner ring, the Y-complex, the cytoplasmically exposed Nup82 complex, three members of the transmembrane Nups

3. RESULTS

(Pom34, Pom152 and Ndc1), as well as the strong membrane-associated Nup53 were identified (Figure 3.16A). Subsequent analysis of EGFP-Atg8 immunoprecipitates by Western blotting confirmed these results (Figure 3.16B). Furthermore, this interaction of Atg8 with Nups was observed even without starvation when Atg8 was overexpressed (Figure 3.16C).

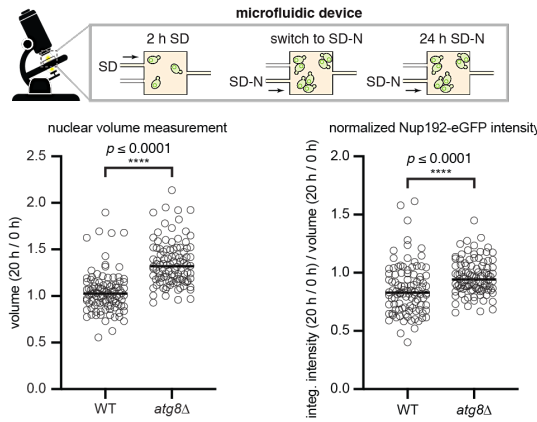
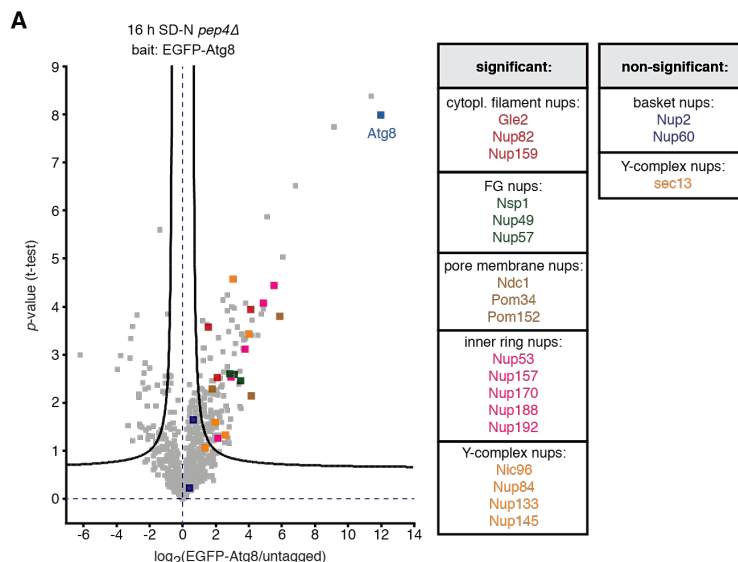


Figure 3.15: Single-cell tracking for membrane-embedded NPC levels quantification.

Quantitative analysis of Nup192-EGFP fluorescence signal and nuclear volume before and after nitrogen starvation. *Wildtype* or *atg8Δ* mutant cells expressing Nup192-EGFP were trapped in a microfluidic device and incubated for two hours with regular growth media before the buffer stream was changed and cells were incubated with medium lacking any nitrogen source (SD-N) for 24 hours. Every hour a z-stack for the Nup192-EGFP signal was recorded. The nuclear volume and the Nup192-EGFP intensity within this volume were followed in individual cells (total at least 100 cells) before and after 24 hours of SD-N treatment. ***p ≤ 0.0001, two-tailed Student's t-Test.



(Figure continued on next page, legend follows.)

3. RESULTS

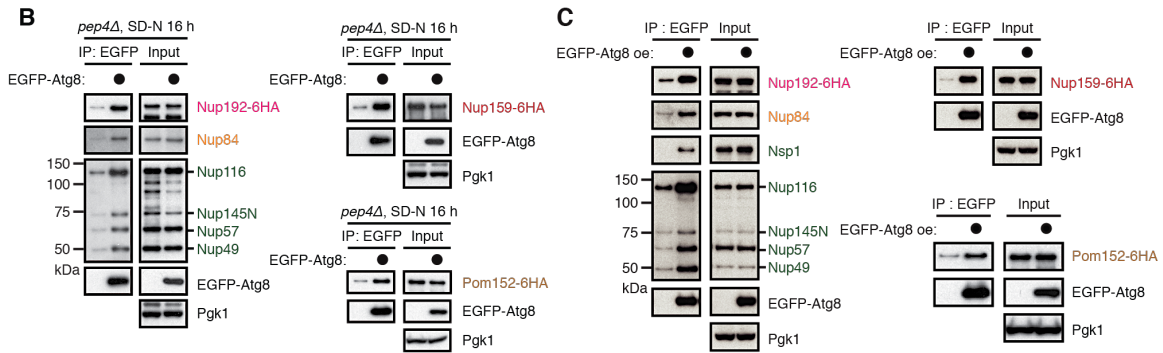


Figure 3.16: qMS identified nucleoporins as autophagosomal substrates.

(A) Volcano plot visualization ($n=4$) of quantitative mass spectrometric analysis of Atg8-interacting proteins determined by EGFP-Atg8 Co-IP under nitrogen starvation conditions. *pep4 Δ* cells expressing N-terminally EGFP-tagged or untagged Atg8 under control of ADH-promoter were subjected to nitrogen starvation for 16h before immunoprecipitation with EGFP-Trap matrix. Depicted are logarithmic ratios of protein intensities against negative logarithmic p-values of t test performed from quadruplicates. The hyperbolic curve separates specifically interacting proteins from background (square) (FDR: 0.05, S0: 0.5). The bait protein Atg8 and different Nups are highlighted in the respective color and sorted by quality of enrichment.

(B) Validation of Nup-Atg8 interactions identified in (A) by Co-IP followed by Western blot with anti-EGFP, anti-Nup98 (reacts multiple FG-nucleoporins), anti-Nup84, and anti-HA (recognizes Nup192-HA (left), Nup159-HA (right, upper) and Pom152-6HA (right, lower)) antibodies.

(C) EGFP-Atg8 interacting proteins were measured by EGFP-Atg8 Co-IP as in (B), with EGFP-Atg8 under control of the ADH promoter. For this analysis cells with tagged Nup159-6HA (upper right panel), Pom152-6HA (bottom right panel) or Nup192-6HA (left panel) were subjected to immunoprecipitation with EGFP-Trap matrix. Immunoprecipitates were probed with antibodies against EGFP tag, HA tag, Nup84, Nup98 (multiple FG-nucleoporins), Nsp1 and Pgk1 as control.

To visualize intermediates of autophagosomal NPC degradation, starvation was induced in a strain in which the vacuolar lipase *ATG15* was deleted. Atg15 is indispensable for digesting autophagosomal membranes in the vacuolar lumen (Epple et al., 2001). Under these conditions, Nup192-EGFP-containing structures trapped inside the vacuole could be observed, most likely resembling autophagosomes (Figure 3.17A). Moreover, these vacuolar structures, not only contained Nup192-EGFP, but also colocalized with different Nups from other subcomplexes such as outer scaffold Nup84-mars, cytoplasmic filament Nup159-mars and, importantly, transmembrane Nup Ndc1-mars (Figure 3.17B), indicating that indeed membrane-embedded NPCs are targeted by

3. RESULTS

the autophagy machinery. Furthermore, appearance of the Nup192-EGFP foci inside the vacuole was entirely dependent on the presence of Atg8, validating that Nups are degraded by autophagy upon nitrogen starvation (Figure 3.17C).

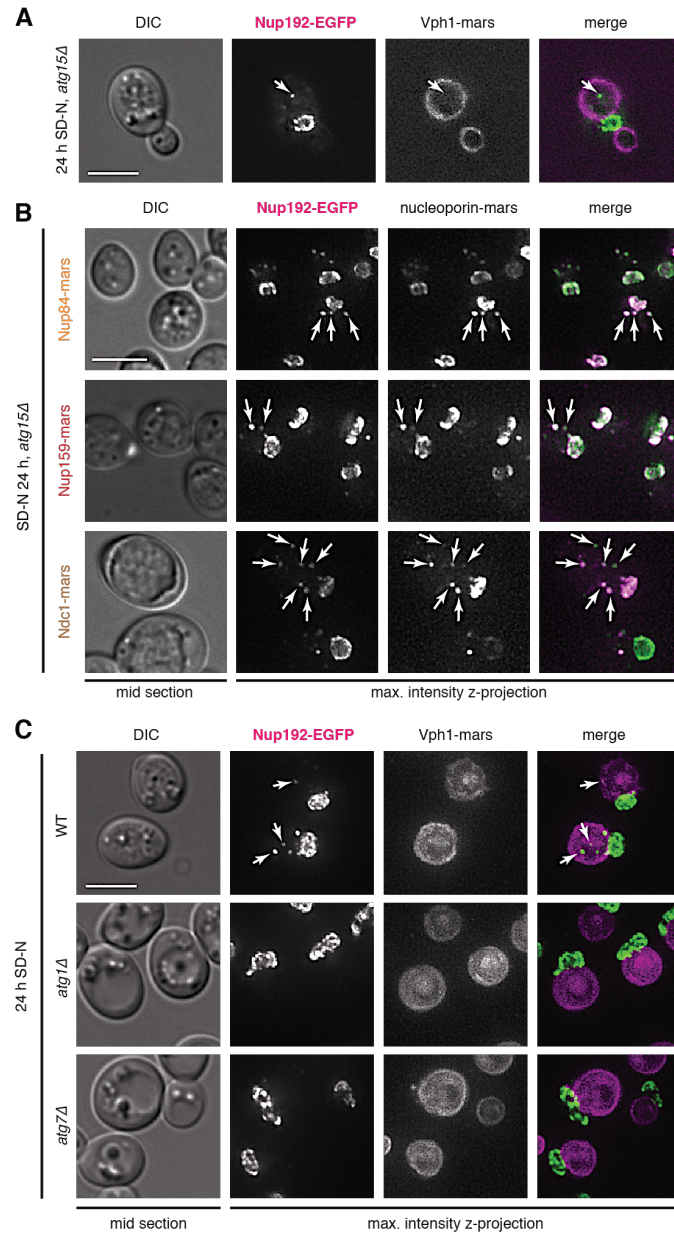


Figure 3.17: Vacuolar accumulation of Nups-containing autophagosomes in *atg15Δ* cells after nitrogen deprivation.

(A) EGFP-tagged Nup192 accumulates in the vacuole in the absence of the vacuolar lipase Atg15. Representative midsection image of the localization of C-terminally EGFP-tagged Nup192 in Atg15-deficient (*atg15Δ*) cells was measured by fluorescence microscopy after 24 hours of nitrogen starvation. Vph1-mars served as marker for the vacuolar membrane. Arrows indicate autophagic bodies within the vacuole. Scale bar, 5 μm.

(Legend continued on next page.)

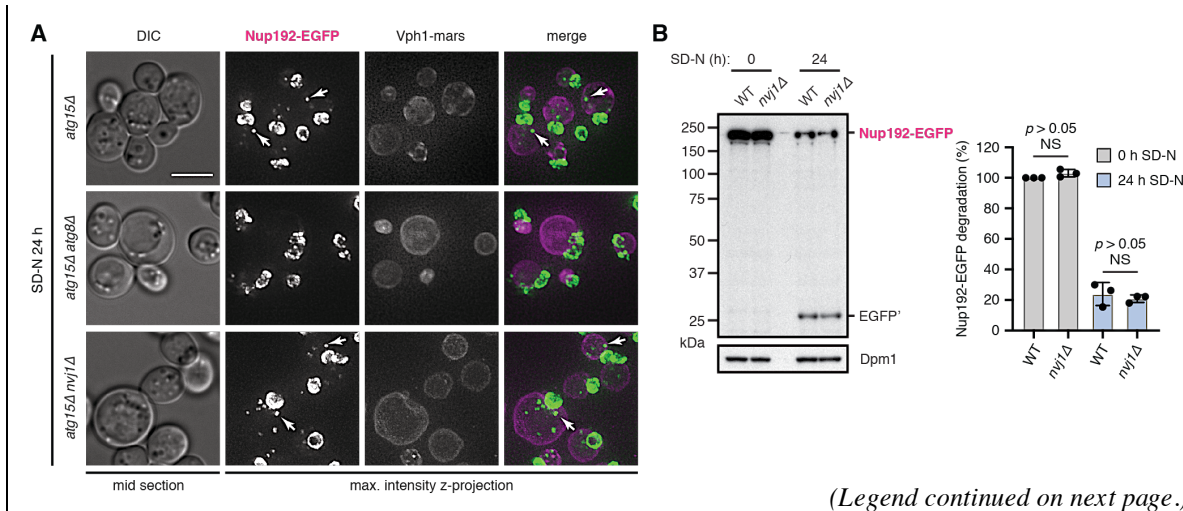
3. RESULTS

(Figure 3.17, legend continued from last page.)

- (B) In the absence of the vacuolar lipase Atg15, colocalization of EGFP-tagged Nup192 with outer scaffold Nup84-mars, cytoplasmic filament Nup159-mars and transmembrane (Pom) Nup Ndc1-mars can be observed in focus like accumulations, resembling vacuole-engulfed autophagosomes. Arrows indicate autophagic bodies within the vacuole. Scale bar, 5 μ m.
- (C) Focal accumulations are dependent on core autophagy machinery proteins as monitored by Nup192-EGFP staining in *wildtype*, *atg1 Δ* and *atg7 Δ* cells. Arrows indicate autophagic bodies within the vacuole. Scale bar, 5 μ m. Vph1-mars served as marker for the vacuolar membrane.

3.6 The Core Autophagy Machinery is Crucial for NPC Degradation in Contrast to Other Characterized Selective Autophagy Pathways

Having established that NPCs are degraded by autophagy, we set out to investigate how autophagy recognizes certain NPCs. One previously described microautophagic pathway for pinching-off nonessential portion of nucleus into vacuole in yeast is the piecemeal mircoautophagy of the nucleus (PMN) (Roberts et al., 2003). The nuclear envelope protein Nvj1 interacts with vacuolar membrane protein Vac8 to form unique membrane contact sites called nucleus-vacuole (NV) junctions, which is essential for PMN. While deletion of *NVJ1* implicated in PMN not only showed no effect on focal accumulation of Nup192-EGFP inside the vacuole, it further did not affect the turnover of Nup192-EGFP (Figures 3.18B and 3.18C), suggesting that NPC turnover is independent of piecemeal autophagy.



(Legend continued on next page.)

3. RESULTS

Figure 3.18: The core autophagy machinery, but not PMN is needed for Nups-vacuole targeting.

(A) Fluorescent images of cells with Nup192-EGFP-containing *ATG8*-dependent structures (marked by arrows) inside the vacuole after 24 h of nitrogen starvation. *ATG15* was deleted in order to block vacuolar digestion of inner autophagosomal membrane. Deletion of *ATG8*, but not *NVJ1* abolished accumulation of Nup192-EGFP-containing structures inside the vacuole. Vph1-mars was used as marker of the vacuolar membrane. Scale bar, 5 μ m.

(C) Degradation of Nup192-EGFP after induction of autophagy by nitrogen starvation (24 h) was measured by immunoblotting against EGFP in *wildtype* and *nvj1* Δ mutant cells as in Figure 3.6. Dmp1 serves as loading control.

Another type of nucleophagy uses the selective autophagy receptors Atg39 and Atg40. Both, Atg39 and Atg40 have been identified as ER-phagy receptors (Khaminets et al., 2015; Mochida et al., 2015). Atg40 is important for degradation of cortical ER whereas Atg39 degrades the perinuclear ER together with nuclear content. Therefore, I next tested if these receptors are important for autophagic NPC degradation. Surprisingly, neither the single deletion of *ATG39* or *ATG40*, nor the *atg39* Δ *atg40* Δ double mutant could stabilize Nup192-EGFP (Figure 3.19A). Likewise, deletions of other current known Atg8-receptors such as *CUE5* (ubiquitin-Atg8 adaptor) or *ATG19* (Cvt pathway) (Lu et al., 2014; Scott et al., 2001) also failed to rescue autophagic degradation of Nup192-EGFP (Figures 3.19B and 3.19C). Also, the distribution of Nup192-EGFP along the nuclear membrane is not altered in these mutants (Figure 3.20).

Most receptors need to interact with the autophagic scaffold protein Atg11, which is important for local formation of autophagic membranes around the cargo (Farre and Subramani, 2016). To test whether Nup159 also follows this concept, co-immunoprecipitation experiments against EGFP-tagged Atg11 were conducted. In these experiments, Nup159 indeed interacts with Atg11 and can be specifically enriched by pulldown of HA-tagged Atg11 (Figure 3.19D). Furthermore, deletion of the autophagic scaffold protein Atg11 partially impaired the degradation of Nup192-EGFP and Nup159-EGFP (Figures 3.19C and 3.19E). Collectively, these data demonstrate that autophagic degradation of the NPC requires the scaffold protein Atg11 but is independent of all identified autophagy receptors.

3. RESULTS

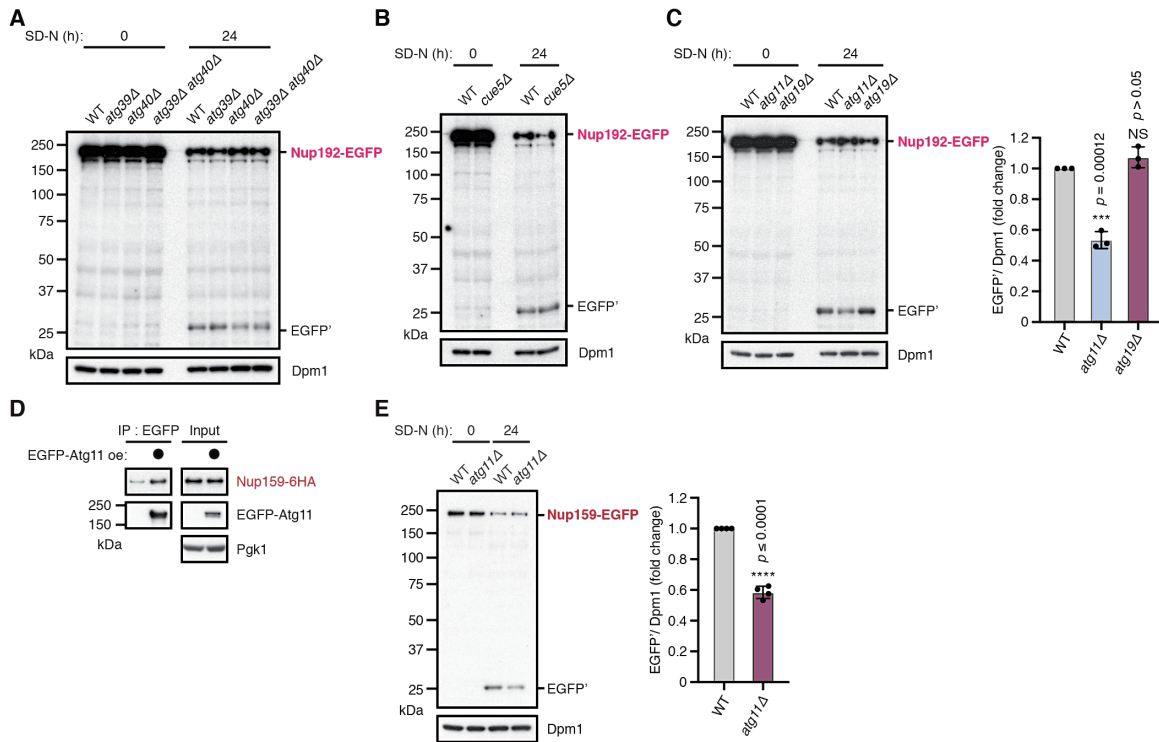


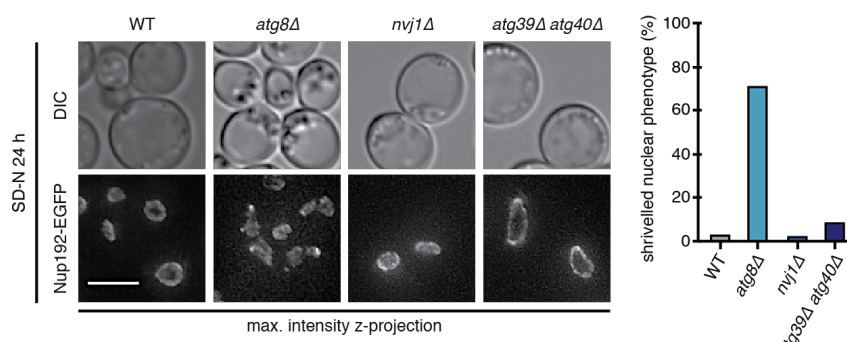
Figure 3.19: Starvation-induced degradation of Nups is independent of nucleophagy, cytoplasm-to-vacuole targeting (Cvt) pathway, and other described autophagic receptors.

(A and B) Starvation-induced degradation of Nup192-EGFP was measured at indicated times as in Figure 3.6, but in *wildtype* and cells deficient in nucleophagic receptors (*atg39Δ*, *atg40Δ* and *atg39Δ atg40Δ*, (A)), as well as in cells deficient for the autophagy receptor Cue5 (*cue5Δ*, (B)). Dpm1 serves as control.

(C) Degradation of Nup192- EGFP was measured by immunoblotting against EGFP in *wildtype*, *atg11Δ*, and *atg19Δ* mutant cells before and after induction of autophagy by nitrogen starvation (24 h).

(D) Co-immunoprecipitation of Nup159-6HA with EGFP- Atg11 in *wildtype* cells. Immunoprecipitates were probed with anti-EGFP and anti-HA antibodies. Anti-Pgk1 serves as control.

(E) Degradation of Nup159-EGFP was measured by immunoblotting against EGFP in *wildtype* and *atg11Δ* mutant cells before and after induction of autophagy by nitrogen starvation (24 h). Depicted are mean \pm s.d. from (n=3) experiments, ***p \leq 0.005, two-tailed Student's t-Test. Dpm1 serves as loading control.



(Legend continued on next page.)

3. RESULTS

Figure 3.20: Malfunction of PMN or other identified nucleophagy receptors have no impact on the distribution of membrane-embedded NPCs upon nitrogen deprivation.

Fluorescence microscopy images of EGFP-tagged Nup192 cells compared to different mutant strains (*atg8Δ*, *nvj1Δ*, and *atg39Δ atg40Δ*) after 24h of nitrogen deprivation (representative of at least 300 cells). Quantification of cells with “shriveled” Nup192-EGFP appearance (300 cells were quantified per condition), scale bar, 5 μ m.

3.7 Nup159 is a Built-in Autophagy Receptor for NPC Degradation

The accessibility of a given autophagy receptor toward Atg8 is important for substrate-autophagosome targeting. Since autophagosomes are formed in the cytoplasm, it is reasonable to hypothesize that the interaction of Atg8 with the NPC occurs at the cytoplasmic face of the NPC. Conceivably, Nups forming the cytoplasmic filaments that consist of the members of Nup82 complex might be most accessible for Atg8 binding. Moreover, Nup159 is the largest member of the Nup82 complex (Beck and Hurt, 2017), it contains a large intrinsically disordered domain that could be accessible for direct interaction with Atg8. To this end recombinantly expressed and purified His-Atg8 and GST-Nup159 was incubated *in vitro* and subsequently enriched for His-Atg8 by Ni-NTA pulldowns. Notably, the Ni-Atg8 eluate is specifically enriched together with GST-Nup159 whereas GST alone is not, emphasizing a direct interaction of both proteins (Figure 3.21).

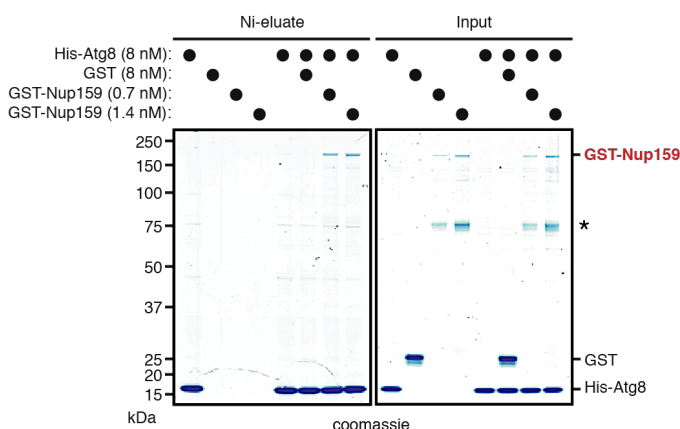


Figure 3.21: Purified Nup159 binds directly to Atg8 *in vitro*.

Ni-pull-down assays were used to enrich a Nup159-Atg8 complex, after recombinant His-tagged Atg8 (His-Atg8, 8 nM) was incubated with GST-Nup159 (at two different concentrations, 0.7 nM and 1.4 nM) or GST as control. The asterisk marks a C-terminal truncation in GST-Nup159 present in the purification of GST-Nup159 that fails however to associate with His-Atg8.

3. RESULTS

Most autophagy receptors bind to two hydrophobic pockets (W-site and L-site) on Atg8 via a small, linear sequence motif called the Atg8 interacting motif (AIM) on the receptor. To test if Nup159 also binds Atg8 in an AIM-dependent manner, GST-Atg8 Y49A, L50A, altered in both hydrophobic pockets and unable to bind AIM containing proteins, was used and tested in its binding to Nup159-6HA in yeast lysate (Noda et al., 2010). The binding of Nup159-6HA to GST-Atg8 Y49A, L50A was strongly decreased in the presence of the Y49A, L50A mutations compared to *wildtype* Atg8 (Figure 3.22), suggesting that Nup159 is a classical AIM-dependent Atg8-binder.

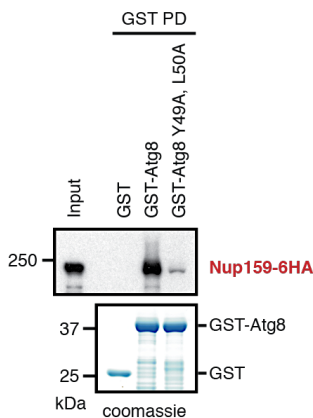


Figure 3.22: Nup159 binds to Atg8 in an AIM-dependent fashion.

Lysates from Nup159-6HA cells were incubated with recombinant His-tagged Atg8 or the Y49A, L50A mutant (defective in AIM-dependent interactions), followed by GST pulldown and immunoblotting with HA antibodies.

Since the C-terminal truncated variants of Nup159 were not recognized by the Atg8 in the previous pulldowns (Figure 3.21, marks with asterisk), this suggested that the AIM lies within the C-terminus. Computational mapping of AIMs in Nup159 unveiled five predicted AIMs in its C-terminus. These putative AIMs were then mutated individually in its respective amino acids at position 1 and 4 to alanine and tested for binding to Atg8 by co-immunoprecipitation experiments. Mutations in AIM1 (Nup159^{AIM1}) strongly impaired the binding between Nup159-6HA and EGFP-Atg8 as compared to *wildtype* or other potential AIM mutants (Figure 3.23A). Furthermore, the interaction of Atg8 with other Nups was also decreased when *wildtype* Nup159 was replaced with the AIM1 mutant, highlighting the Nup159-dependency of Atg8 binding (Figures 3.23A and 3.23B).

3. RESULTS

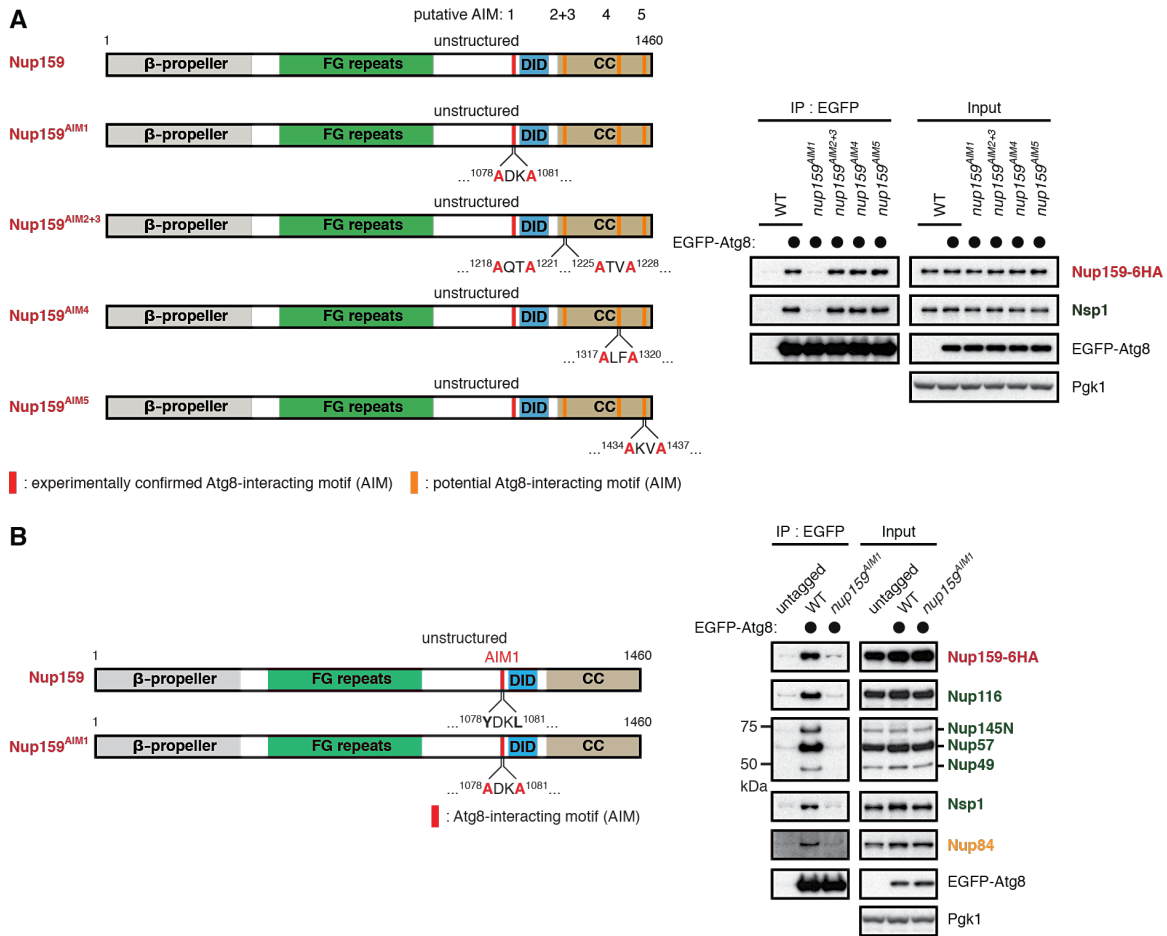


Figure 3.23: Nup159 has an Atg8 interacting motif in its C-terminus.

(A) Depiction of Nup159 protein domains including the AIMs and the corresponding AIM mutations. Co-immunoprecipitation of EGFP-Atg8 with *wildtype* Nup159-6HA or different nup159^{AIM} mutants, followed by Western blot with the indicated antibodies. Schematic overview of Nup159 domain architecture with the potential Atg8 interacting motifs (AIM) depicted.

(B) AIM1 of Nup159 is required for the Nup159-Atg8 interaction. Depiction of Nup159 protein domains including the AIM1 and the corresponding nup159^{AIM1} mutation. Co-immunoprecipitation of Nups with EGFP-Atg8 in *wildtype* or nup159^{AIM1} mutant cells, followed by Western blot with anti-EGFP, anti-Nup98 (multiple FG-nucleoporins), anti-Nup84, anti-Nsp1, and anti-HA (detecting Nup159-6HA) antibodies. Schematic overview of Nup159 domain architecture with depicted Atg8-interacting motif (AIM).

To validate that assembled NPCs are degraded in a Nup159-dependent manner, the Nup159^{AIM1} was introduced *in vivo* and checked for its effect on the degradation of different Nups. Nup159^{AIM1} impaired the starvation-induced autophagic clearance not only of Nup192-EGFP, but also Nup133-EGFP, judged from the levels of cleaved EGFP' (Figures 3.24A and 3.24B).

3. RESULTS

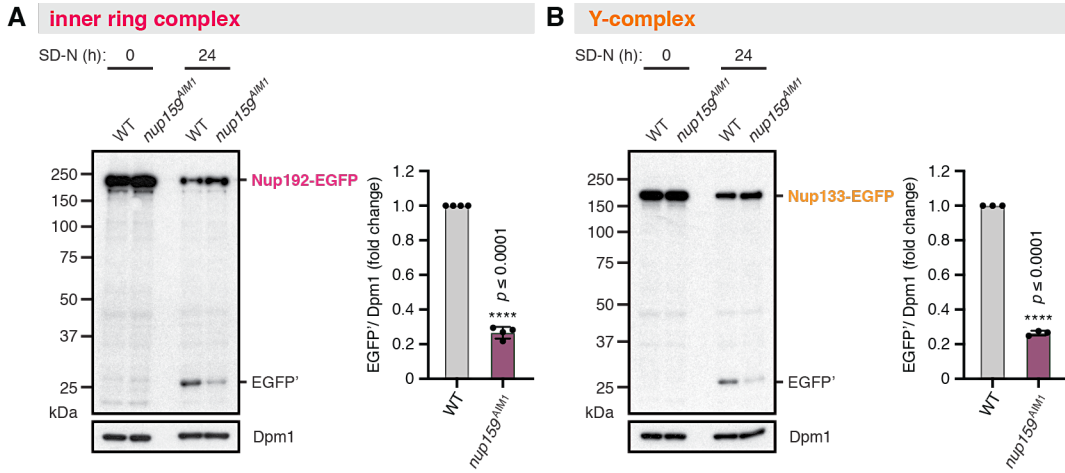


Figure 3.24: Nup159 is an autophagy receptor for degradation of assembled NPCs.

(A and B) Degradation of scaffold nucleoporins (Nup192-EGFP (A) and Nup133-EGFP (B)) in *wildtype* or *nup159^{AIM1}* mutant cells measured upon nitrogen starvation by anti-EGFP immunoblotting. Dpm1 serves as loading control. Quantifications from (n=3) experiments are shown as mean ± s.d..

On the other hand, the *Nup159^{AIM1}* mutant had no effect on autophagy *per se* as degradation of EGFP-Atg8 remained unchanged (Figure 3.25).

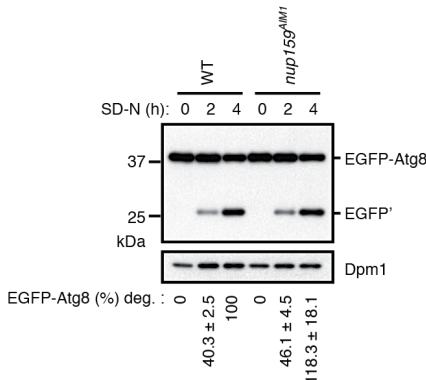


Figure 3.25: Atg8 turnover is not significantly affected in *nup159^{AIM1}* cells.

Degradation of EGFP-Atg8 was measured by immunoblotting against EGFP in *wildtype* cells or *nup159^{AIM1}* mutant cells. Quantifications from (n=3) experiments are shown as mean ± s.d..

Having established that Nup159 interacts with Atg8 *in vivo*, I aimed to visualize these sites of interaction. Therefore, I turned to a bimolecular fluorescence complementation (BiFC) strategy (Kerppola, 2008), by labelling Nup159 and Atg8 with either the C-terminal (VC) or N-terminal (VN) half of the Venus fragments, respectively. A fluorescent signal could be detected when the full Venus reconstituted by the interaction between Nup159 and Atg8. Consistent with previous Atg8 interaction data (Figures 3.21-3.23), a BiFC signal for the Atg8-Nup159 interaction was observed even in the absence of nitrogen starvation, when VN-Atg8 was overexpressed (Figure 3.26A). The co-

3. RESULTS

localization of the BiFC signal and the membrane-associated Nup170-mars demonstrated that Atg8-Nup159 interacts directly at nuclear envelope. Notably, upon nitrogen starvation the BiFC signal was enhanced in a focus, which nicely co-localized with the scaffold Nup170-mars (Figure 3.26A). This BiFC approach was specific for the Atg8-Nup159 interaction, since it remained undetected when Nup159-VC was replaced by either the inner ring Nup192-VC or the nuclear basket Mlp1-VC (Figure 3.26B). Furthermore, the signal was strongly decreased when *wildtype* VN-Atg8 was replaced by the AIM-binding deficient mutant (VN-Atg8 Y49A, L50A) (Figure 3.27). Overall, these data indicate that Atg8-Nup159 interacts directly at the nuclear envelope, presumably at membrane-embedded NPCs.

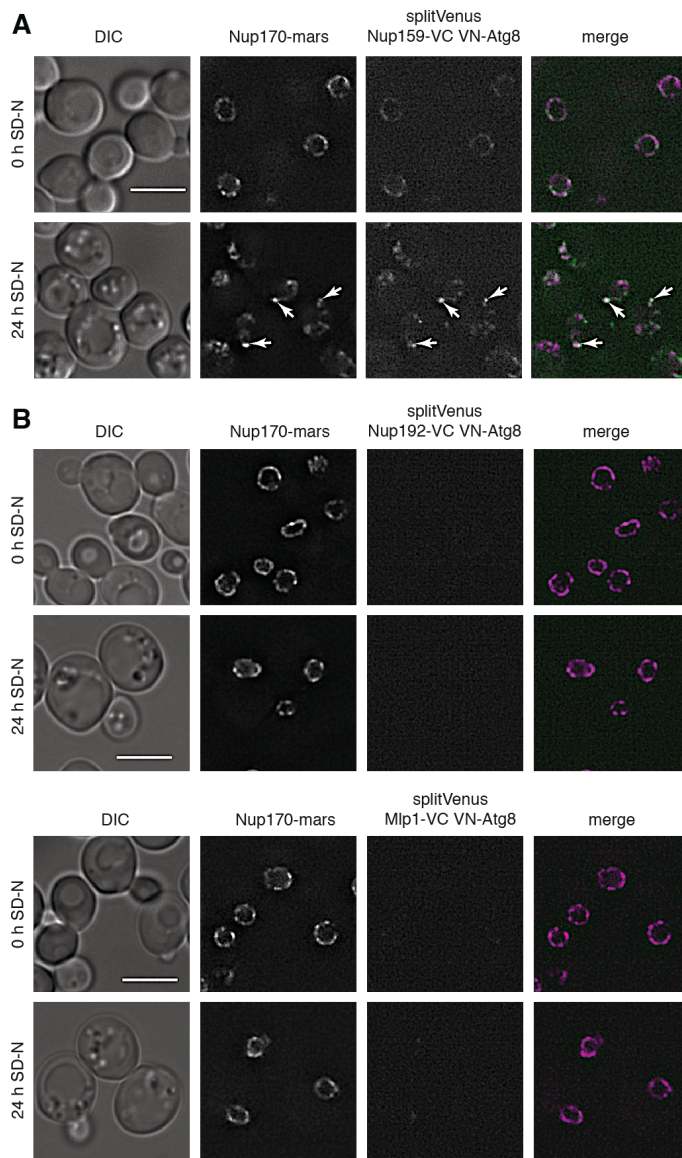


Figure 3.26: Nup159 interact with Atg8 at the nuclear envelope.

(A and B) Fluorescent micrographs of the BiFC signal arising from pADH::VN-Atg8 and Nup159-VC (A), or pADH::VN-Atg8 and Nup192-VC or Mlp1-VC (B) are examined before and after 24h of nitrogen starvation. Inner-ring nucleoporin Nup170-mars marks NPCs. Starvation induced formation of an VN-Atg8-, Nup159-VC- and Nup170-containing NPC focus is indicated by arrows. Scale bar, 5 μ m.

3. RESULTS

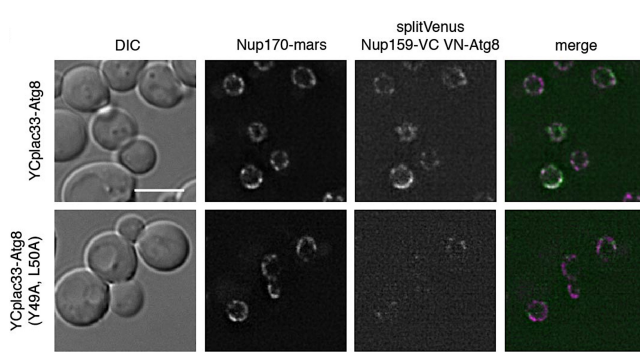


Figure 3.27: The VN-Atg8 Y49A, L50A mutant does not interact with Nup159-VC at nuclear envelope.

Fluorescent micrographs of the BiFC signal arising from pADH::VN-Atg8 or pADH::VN-Atg8 Y49A, L50A mutant with Nup159-VC are examined at normal growth condition. Inner-ring nucleoporin Nup170-mars marks fully assembled NPCs. Scale

Additionally, the focus-like accumulation of the BiFC signal and the Nup170-mars upon nitrogen starvation hints that NPCs cluster at specific sites, where they are targeted by autophagy. To understand whether Atg8-Nup159 interaction results in targeting of NPCs to the vacuole, the number of cells with vacuolar Nup192-EGFP foci was counted for cells lacking the vacuolar lipase Atg15 with *wildtype* Nup159 or the Nup159^{AIM1} mutant present. Strikingly, disruption of the Atg8-Nup159 interaction strongly reduced vacuolar focus accumulation (Figure 3.28).

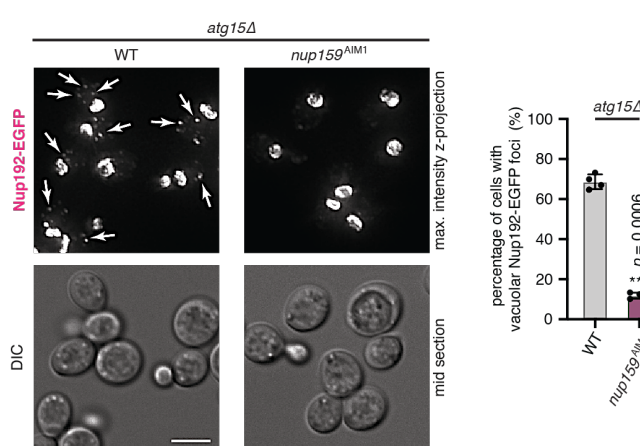


Figure 3.28: Focal accumulations of scaffold Nups in the vacuole are dependent on Atg8-Nup159 interaction.

Focal accumulations of Nup192-EGFP in the vacuole in the *atg15Δ* cells as monitored by Nup192-EGFP staining in *wildtype* and *nup159^{AIM1}* cells. Arrows indicate autophagic bodies marked by Nup192- EGFP. Scale bar, 5 μ m. Depicted are mean \pm s.d. from (n=3) experiments (above 300 cells were quantified per condition each time), ***p \leq 0.005, two-tailed Student's t-Test.

To gain insights into the architecture of these Nups-containing structures, correlative light and electron microscopy (CLEM) was performed on a Nup159 mars-tagged strain in

3. RESULTS

which *ATG15* was deleted. The accumulated single-membrane autophagic bodies within the vacuole could be tracked by correlating the Nup159-mars fluorescence signal. Indeed, nuclear membrane-derived vesicles decorated with assembled NPCs were enriched in these correlated autophagic bodies, demonstrating that membrane-embedded NPCs are truly a target of Nup159-dependent autophagic degradation (Figures 3.29A and 3.29B). Intriguingly, the interior of these nuclear vesicles retained an electron dense material that resembled the density seen for the nucleus suggesting the idea that nuclear material could be degraded via this pathway (Figures 3.29A and 3.29B).

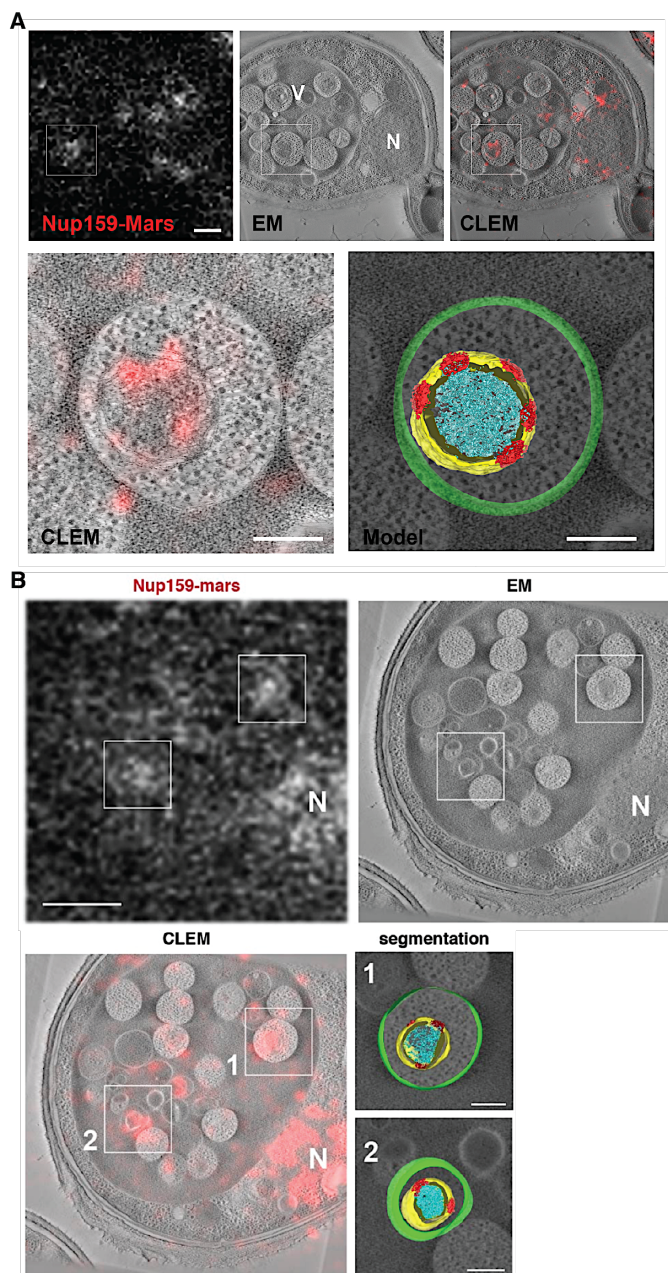
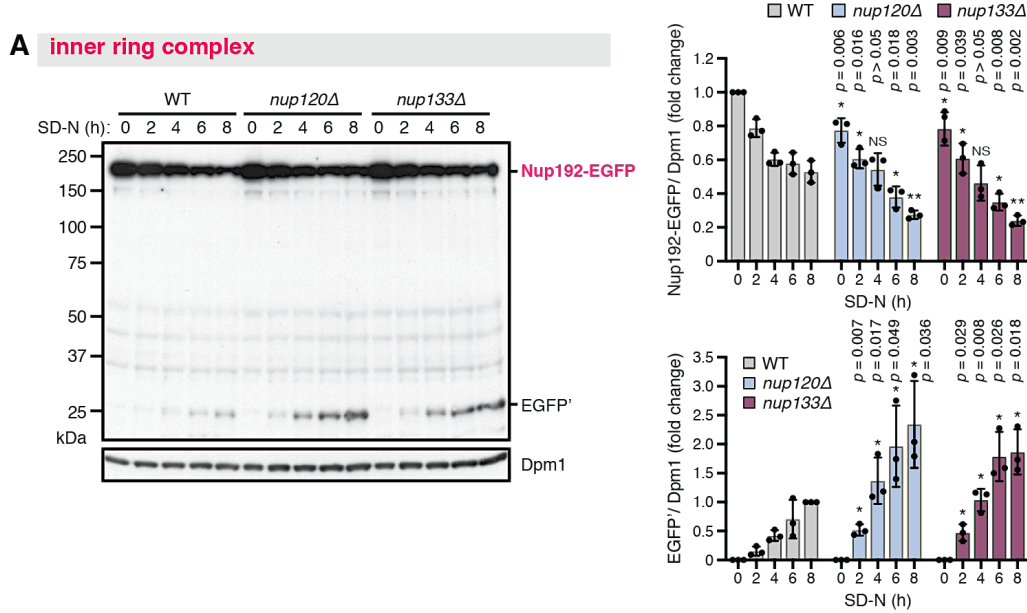


Figure 3.29: The visualization of NPC-containing nuclear vesicles by CLEM.
(A and B) Nup159 mars-tagged cells starved for 24 h and deleted for the vacuolar lipase Atg15 were subjected to correlative light and electron microscopy (CLEM). (A) Top left shows the Nup159-mars signal, top middle a single plain image of an EM tomogram and top right a merge of the two corresponding images. Bottom left shows an inset of an autophagic body loaded with an NPC-containing vesicle. On the right is a manual segmentation of the corresponding tomogram. NPCs in red, nuclear membrane in yellow, autophagosomal membrane in green, nuclear content in cyan. (B) Additional examples of CLEM visualized vacuolar trapped autophagic bodies in *atg15Δ* cells loaded with NPC-containing nuclear vesicles (as in A). Scale bar, 500 nm and 200 nm for inset.

3. RESULTS

3.8 Selective Autophagy is Important for the Clearance of Aberrant NPCs

NPC clustering in mother cells was thought to be a protective mechanism for preventing daughter cells from inheriting damaged or misassembled NPC species (Shintani and Klionsky, 2004). Deletion of certain scaffold nucleoporins, particularly Nup120 and Nup133, leads to constitutive clustering of NPCs at one side of the nuclear envelope and strongly compromises nucleocytoplasmic transport (Aitchison et al., 1995; Doye et al., 1994; Heath et al., 1995). If and how these defective NPC clusters are removed is currently unknown. Given the initial finding that upon starvation NPCs cluster at sites of Atg8 interaction (Figure 3.26), it was reasonable to test if NPC clusters are a preferred target of autophagic removal. Therefore, the degradation of Nup192-EGFP or Nic96-EGFP in *wildtype* cells was compared to mutant cells (*nup120Δ* or *nup133Δ*), which cause NPC clustering. Interestingly, free EGFP appeared more rapidly in both *nup120Δ* and *nup133Δ* cells as compared to *wildtype* cells (Figures 3.30A and 3.30B). Moreover, interaction between Atg8 and Nups, which was measured by coimmunoprecipitation of EGFP-Atg8 expressed from the ADH promoter, was enhanced in *nup120Δ* cells (Figure 3.31), supporting the idea that clustered NPCs are preferentially degraded by autophagy.



(Figure continued on next page, legend follows.)

3. RESULTS

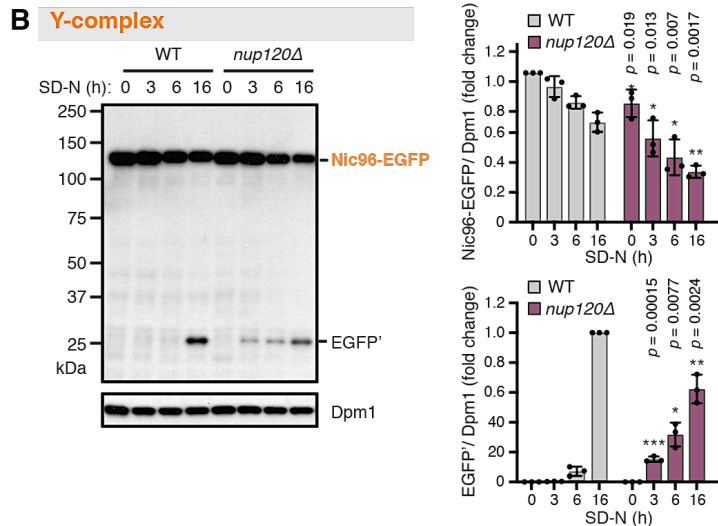
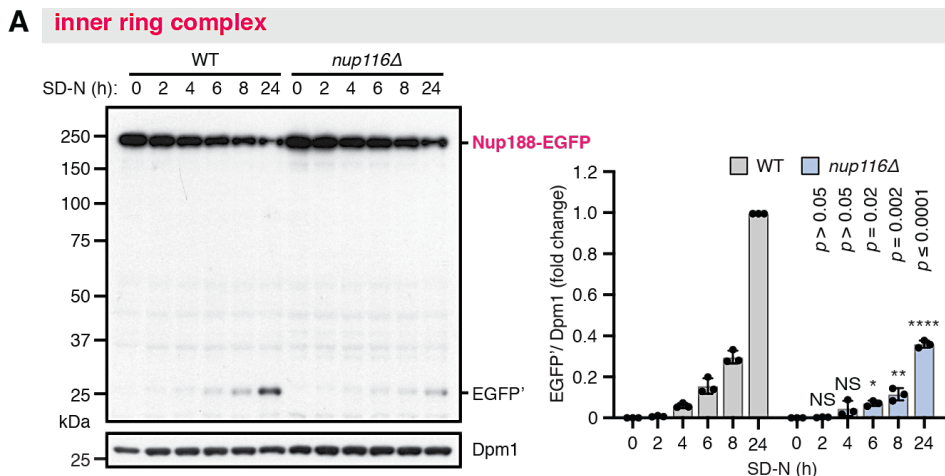


Figure 3.30: Mutations that cause NPC clustering trigger enhanced NPC degradation.

(A and B) Starvation-induced degradation of Nup192-EGFP (A) or Nic96-EGFP (B) in *wildtype*, *nup120Δ* or *nup133Δ* mutant background, which cause the appearance of NPC clusters, was analysed as in Figure 3.24, but the disappearance of the Nup192-EGFP or Nic96-EGFP (normalized to loading control) as well as appearance of the free EGFP band was quantified and shown as mean±s.d. (n=3), *p ≤ 0.05; **p ≤ 0.01, two-tailed Student's t-Test. Dpm1 served as a control.

In contrast, the faster turnover of Nups was not seen when NPC assembly was impaired by deletion of *NUP116*. Nup116 forms a stable association with Nup82 complex, which thus is critical for nuclear RNA export (Wente and Blobel, 1993). Particularly, deletion of *NUP116* did not cause NPC clustering, but abolished autophagic degradation of Nups (Figures 3.31A and 3.31B), suggesting that NPC clustering is important for autophagic NPC turnover.



(Figure continued on next page, legend follows.)

3. RESULTS

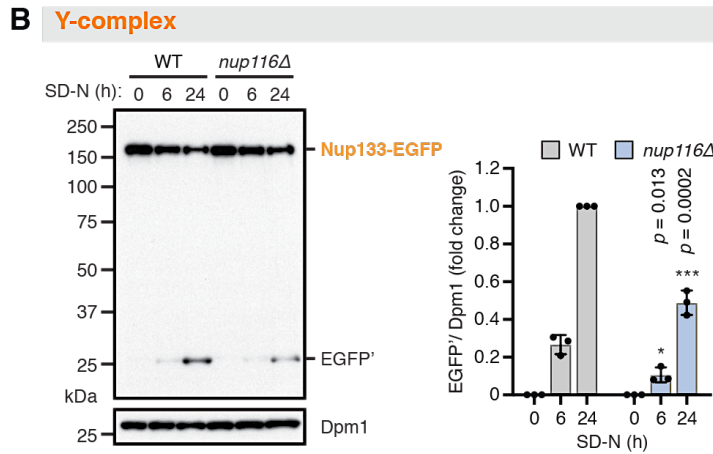


Figure 3.31: Degradation of scaffold Nups in Nup116-deficient cells is strongly impaired.

(A and B) Starvation-induced degradation of Nup188-EGFP (A) or Nic96-EGFP (B) in *nup116Δ* mutant background, was analysed as in Figure 3.24. Dpm1 served as a control and was used for normalization (bottom). Depicted are mean \pm s.d. from (n=3) experiments, ***p \leq 0.005, two-tailed Student's t-Test.

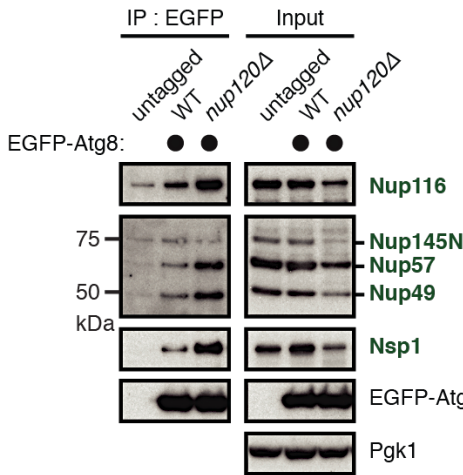


Figure 3.32: Interaction of Atg8-Nups is enhanced in NPC-clustering mutants.

Co-immunoprecipitation of nucleoporins with EGFP-Atg8 in *wildtype* and *nup120Δ* cells. Immunoprecipitates were probed with anti-EGFP, anti-Nup98 (multiple FG-nucleoporins) and anti-Nsp1 antibodies. Anti-Pgk1 serves as control.

The *nup116Δ* cells show assembly defects at higher temperatures, which lead to herniation of single NPCs (Wente and Blobel, 1993). Therefore, it was reasonable to hypothesize that the cytosolic filaments could not assemble properly leading to the absence of the receptor Nup159. Indeed, the cytosolic filaments seemed to dissociate from the NPCs in *nup116Δ* cells since EGFP-Atg8 pulldowns only enriched members of the Nup82 subcomplex, but not other Nups (Figure 3.33A). Additionally, immunoprecipitates of the Y-complex protein Nup84-EGFP failed to enrich members of the cytosolic

3. RESULTS

filaments in the *nup116 Δ* background (Figure 3.33B), suggesting that the Nup82 subcomplex is not present on these misassembled NPCs which renders them unrecognizable for autophagic turnover.

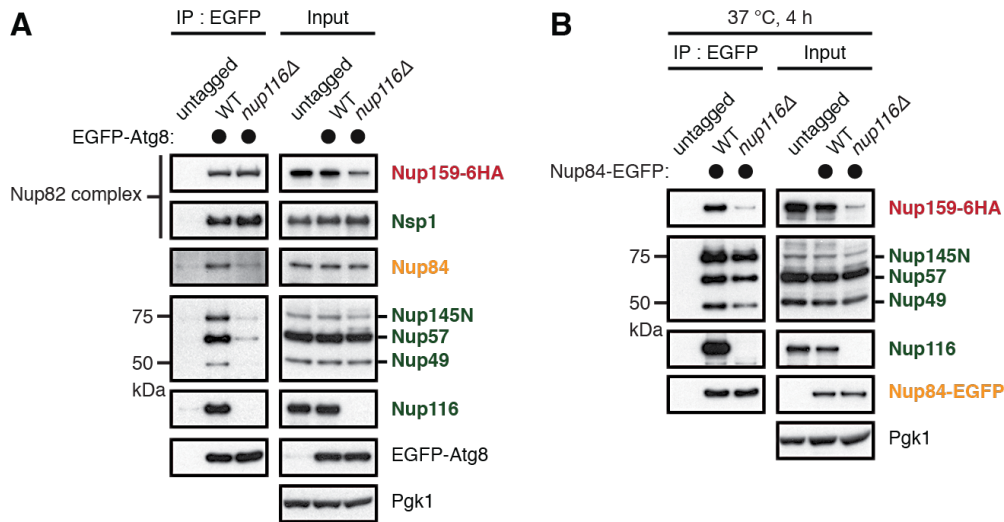


Figure 3.33: Depletion of Nup116 leads to dissociation of the cytosolic filaments from NPCs and abolishes Atg8-NPC binding.

(A) EGFP-Atg8 interacting proteins were measured by EGFP-Atg8 Co-IP as in Figure 20B, for *wildtype* or *nup116 Δ* mutant cells. For this analysis cells with tagged Nup159-6HA, were subjected to immunoprecipitation with EGFP-Trap matrix. Immunoprecipitates were probed with antibodies against EGFP tag, HA tag, Nup84, Nup98 (multiple FG-nucleoporins), Nsp1 and Pgk1 as control.

(B) Nup159 does not interact with NPC at non-permissive temperature. Cells with tagged Nup159-6HA and Nup84-EGFP, were subjected to immunoprecipitation with EGFP-Trap matrix and probed with antibodies against EGFP tag, HA tag, Nup98 (multiple FG-nucleoporins) and Pgk1 as control.

Interestingly, a patch-like BiFC signal was detected specifically at the site where NPCs cluster using the previously reported approach (Figure 3.34). After 24h of nitrogen starvation, this signal collapsed into a dot like structure, further implying that aberrant NPCs are indeed degraded in an autophagy-dependent manner (Figure 3.34).

3. RESULTS

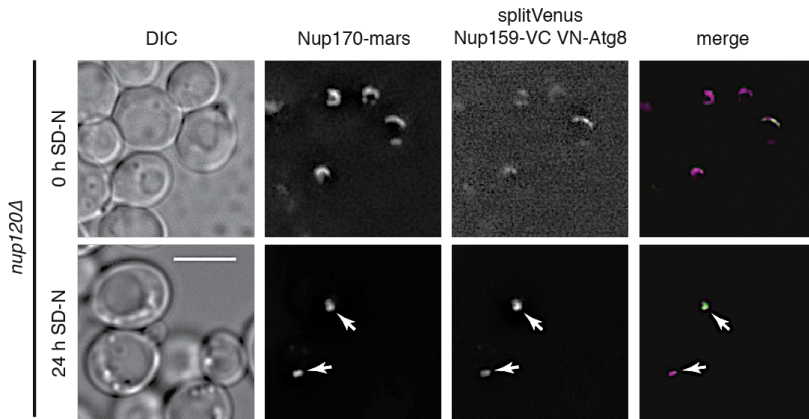


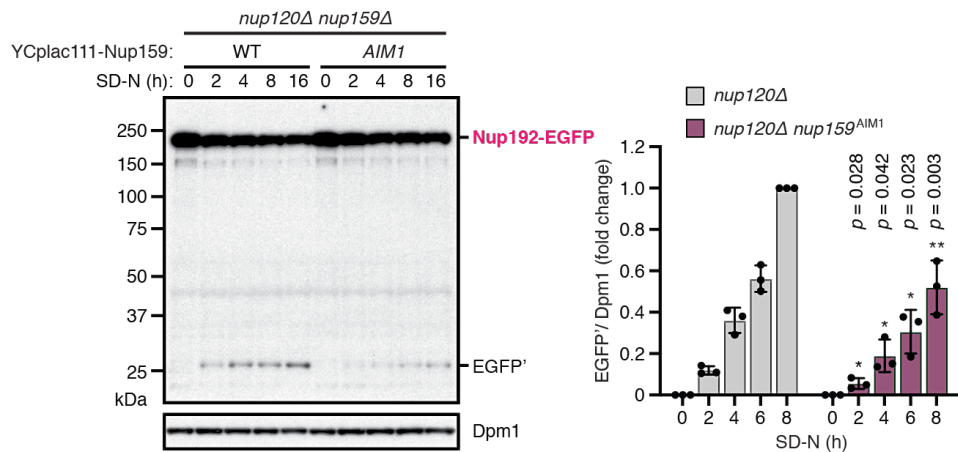
Figure 3.34: Atg8 interacts with Nup159 at the site of the NPC cluster.

Fluorescent micrographs of Atg8-Nup159 BiFC assay as in Figure 3.26 were examined before and after 24h of nitrogen starvation in the *nup120Δ* background. Inner-ring nucleoporin Nup170-mars marks NPCs. Starvation-induced formation of a Nup159-Atg8 and Nup170 containing focus is indicated by arrows. Scale bar, 5 μ m.

Finally, I tested whether the clearance of NPC clusters is also mediated by the autophagy receptor Nup159. For this, the *nup159^{AIM1}* mutant was introduced into the *nup120Δ* cluster strain and EGFP-tagged Nup192-EGFP and Nic96-EGFP were monitored using the EGFP-cleavage assay for their degradation under nitrogen starvation. Remarkably, the degradation of both scaffold Nups was strongly impaired which further confirmed that Nup159 functions as a autophagy receptor to remove NPCs (Figures 3.35A and 3.35B). Altogether this provides strong evidence that Nup159 functions as a selective autophagy receptor and its loss makes NPCs resistant to autophagic degradation. Furthermore, selective autophagy plays an important role in clearance of NPCs under specific conditions such as nitrogen starvation or when NPC architecture is dysfunctional.

3. RESULTS

A inner ring complex



B Y-complex

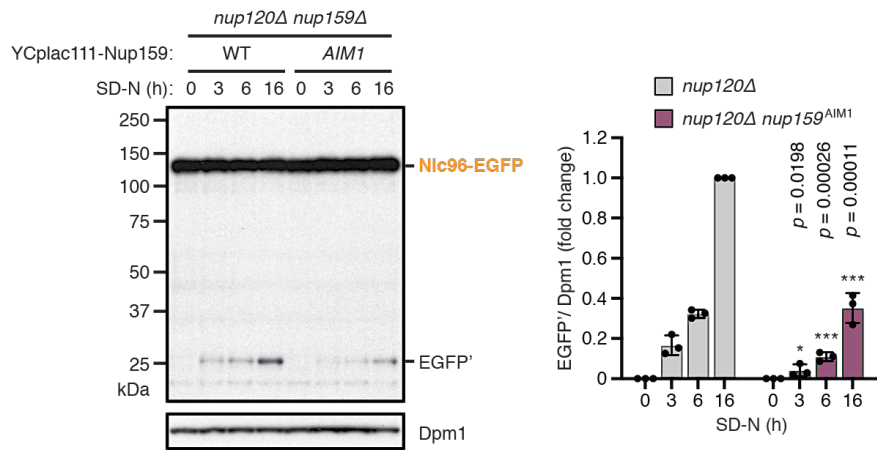


Figure 3.35: Nup159-mediated degradation of clustered NPCs.

(A and B) Starvation-induced degradation of Nup192-EGFP (A) or Nic96-EGFP (B) in *nup120 Δ nup159 Δ* mutant background complemented with *wildtype NUP159* or the *nup159 AIM1* mutant was analysed as in Figure 3.24. Dpm1 served as a control and was used for normalization (right). Depicted are mean \pm s.d. from (n=3) experiments, ***p \leq 0.005, two-tailed Student's t-Test.

4 Conclusions and Discussion

An extended model of NPC quality control, in which the number of NPCs is controlled and misassembled or perhaps damaged NPCs are turned over by proteasome or the autophagy machinery, was proposed (Figure 4.1). In case of proteasomal degradation, the defective NPCs are first earmarked by the ESCRT machinery and then handed over to the proteasome (Webster et al., 2014). In case of autophagic degradation, it is at the moment unclear whether earmarking by ESCRT is involved and at which stage it may act. However, this appears to undergo via a route that is distinct from piecemeal autophagy or nucleophagy and which is also independent of previously characterized autophagy receptors, but rather appears to involve an intrinsic receptor Nup159 or possible other proteins as receptors.

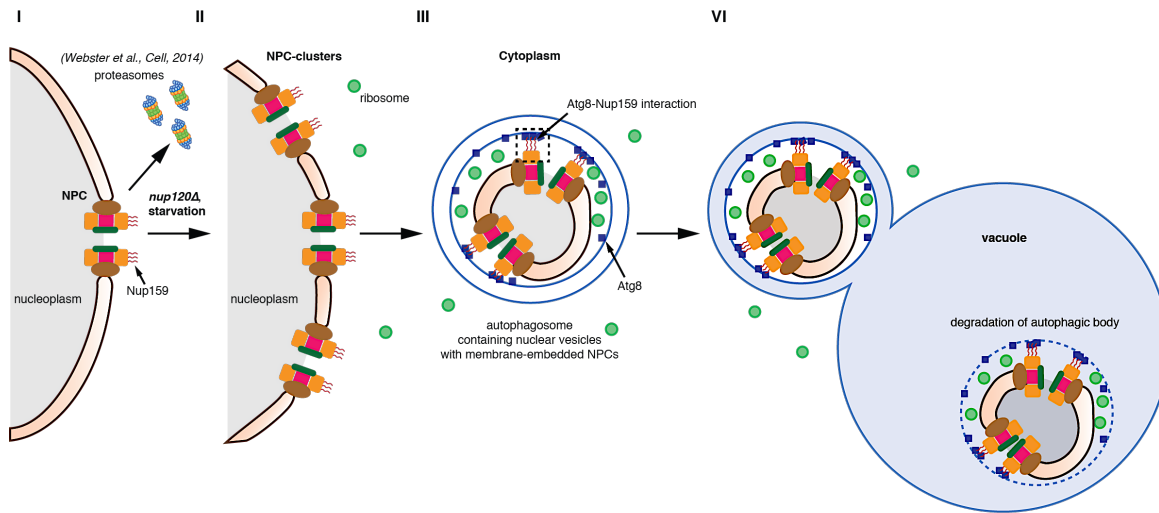


Figure 4.1: Cartoon model of membrane remodeling during NPC turnover by selective autophagy.

A fraction of fully assembled NPCs (I) clusters upon nitrogen starvation or even more dramatic upon genetic perturbation (*nup120Δ*) (II). This leads to interaction of the intrinsic receptor Nup159 with Atg8 and packaging of nuclear vesicles into autophagosomes (III), which our data predicts as cellular intermediate. These autophagosomes will subsequently fuse with the vacuole for degradation (IV). Color-code of NPC is analogue to the NPC model (Figure 1.1)

4.1 Nup159 Specifically Target Membrane-embedded NPCs for Autophagic Turnover

Multiple lines of evidence support that Nup159-dependent autophagy is specifically involved in degradation of nuclear envelope-embedded NPCs rather than orphan subunits. (I) The interaction of Atg8 with other Nups is Nup159-mediated (Figure 3.23). (II) Nup159 controls the degradation of Nups even from other subcomplexes (Figure 3.24). (III) The interaction of Atg8 with NPCs is spatially associated with the nuclear periphery (Figure 3.26A and 3.34). (IV) NPC-containing vesicles are observed in the vacuole if the degradation is blocked (Figure 3.29). (V) Nup159 is incorporated into NPCs late during interphase assembly (Otsuka and Ellenberg, 2018). (VI) The in cell structural analysis of Nup159 complex from our co-workers further revealed that AIM of Nup159 is favouring the recruitment of cytoplasmic Atg8 without a spatial hindrance (Allegretti et al., 2020). This mechanism serves as an elegant solution of how cells can control the number (Cantwell and Nurse, 2019; McCloskey et al., 2018) or the integrity of individual nuclear envelope-embedded NPCs (Thaller and Patrick Lusk, 2018) in organisms with closed mitosis, where chromosomes are segregated inside intact nucleus and nuclei divide without the nuclear envelope breakdown. However, whether this concept can be implemented to higher eukaryotes with open mitosis, especially in terminally differentiated, non-dividing cells (Mathieson et al., 2018), remains to be investigated in the future. It is noteworthy that an initial experiment with autophagy inhibitors so far failed to provide supporting evidence for clearance by autophagy in quiescent mammalian cells (Toyama et al., 2019).

4.2 Nup159 Functions Intrinsically as a New Type of Autophagy Receptor

This study demonstrates that Nup159 act as an autophagy receptor for NPC degradation. Besides, Nup159 is also the first among other identified autophagy receptors that is an integral and functional part of the complex destined for degradation. A similar example appears to be the translocon subunit Sec62 in a process called recovER-phagy, regulating maintenance and recovery of ER homeostasis (Fumagalli et al., 2016). We therefore

4. CONCLUSIONS AND DISCUSSION

name this kind of autophagy receptor “intrinsic receptor”. Such intrinsic receptors are ideally positioned to discriminate normal from misassembled or unproductive protein complexes, thus provided a very elegant solution to the problem of how to handle toxic misassembled intermediates that would perhaps interfere with the normal assembly of macromolecular machines.

In the initial qMS experiment (Figure 3.16), subunits of other macromolecular complexes such as ribosomes and endocytic machinery were actually found enriched in the EGFP-Atg8 pulldown. Since many of the published mass spectrometry results revealed proteins with annotated function in other pathways, these proteins may have been mostly overlooked or ignored. This study thus suggests to revisit these aspects and shows that autophagy plays a much broader role in cellular homeostasis.

4.3 The Generation of Nuclear Envelope-derived Vesicles

The CLEM approach by correlating the Nup159-mars fluorescence signal allowed the first-time observation of NPC-containing nuclear vesicles in the vacuole after inhibition of degradation (Figures 3.29). Such degradative intermediates display that autophagy degrade not only the membrane-embedded NPCs, but also the remnants in particular for the nuclear membrane and trapped nuclear material. It additionally offers an escape road for nuclear material, which could become sequestered to NPCs during the vesicle formation step and accumulates inside the NPC-containing vesicles.

Another intriguing puzzle is how to produce these NPC-containing nuclear vesicles from the intact nuclear envelope. Although it is remain unclear, but presumably the nuclear envelope evagination or herniation, a phenotype in which NPCs are engulfed by the NE membranes might cause the formation of nuclear vesicles (Thaller et al., 2019). Previous study showed that the number of NE hernia was drastically increased in *nup116Δ* strain at non-permissive temperature (Wente and Blobel, 1993), but I found that these hernia which lost the Nup159 complex are resistant to autophagic degradation (Figures 3.31 and 3.33). While genetic interference of *NUP120* not only linked to cluster of NPCs, a preferred substrate of autophagy (Figure 3.30), but exhibited an agglomerate of NE herniae at the place of NPC cluster (Heath et al., 1995) and thus could possibly

4. CONCLUSIONS AND DISCUSSION

assist the formation of nuclear vesicles. This type of NE alteration was also detected when deletion in the amino-terminal half of *NUP145* (*nup145ΔN*) or other Nup159 complex associated Nups, such as Gle2, were genetically perturbed or under other unrelated conditions, such as mutation of inner nuclear membrane proteins (Murphy et al., 1996; Scarcelli et al., 2007; Vallotton et al., 2019; Webster et al., 2014; Webster et al., 2016; Wente and Blobel, 1993; Wente and Blobel, 1993; Zhang et al., 2018). This implicate herniation is a general response to maintain NE integrity. Nevertheless, whether the generation of NE herniae is prerequisite for nuclear vesicle formation and what is the cause for NPC clustering requires further examination.

4.4 Cross-regulation between ESCRT, proteasome and autophagy in NPC Degradation

Apart from selective autophagy, pathways like ESCRT and proteasome are involved in NPC surveillance (Thaller et al., 2019; Webster et al., 2014; Webster et al., 2016). It has been shown, when ESCRT function was compromised, the malformed NPCs clustered and accumulated in the SINC (Webster et al., 2014). Since the clustering of defective NPCs is a hallmark for autophagic turnover based on my observation of Nups degradation in *nup120Δ* strain (Figure 3.30), one may speculate whether the SINC is under surveillance by autophagy. However, ESCRT mutation (*vps4Δ*) as well as *cim3-1* mutation strongly impaired the general autophagy flux, suggesting the secondary effects on autophagy (Figure 3.12) and made it hard to dissect the contribution of the individual pathways.

Alternatively, substrates degraded by the proteasome require protein unfolding in order to pass through the narrow opening and reach the proteolytic center of proteasome (Tanaka, 2009). This indicate only the orphan subunits rather than whole protein complexes are subjected directly to proteasomal turnover and hence, as the proteasome substrates, protein complex disassembly must exist. A previous study has shown that the defective NPC assembly intermediates are eliminated in a proteasome-dependent, but vacuolar peptidases-independent manner (Webster et al., 2014). However, this conclusion was drawn by monitoring the degradation of the Y-complex Nup85 in *nic96-1* mutant cells at non-permissive temperature. Since Nic96 is essential for NPC formation (Zabel et

4. CONCLUSIONS AND DISCUSSION

al., 1996), mutation in Nic96 may lead to partially dismantle the complex and results in orphan subunits, which are preferentially degraded by proteasome. Consequently, whether the defective NPC mutants are indeed represented the genuine damaged NPC, especially for this type of quality control study, should be always considered and checked carefully.

It remains an open question of how ESCRT machinery surveils the assembly of NPCs as the primary function of this multi-subunit machinery is involved in membrane remodelling. Evidence that accumulation of balloon-like NE herinae at sites of where Chm7, a NE-specific ESCRT, and SINC interacted in *vps4Δ pom152Δ* cells (Thaller et al., 2019), hinted that ESCRT function may assist the formation of NPC-containing nuclear vesicles. Moreover, it additionally suggested the ESCRT may act upstream of autophagy-mediated NPC degradation since the generation of nuclear vesicles is prerequisite for their autophagic removal (Figure 3.29). This offering an explanation of how the membrane remodelling capability of ESCRT can clear the defective NPC assemblies, albeit the mechanistic details remain enigmatic and yet to be determined.

References

- Adams, R.L., Terry, L.J., and Wente, S.R. (2014). Nucleoporin FG domains facilitate mRNP remodeling at the cytoplasmic face of the nuclear pore complex. *Genetics* *197*, 1213-1224.
- Aitchison, J.D., Blobel, G., and Rout, M.P. (1995). Nup120p: a yeast nucleoporin required for NPC distribution and mRNA transport. *J Cell Biol* *131*, 1659-1675.
- Allegretti, M., Zimmerli, C.E., Rantos, V., Wilfling, F., Ronchi, P., Herman K.H. Fung, H.K.H., Lee, C.W., Hagen, W., Turonova, B., Karius, K., Zhang, X.J., Müller, C., Schwab, Y., Mahamid, J., Pfander, B., Kosinski, J., and Martin Beck, M. (2020) In cell architecture of the nuclear pore complex and snapshots of its turnover. *BioRxiv*.
- Anderson, D.J., and Hetzer, M.W. (2007). Nuclear envelope formation by chromatin-mediated reorganization of the endoplasmic reticulum. *Nat Cell Biol* *9*, 1160-1166.
- Anderson, D.J., and Hetzer, M.W. (2008). Reshaping of the endoplasmic reticulum limits the rate for nuclear envelope formation. *J Cell Biol* *182*, 911-924.
- Antonin, W., Ellenberg, J., and Dultz, E. (2008). Nuclear pore complex assembly through the cell cycle: regulation and membrane organization. *FEBS Lett* *582*, 2004-2016.
- Antonin, W., Franz, C., Haselmann, U., Antony, C., and Mattaj, I.W. (2005). The integral membrane nucleoporin pom121 functionally links nuclear pore complex assembly and nuclear envelope formation. *Mol Cell* *17*, 83-92.
- Beck, M., and Hurt, E. (2017). The nuclear pore complex: understanding its function through structural insight. *Nat Rev Mol Cell Biol* *18*, 73-89.
- Birgisdottir, A.B., Lamark, T., and Johansen, T. (2013). The LIR motif - crucial for selective autophagy. *J Cell Sci* *126*, 3237-3247.
- Cantwell, H., and Nurse, P. (2019). Unravelling nuclear size control. *Curr Genet*.
- Cheong, H. & Klionsky, D.J. (2008). Biochemical methods to monitor autophagy-related processes in yeast. *Methods Enzymol* *451*, 1-26.
- Chew, L.H., Lu, S., Liu, X., Li, F.K., Yu, A.Y., Klionsky, D.J., Dong, M.Q., and Yip, C.K. (2015). Molecular interactions of the *Saccharomyces cerevisiae* Atg1 complex provide insights into assembly and regulatory mechanisms. *Autophagy* *11*, 891-905.

REFERENCES

- Chial, H.J., Rout, M.P., Giddings, T.H., and Winey, M. (1998). *Saccharomyces cerevisiae Ndc1p* is a shared component of nuclear pore complexes and spindle pole bodies. *J Cell Biol* *143*, 1789-1800.
- Christ, L., Wenzel, E.M., Liestol, K., Raiborg, C., Campsteijn, C., and Stenmark, H. (2016). ALIX and ESCRT-I/II function as parallel ESCRT-III recruiters in cytokinetic abscission. *J Cell Biol* *212*, 499-513.
- Colombi, P., Webster, B.M., Frohlich, F., and Lusk, C.P. (2013). The transmission of nuclear pore complexes to daughter cells requires a cytoplasmic pool of Nsp1. *J Cell Biol* *203*, 215-232.
- Cordes, V.C., Reidenbach, S., Rackwitz, H.R., and Franke, W.W. (1997). Identification of protein p270/Tpr as a constitutive component of the nuclear pore complex-attached intranuclear filaments. *J Cell Biol* *136*, 515-529.
- Cox, J., Hein, M.Y., Luber, C.A., Paron, I., Nagaraj, N., and Mann, M. (2014). Accurate proteome-wide label-free quantification by delayed normalization and maximal peptide ratio extraction, termed MaxLFQ. *Mol Cell Proteomics* *13*, 2513-2526.
- Cox, J., and Mann, M. (2008). MaxQuant enables high peptide identification rates, individualized p.p.b.-range mass accuracies and proteome-wide protein quantification. *Nat Biotechnol* *26*, 1367-1372.
- D'Angelo, M.A., Anderson, D.J., Richard, E., and Hetzer, M.W. (2006). Nuclear pores form de novo from both sides of the nuclear envelope. *Science* *312*, 440-443.
- D'Angelo, M.A., Raices, M., Panowski, S.H., and Hetzer, M.W. (2009). Age-dependent deterioration of nuclear pore complexes causes a loss of nuclear integrity in postmitotic cells. *Cell* *136*, 284-295.
- Dawson, T.R., Lazarus, M.D., Hetzer, M.W., and Wente, S.R. (2009). ER membrane-bending proteins are necessary for de novo nuclear pore formation. *J Cell Biol* *184*, 659-675.
- de Chaumont, F., Dallongeville, S., Chenouard, N., Herve, N., Pop, S., Provoost, T., Meas-Yedid, V., Pankajakshan, P., Lecomte, T., Le Montagner, Y., *et al.* (2012). Icy: an open bioimage informatics platform for extended reproducible research. *Nat Methods* *9*, 690-696.

REFERENCES

- Deretic, V., Saitoh, T., and Akira, S. (2013). Autophagy in infection, inflammation and immunity. *Nat Rev Immunol* *13*, 722-737.
- Dikic, I. (2017). Proteasomal and Autophagic Degradation Systems. *Annu Rev Biochem* *86*, 193-224.
- Dilworth, D.J., Suprapto, A., Padovan, J.C., Chait, B.T., Wozniak, R.W., Rout, M.P., and Aitchison, J.D. (2001). Nup2p dynamically associates with the distal regions of the yeast nuclear pore complex. *J Cell Biol* *153*, 1465-1478.
- Doye, V., Wepf, R., and Hurt, E.C. (1994). A novel nuclear pore protein Nup133p with distinct roles in poly(A)+ RNA transport and nuclear pore distribution. *EMBO J* *13*, 6062-6075.
- Dultz, E., Zanin, E., Wurzenberger, C., Braun, M., Rabut, G., Sironi, L., and Ellenberg, J. (2008). Systematic kinetic analysis of mitotic dis- and reassembly of the nuclear pore in living cells. *J Cell Biol* *180*, 857-865.
- Epple, U.D., Suriapranata, I., Eskelinen, E.L., and Thumm, M. (2001). Aut5/Cvt17p, a putative lipase essential for disintegration of autophagic bodies inside the vacuole. *J Bacteriol* *183*, 5942-5955.
- Farre, J.C., and Subramani, S. (2016). Mechanistic insights into selective autophagy pathways: lessons from yeast. *Nat Rev Mol Cell Biol* *17*, 537-552.
- Fernandez-Martinez, J., Kim, S.J., Shi, Y., Upla, P., Pellarin, R., Gagnon, M., Chemmama, I.E., Wang, J., Nudelman, I., Zhang, W., et al. (2016). Structure and Function of the Nuclear Pore Complex Cytoplasmic mRNA Export Platform. *Cell* *167*, 1215-1228 e1225.
- Finley, D., Ozkaynak, E., and Varshavsky, A. (1987). The yeast polyubiquitin gene is essential for resistance to high temperatures, starvation, and other stresses. *Cell* *48*, 1035-1046.
- Finley, D., Ulrich, H.D., Sommer, T., and Kaiser, P. (2012) The ubiquitin–proteasome system of *Saccharomyces cerevisiae*. *Genetics* *192*, 319-360.
- Frey, S., and Gorlich, D. (2009). FG/FxFG as well as GLFG repeats form a selective permeability barrier with self-healing properties. *EMBO J* *28*, 2554-2567.

REFERENCES

- Fumagalli, F., Noack, J., Bergmann, T.J., Cebollero, E., Pisoni, G.B., Fasana, E., Fregno, I., Galli, C., Loi, M., Solda, T., *et al.* (2016). Translocon component Sec62 acts in endoplasmic reticulum turnover during stress recovery. *Nat Cell Biol* *18*, 1173-1184.
- Gaik, M., Flemming, D., von Appen, A., Kastritis, P., Mucke, N., Fischer, J., Stelter, P., Ori, A., Bui, K.H., Bassler, J., *et al.* (2015). Structural basis for assembly and function of the Nup82 complex in the nuclear pore scaffold. *J Cell Biol* *208*, 283-297.
- Grumati, P., Dikic, I., and Stoltz, A. (2018). ER-phagy at a glance. *J Cell Sci* *131*.
- Gu, Y., Zavaliev, R., and Dong, X. (2017). Membrane Trafficking in Plant Immunity. *Mol Plant* *10*, 1026-1034.
- Hampoelz, B., Andres-Pons, A., Kastritis, P., and Beck, M. (2019). Structure and Assembly of the Nuclear Pore Complex. *Annu Rev Biophys* *48*, 515-536.
- Harper, J.W., Ordureau, A., and Heo, J.M. (2018). Building and decoding ubiquitin chains for mitophagy. *Nat Rev Mol Cell Biol* *19*, 93-108.
- Heath, C.V., Copeland, C.S., Amberg, D.C., Del Priore, V., Snyder, M., and Cole, C.N. (1995). Nuclear pore complex clustering and nuclear accumulation of poly(A)+ RNA associated with mutation of the *Saccharomyces cerevisiae* RAT2/NUP120 gene. *J Cell Biol* *131*, 1677-1697.
- Hetzer, M.W., and Wente, S.R. (2009). Border control at the nucleus: biogenesis and organization of the nuclear membrane and pore complexes. *Dev Cell* *17*, 606-616.
- Hodge, C. A., Colot, H. V., Stafford, P., Cole, C. N. (1999). Rat8p/Dbp5p is a shuttling transport factor that interacts with Rat7p/Nup159p and Gle1p and suppresses the mRNA export defect of xpo1-1 cells. *EMBO J* *18*, 5778-5788
- Hulsmann, B.B., Labokha, A.A., and Gorlich, D. (2012). The permeability of reconstituted nuclear pores provides direct evidence for the selective phase model. *Cell* *150*, 738-751.
- Janke, C., Magiera, M.M., Rathfelder, N., Taxis, C., Reber, S., Maekawa, H., Moreno-Borchart, A., Doenges, G., Schwob, E., Schiebel, E., *et al.* (2004). A versatile toolbox for PCR-based tagging of yeast genes: new fluorescent proteins, more markers and promoter substitution cassettes. *Yeast* *21*, 947-962.
- Kabachinski, G., and Schwartz, T.U. (2015). The nuclear pore complex--structure and function at a glance. *J Cell Sci* *128*, 423-429.

REFERENCES

- Kerppola, T.K. (2008). Bimolecular fluorescence complementation (BiFC) analysis as a probe of protein interactions in living cells. *Annu Rev Biophys* *37*, 465-487.
- Khaminets, A., Heinrich, T., Mari, M., Grumati, P., Huebner, A.K., Akutsu, M., Liebmann, L., Stolz, A., Nietzsche, S., Koch, N., *et al.* (2015). Regulation of endoplasmic reticulum turnover by selective autophagy. *Nature* *522*, 354-358.
- Kirisako, T., Baba, M., Ishihara, N., Miyazawa, K., Ohsumi, M., Yoshimori, T., Noda, T., and Ohsumi, Y. (1999). Formation process of autophagosome is traced with Apg8/Aut7p in yeast. *J Cell Biol* *147*, 435-446.
- Knop, M., Siegers, K., Pereira, G., Zachariae, W., Winsor, B., Nasmyth, K., and Schiebel, E. (1999). Epitope tagging of yeast genes using a PCR-based strategy: more tags and improved practical routines. *Yeast* *15*, 963-972.
- Kraft, C., Deplazes, A., Sohrmann, M., and Peter, M. (2008). Mature ribosomes are selectively degraded upon starvation by an autophagy pathway requiring the Ubp3p/Bre5p ubiquitin protease. *Nat Cell Biol* *10*, 602-610.
- Kremer, J.R., Mastronarde, D.N., and McIntosh, J.R. (1996). Computer visualization of three-dimensional image data using IMOD. *J Struct Biol* *116*, 71-76.
- Kukulski, W., Schorb, M., Welsch, S., Picco, A., Kaksonen, M., and Briggs, J.A. (2011). Correlated fluorescence and 3D electron microscopy with high sensitivity and spatial precision. *J Cell Biol* *192*, 111-119.
- Lau, C.K., Delmar, V.A., and Forbes, D.J. (2006). Topology of yeast Ndc1p: predictions for the human NDC1/NET3 homologue. *Anat Rec A Discov Mol Cell Evol Biol* *288*, 681-694.
- Lau, C.K., Giddings, T.H., Jr., and Winey, M. (2004). A novel allele of *Saccharomyces cerevisiae* NDC1 reveals a potential role for the spindle pole body component Ndc1p in nuclear pore assembly. *Eukaryot Cell* *3*, 447-458.
- Laurell, E., Beck, K., Krupina, K., Theerthagiri, G., Bodenmiller, B., Horvath, P., Aebersold, R., Antonin, W., and Kutay, U. (2011). Phosphorylation of Nup98 by multiple kinases is crucial for NPC disassembly during mitotic entry. *Cell* *144*, 539-550.

REFERENCES

- Levine, B., and Klionsky, D.J. (2017). Autophagy wins the 2016 Nobel Prize in Physiology or Medicine: Breakthroughs in baker's yeast fuel advances in biomedical research. *Proc Natl Acad Sci U S A* *114*, 201-205.
- Levine, B., and Kroemer, G. (2008). Autophagy in the pathogenesis of disease. *Cell* *132*, 27-42.
- Linder, M.I., Kohler, M., Boersema, P., Weberruss, M., Wandke, C., Marino, J., Ashiono, C., Picotti, P., Antonin, W., and Kutay, U. (2017). Mitotic Disassembly of Nuclear Pore Complexes Involves CDK1- and PLK1-Mediated Phosphorylation of Key Interconnecting Nucleoporins. *Dev Cell* *43*, 141-156 e147.
- Lord, C.L., Timney, B.L., Rout, M.P., and Wente, S.R. (2015). Altering nuclear pore complex function impacts longevity and mitochondrial function in *S. cerevisiae*. *J Cell Biol* *208*, 729-744.
- Lu, K., Psakhye, I., and Jentsch, S. (2014). Autophagic clearance of polyQ proteins mediated by ubiquitin-Atg8 adaptors of the conserved CUET protein family. *Cell* *158*, 549-563.
- Lusk, C.P., and Colombi, P. (2014). Toward a consensus on the mechanism of nuclear pore complex inheritance. *Nucleus* *5*, 97-102.
- Lynch-Day, M.A., and Klionsky, D.J. (2010). The Cvt pathway as a model for selective autophagy. *FEBS Lett* *584*, 1359-1366.
- Madrid, A.S., Mancuso, J., Cande, W.Z., and Weis, K. (2006). The role of the integral membrane nucleoporins Ndc1p and Pom152p in nuclear pore complex assembly and function. *J Cell Biol* *173*, 361-371.
- Makio, T., Lapetina, D.L., and Wozniak, R.W. (2013). Inheritance of yeast nuclear pore complexes requires the Nsp1p subcomplex. *J Cell Biol* *203*, 187-196.
- Mancias, J.D., Wang, X., Gygi, S.P., Harper, J.W., and Kimmelman, A.C. (2014). Quantitative proteomics identifies NCOA4 as the cargo receptor mediating ferritinophagy. *Nature* *509*, 105-109.
- Marshall, R.S., McLoughlin, F., and Vierstra, R.D. (2016). Autophagic Turnover of Inactive 26S Proteasomes in Yeast Is Directed by the Ubiquitin Receptor Cue5 and the Hsp42 Chaperone. *Cell Rep* *16*, 1717-1732.

REFERENCES

- Mastronarde, D.N. (2005). Automated electron microscope tomography using robust prediction of specimen movements. *J Struct Biol* 152, 36-51.
- Mathew, R., Karantza-Wadsworth, V., and White, E. (2007). Role of autophagy in cancer. *Nat Rev Cancer* 7, 961-967.
- Mathieson, T., Franken, H., Kosinski, J., Kurzawa, N., Zinn, N., Sweetman, G., Poeckel, D., Ratnu, V.S., Schramm, M., Becher, I., *et al.* (2018). Systematic analysis of protein turnover in primary cells. *Nat Commun* 9, 689.
- Maul, G.G., Price, J.W., and Lieberman, M.W. (1971). Formation and distribution of nuclear pore complexes in interphase. *J Cell Biol* 51, 405-418.
- McCloskey, A., Ibarra, A., and Hetzer, M.W. (2018). Tpr regulates the total number of nuclear pore complexes per cell nucleus. *Genes Dev* 32, 1321-1331.
- Mei, Y., Thompson, M.D., Cohen, R.A., and Tong, X. (2015). Autophagy and oxidative stress in cardiovascular diseases. *Biochim Biophys Acta* 1852, 243-251.
- Meszaros, N., Cibulka, J., Mendiburo, M.J., Romanauska, A., Schneider, M., and Kohler, A. (2015). Nuclear pore basket proteins are tethered to the nuclear envelope and can regulate membrane curvature. *Dev Cell* 33, 285-298.
- Miao, M., Ryan, K.J., and Wente, S.R. (2006). The integral membrane protein Pom34p functionally links nucleoporin subcomplexes. *Genetics* 172, 1441-1457.
- Mizushima, N., Yoshimori, T., and Ohsumi, Y. (2011). The role of Atg proteins in autophagosome formation. *Annu Rev Cell Dev Biol* 27, 107-132.
- Mochida, K., Oikawa, Y., Kimura, Y., Kirisako, H., Hirano, H., Ohsumi, Y., and Nakatogawa, H. (2015). Receptor-mediated selective autophagy degrades the endoplasmic reticulum and the nucleus. *Nature* 522, 359-362.
- Murphy, R., Watkins, J.L., and Wente, S.R. (1996). GLE2, a *Saccharomyces cerevisiae* homologue of the *Schizosaccharomyces pombe* export factor RAE1, is required for nuclear pore complex structure and function. *Mol Biol Cell* 7, 1921-1937.
- Nakatogawa, H., Suzuki, K., Kamada, Y., and Ohsumi, Y. (2009). Dynamics and diversity in autophagy mechanisms: lessons from yeast. *Nat Rev Mol Cell Biol* 10, 458-467.
- Nixon, R.A. (2013). The role of autophagy in neurodegenerative disease. *Nat Med* 19, 983-997.

REFERENCES

- Noda, N.N., Ohsumi, Y., and Inagaki, F. (2010). Atg8-family interacting motif crucial for selective autophagy. *FEBS Lett* 584, 1379-1385.
- Olmos, Y., Hodgson, L., Mantell, J., Verkade, P., and Carlton, J.G. (2015). ESCRT-III controls nuclear envelope reformation. *Nature* 522, 236-239.
- Olmos, Y., Perdrix-Rosell, A., and Carlton, J.G. (2016). Membrane Binding by CHMP7 Coordinates ESCRT-III-Dependent Nuclear Envelope Reformation. *Curr Biol* 26, 2635-2641.
- Otsuka, S., and Ellenberg, J. (2018). Mechanisms of nuclear pore complex assembly - two different ways of building one molecular machine. *FEBS Lett* 592, 475-488.
- Patel, S.S., Belmont, B.J., Sante, J.M., and Rexach, M.F. (2007). Natively unfolded nucleoporins gate protein diffusion across the nuclear pore complex. *Cell* 129, 83-96.
- Paul-Gilloteaux, P., Heiligenstein, X., Belle, M., Domart, M.C., Larijani, B., Collinson, L., Raposo, G., and Salamero, J. (2017). eC-CLEM: flexible multidimensional registration software for correlative microscopies. *Nat Methods* 14, 102-103.
- Popken, P., Ghavami, A., Onck, P.R., Poolman, B., and Veenhoff, L.M. (2015). Size-dependent leak of soluble and membrane proteins through the yeast nuclear pore complex. *Mol Biol Cell* 26, 1386-1394.
- Quan, W., Lim, Y.M., and Lee, M.S. (2012). Role of autophagy in diabetes and endoplasmic reticulum stress of pancreatic beta-cells. *Exp Mol Med* 44, 81-88.
- Rappaport, J., Ishihama, Y., and Mann, M. (2003). Stop and go extraction tips for matrix-assisted laser desorption/ionization, nanoelectrospray, and LC/MS sample pretreatment in proteomics. *Anal Chem* 75, 663-670.
- Reggiori, F., and Klionsky, D.J. (2013). Autophagic processes in yeast: mechanism, machinery and regulation. *Genetics* 194, 341-361.
- Reggiori, F., Komatsu, M., Finley, K., and Simonsen, A. (2012). Autophagy: more than a nonselective pathway. *Int J Cell Biol* 2012, 219625.
- Roberts, P., Moshitch-Moshkovitz, S., Kvam, E., O'Toole, E., Winey, M., and Goldfarb, D.S. (2003). Piecemeal microautophagy of nucleus in *Saccharomyces cerevisiae*. *Mol Biol Cell* 14, 129-141.

REFERENCES

- Rout, M.P., Aitchison, J.D., Suprapto, A., Hjertaas, K., Zhao, Y., and Chait, B.T. (2000). The yeast nuclear pore complex: composition, architecture, and transport mechanism. *J Cell Biol* *148*, 635-651.
- Rout, M.P., Blobel, G., and Aitchison, J.D. (1997). A distinct nuclear import pathway used by ribosomal proteins. *Cell* *89*, 715-725.
- Ryan, K.J., McCaffery, J.M., and Wente, S.R. (2003). The Ran GTPase cycle is required for yeast nuclear pore complex assembly. *J Cell Biol* *160*, 1041-1053.
- Ryan, K.J., Zhou, Y., and Wente, S.R. (2007). The karyopherin Kap95 regulates nuclear pore complex assembly into intact nuclear envelopes in vivo. *Mol Biol Cell* *18*, 886-898.
- Sakai, Y., Oku, M., van der Klei, I.J., and Kiel, J.A. (2006). Pexophagy: autophagic degradation of peroxisomes. *Biochim Biophys Acta* *1763*, 1767-1775.
- Sakuma, S., and D'Angelo, M.A. (2017). The roles of the nuclear pore complex in cellular dysfunction, aging and disease. *Semin Cell Dev Biol* *68*, 72-84.
- Savas, J.N., Toyama, B.H., Xu, T., Yates, J.R., 3rd, and Hetzer, M.W. (2012). Extremely long-lived nuclear pore proteins in the rat brain. *Science* *335*, 942.
- Sawa-Makarska, J., Abert, C., Romanov, J., Zens, B., Ibiricu, I., and Martens, S. (2014). Cargo binding to Atg19 unmasks additional Atg8 binding sites to mediate membrane-cargo apposition during selective autophagy. *Nat Cell Biol* *16*, 425-433.
- Scarcelli, J.J., Hodge, C.A., and Cole, C.N. (2007). The yeast integral membrane protein Apq12 potentially links membrane dynamics to assembly of nuclear pore complexes. *J Cell Biol* *178*, 799-812.
- Schwartz, T.U. (2016). The Structure Inventory of the Nuclear Pore Complex. *J Mol Biol* *428*, 1986-2000.
- Scott, S.V., Guan, J., Hutchins, M.U., Kim, J., and Klionsky, D.J. (2001). Cvt19 is a receptor for the cytoplasm-to-vacuole targeting pathway. *Mol Cell* *7*, 1131-1141.
- Shcheprova, Z., Baldi, S., Frei, S.B., Gonnet, G., and Barral, Y. (2008). A mechanism for asymmetric segregation of age during yeast budding. *Nature* *454*, 728-734.
- Shintani, T., and Klionsky, D.J. (2004). Cargo proteins facilitate the formation of transport vesicles in the cytoplasm to vacuole targeting pathway. *J Biol Chem* *279*, 29889-29894.

REFERENCES

- Shpilka, T., Welter, E., Borovsky, N., Amar, N., Shimron, F., Peleg, Y., and Elazar, Z. (2015). Fatty acid synthase is preferentially degraded by autophagy upon nitrogen starvation in yeast. *Proc Natl Acad Sci U S A* *112*, 1434-1439.
- Simon, D.N., and Rout, M.P. (2014). Cancer and the nuclear pore complex. *Adv Exp Med Biol* *773*, 285-307.
- Stoten, C.L., and Carlton, J.G. (2018). ESCRT-dependent control of membrane remodelling during cell division. *Semin Cell Dev Biol* *74*, 50-65.
- Strambio-de-Castillia, C., Blobel, G., and Rout, M.P. (1999). Proteins connecting the nuclear pore complex with the nuclear interior. *J Cell Biol* *144*, 839-855.
- Strambio-De-Castillia, C., Niepel, M., and Rout, M.P. (2010). The nuclear pore complex: bridging nuclear transport and gene regulation. *Nat Rev Mol Cell Biol* *11*, 490-501.
- Tanaka, K. (2009). The proteasome: Overview of structure and functions. *Proc Jpn Acad Ser B Phys Biol Sci.* *85*, 12-36.
- Terry, L.J., and Wente, S.R. (2007). Nuclear mRNA export requires specific FG nucleoporins for translocation through the nuclear pore complex. *J Cell Biol* *178*, 1121-1132.
- Terry, L.J., and Wente, S.R. (2009). Flexible gates: dynamic topologies and functions for FG nucleoporins in nucleocytoplasmic transport. *Eukaryot Cell* *8*, 1814-1827.
- Thaller, D.J., Allegretti, M., Borah, S., Ronchi, P., Beck, M., and Lusk, C.P. (2019). An ESCRT-LEM protein surveillance system is poised to directly monitor the nuclear envelope and nuclear transport system. *Elife* *8*.
- Thaller, D.J., and Patrick Lusk, C. (2018). Fantastic nuclear envelope herniations and where to find them. *Biochem Soc Trans* *46*, 877-889.
- Timney, B.L., Raveh, B., Mironksa, R., Trivedi, J.M., Kim, S.J., Russel, D., Wente, S.R., Sali, A., and Rout, M.P. (2016). Simple rules for passive diffusion through the nuclear pore complex. *J Cell Biol* *215*, 57-76.
- Toyama, B.H., Arrojo, E.D.R., Lev-Ram, V., Ramachandra, R., Deerinck, T.J., Lechene, C., Ellisman, M.H., and Hetzer, M.W. (2019). Visualization of long-lived proteins reveals age mosaicism within nuclei of postmitotic cells. *J Cell Biol* *218*, 433-444.

REFERENCES

- Toyama, B.H., Savas, J.N., Park, S.K., Harris, M.S., Ingolia, N.T., Yates, J.R., 3rd, and Hetzer, M.W. (2013). Identification of long-lived proteins reveals exceptional stability of essential cellular structures. *Cell* *154*, 971-982.
- Tyanova, S., Temu, T., Sinitcyn, P., Carlson, A., Hein, M.Y., Geiger, T., Mann, M., and Cox, J. (2016). The Perseus computational platform for comprehensive analysis of (prote)omics data. *Nat Methods* *13*, 731-740.
- Ungermann, C., and Reggiori, F. (2018). Atg9 proteins, not so different after all. *Autophagy* *14*, 1456-1459.
- Vallotton, P., Rajoo, S., Wojtynek, M., Onischenko, E., Kralt, A., Derrer, C.P., and Weis, K. (2019). Mapping the native organization of the yeast nuclear pore complex using nuclear radial intensity measurements. *Proc Natl Acad Sci U S A* *116*, 14606-14613.
- Vietri, M., Schink, K.O., Campsteijn, C., Wegner, C.S., Schultz, S.W., Christ, L., Thoresen, S.B., Brech, A., Raiborg, C., and Stenmark, H. (2015). Spastin and ESCRT-III coordinate mitotic spindle disassembly and nuclear envelope sealing. *Nature* *522*, 231-235.
- Vollmer, B., Schooley, A., Sachdev, R., Eisenhardt, N., Schneider, A.M., Sieverding, C., Madlung, J., Gerken, U., Macek, B., and Antonin, W. (2012). Dimerization and direct membrane interaction of Nup53 contribute to nuclear pore complex assembly. *EMBO J* *31*, 4072-4084.
- Walther, T.C., Alves, A., Pickersgill, H., Loiodice, I., Hetzer, M., Galy, V., Hulsmann, B.B., Kocher, T., Wilm, M., Allen, T., *et al.* (2003a). The conserved Nup107-160 complex is critical for nuclear pore complex assembly. *Cell* *113*, 195-206.
- Walther, T.C., Askjaer, P., Gentzel, M., Habermann, A., Griffiths, G., Wilm, M., Mattaj, I.W., and Hetzer, M. (2003b). RanGTP mediates nuclear pore complex assembly. *Nature* *424*, 689-694.
- Webster, B.M., Colombi, P., Jager, J., and Lusk, C.P. (2014). Surveillance of nuclear pore complex assembly by ESCRT-III/Vps4. *Cell* *159*, 388-401.
- Webster, B.M., Thaller, D.J., Jager, J., Ochmann, S.E., Borah, S., and Lusk, C.P. (2016). Chm7 and Heh1 collaborate to link nuclear pore complex quality control with nuclear envelope sealing. *EMBO J* *35*, 2447-2467.

REFERENCES

- Weirich, C.S., Erzberger, J.P., Berger, J.M., and Weis, K. (2004). The N-terminal domain of Nup159 forms a beta-propeller that functions in mRNA export by tethering the helicase Dbp5 to the nuclear pore. *Mol Cell* *16*, 749-760.
- Wen, X., and Klionsky, D.J. (2016). An overview of macroautophagy in yeast. *J Mol Biol* *428*, 1681-1699.
- Wente, S.R., and Blobel, G. (1993). A temperature-sensitive NUP116 null mutant forms a nuclear envelope seal over the yeast nuclear pore complex thereby blocking nucleocytoplasmic traffic. *J Cell Biol* *123*, 275-284.
- Wente, S.R., and Blobel, G. (1994). NUP145 encodes a novel yeast glycine-leucine-phenylalanine-glycine (GLFG) nucleoporin required for nuclear envelope structure. *J Cell Biol* *125*, 955-969.
- Wente, S.R., and Rout, M.P. (2010). The nuclear pore complex and nuclear transport. *Cold Spring Harb Perspect Biol* *2*, a000562.
- Wozniak, R.W., Blobel, G., and Rout, M.P. (1994). POM152 is an integral protein of the pore membrane domain of the yeast nuclear envelope. *J Cell Biol* *125*, 31-42.
- Wyant, G.A., Abu-Remaileh, M., Frenkel, E.M., Laqtom, N.N., Dharamdasani, V., Lewis, C.A., Chan, S.H., Heinze, I., Ori, A., and Sabatini, D.M. (2018). NUFIP1 is a ribosome receptor for starvation-induced ribophagy. *Science* *360*, 751-758.
- Yewdell, W.T., Colombi, P., Makhnevych, T., and Lusk, C.P. (2011). Luminal interactions in nuclear pore complex assembly and stability. *Mol Biol Cell* *22*, 1375-1388.
- Yu, X., Long, Y.C., and Shen, H.M. (2015). Differential regulatory functions of three classes of phosphatidylinositol and phosphoinositide 3-kinases in autophagy. *Autophagy* *11*, 1711-1728.
- Zabel U., Doye V., Tekotte H., Wepf R., Grandi P., and Hurt E.C. (1996). Nic96p is required for nuclear pore formation and functionally interacts with a novel nucleoporin, Nup188p. *IUBMB Life* *38*, 1141-52.
- Zhang, W., Neuner, A., Ruthnick, D., Sachsenheimer, T., Luchtenborg, C., Brugger, B., and Schiebel, E. (2018). Brr6 and Brl1 locate to nuclear pore complex assembly sites to promote their biogenesis. *J Cell Biol* *217*, 877-894.

Abbreviations

Abbreviations for nucleotides and amino acids were used according to the standard definitions (1-letter or 3-letter code) and are not specifically listed in this section.

aa	amino acid(s)
AIM	Atg8-interacting motif
ATG	autophagy-related genes
bp	base pair(s)
°C	degree Celsius
C-	carboxyl-
Can	canavanine
CdCl ₂	cadmium chloride
CDK1	cyclin - dependent kinase 1
CHX	cyclohexamide
CLEM	correlative light and electron microscopy
ConA	concanavalin A
COPII	coat protein complex II
CR	cytoplasmic ring
Cvt	cytoplasm-to-vacuole targeting
d	day(s)
D	dextrose
DID	dynein light chain-interaction domain
DMSO	dimethyl sulfoxide
DNA	deoxyribonucleic acid
DNase	deoxyribonuclease
dNTP	2'-deoxyribonucleoside-5'-triphosphate
DTT	dithiothreitol
Dyn2	dynein light chain 2
<i>E. coli</i>	Escherichia coli
e.g.	exempli gratia, for example
ECL	enhanced chemiluminescence
EDTA	ethylenediaminetetraacetic acid

ABBREVIATIONS

ELYS	embryonic large molecule derived from yolk sac
ER	endoplasmic reticulum
ESCRT	endosomal sorting complexes required for transport pathway
EtBr	ethidium bromide
EtOH	ethyl alcohol
g	gram
g	gravity
G418	geneticine disulfate
Gal	galactose
GFP	green fluorescent protein
GST	glutathione S-transferases
h	hours
H ₂ O ₂	hydrogen peroxide
HA	hemagglutinin
HEPES	N-(2-hydroxyethyl)-piperazin-N'-(2-ethanesulfonate)
His	histidine
<i>hphNT1</i>	gene conferring resistance to hygromycin
IgG	immunoglobulin G
INM	inner nuclear membrane
IP	immunoprecipitation
IPTG	isopropyl-β-D-thiogalactopyranoside
IR	inner ring
<i>kanMX6</i>	gene conferring resistance to G418
Kap95	karyopherin 95
kb	kilo base pair(s)
kDa	kilo Dalton
l	liter(s)
LB	(Luria-Bertani)-medium
LEM	Lap2-emerin-MAN1 domain
LIR	LC3-interacting region
log	logarithmic
m	milli ($\times 10^{-3}$)
M	molar

ABBREVIATIONS

μ	micro ($\times 10^6$)
mAb	monoclonal antibody
min	minute
MMS	methyl methanesulfonate
MOPS	3-(N-morpholino) propanesulfonic acid
MVB	multivesicular body
mRNA	messenger RNA
mRNP	messenger ribonucleoprotein
n	nano ($\times 10^{-9}$)
NAT	nourseothricin
<i>natNT2</i>	gene conferring resistance to nourseothricin
NE	nuclear envelope
NEM	N-ethylmaleimide
Ni-NTA	Nickel-nitrilo triacetate
NOC	nocodazole
NR	nuclear ring
NP-40	nonidet p-40
NPCs	nuclear pore complexes
NTR	nuclear transport receptors
Nup	nucleoporin
NV junctions	nucleus-vacuole junctions
OD ₆₀₀	optical density at 600 nm wavelength
ONM	outer nuclear membrane
ORF	open reading frame
<i>p</i>	promoter (with gene names)
<i>p</i> -value	probability value
PAGE	polyacrylamide gel electrophoresis
PAS	pre-autophagosomal structure
PAGE	polyacrylamide gel electrophoresis
PBS	phosphate buffered saline
PCR	polymerase chain reaction
PD	pulldown
PE	phosphatidylethanolamine

ABBREVIATIONS

PEG	Polyethylene glycol
pH	<i>pondus hydrogenii</i>
PI3K	phosphoinositide 3-kinases
PI3P	phosphatidylinositol 3-phosphate
PLK1	polo-like kinase 1
PMSF	phenylmethylsulfonyl fluoride
PtdIns3K-C1	class III phosphatidylinositol 3-kinase complex I
PVDF	polyvinylidene difluoride
Raf	raffinose
RNA	ribonucleic acid
RNase	ribonuclease
rpm	revolutions per minute
RT	room temperature
<i>S. cerevisiae</i>	<i>Saccharomyces cerevisiae</i>
SDS	sodium dodecyl sulfate
sec	second(s)
SINC	storage of improperly assembled NPCs compartment
TBE	tris, boric acid, EDTA
TBS-T	tris-buffered saline with Tween-20
Tris	Tris(hydroxymethyl)-aminomethane
TCA	trichloroacetic acid
Tm	melting temperature
Tm	tunicamycin
TOR	target of rapamycin
TORC1	target of rapamycin complex 1
TRAPP III	transport protein particle III
UPS	ubiquitin-proteasome system
UV	Ultraviolet
V	voltage
v/v	volume per volume
VPS	vacuolar protein sorting
WB	Western blot/immunoblot
WT	wildtype

ABBREVIATIONS

w/v	weight per volume
YNB	yeast nitrogen base
Ypt1	yeast protein two 1

Acknowledgments

It has been a crazy time of my life. Being a PhD student here in MPI and experiencing so many unforeseeable obstacles, depressions, and sadness, to an eventual success. Things that I will never forget...

Foremost I would like to start by thanking my PhD supervisors, Prof. Stefan Jentsch and Prof. Wolfgang Baumeister, who kindly offered me an opportunity to explore such amazing projects in their labs. I really enjoy the working atmosphere here with a lot of scientific freedom and many insightful discussions between colleagues. I appreciate their trust in me from the very beginning of project design, execution and final paper publishing. Moreover, I am sincerely grateful to Prof. Baumeister for the understanding and care with which he helped me overcome the most difficult time after Stefan's death.

In addition, my special thanks go to the members of the Thesis Advisory Committee for refereeing this thesis, in particular, to Prof. Dr. Johannes Buchner for valuable ideas and the kind support. Meanwhile, I also want to acknowledge Dr. Boris Pfander and Prof. Dr. Martin Beck for assisting with the paper publication.

A big thank to my best partner, Florian Wilfling, without him I would never be able accomplish that much. Thank you so much for your patience, generosity, inspiring advices and support. I also want to express my thanks to Ben Engel for coordinating the proteasome project and my stay in the department. I am thankful to Sean Lin and Wojciech Wietrzynski for hands-on teaching of experiments, and André, Chandhuru, Fabian, Ivan, Kefeng, Lucas, Markus, Matias, Paasch, and Yan Xiao for their scientific suggestions and many outdoor activities together. Special thanks to Birgit, Dirk, Klara, Massimo, and Ulla for all kind of technical supports and dealing with the administrative tasks.

Lastly, I would send my gratitude to my parents. Thanks for the unquestioned support and much needed help they offered these years and also for enduring a stubborn child like me.

Curriculum Vitae

Chia-Wei Lee

University Education & Research Experience:

2014 – present **PhD thesis with Prof. Wolfgang Baumeister and Prof. Stefan Jentsch (deceased 10/2016).**

The International Max Planck Research School of Life Science (IMPRS-LS) program, Max Planck Institute of Biochemistry, Martinsried/Munich, Germany.

Degree awarded by the Department of Chemistry, Technical University of Munich, Germany.

Thesis title: Selective autophagy degrades nuclear pore complexes
Research assistant position with Prof. Sheng-Chung Lee.

2013 – 2014 Institute of Molecular Medicine, college of Medicine, National Taiwan University (NTU), Taiwan.

Master thesis with Prof. Sheng-Chung Lee.

MS. Institute of Molecular Medicine, School of Medicine, National Taiwan University (NTU), Taiwan.

Thesis title: Functional interaction between SIK2 and PP2A

GPA: 4.0/ Cumulative Average: 90.48/ Letter Grade: A⁺

2005 – 2009 **Undergraduate research with Prof. Chiu-Ming Wen.**

BS. Department of Life Science, National University of Kaohsiung (NUK), Taiwan.

Major GPA: 3.92/ Cumulative Average: 85.14/ Latter Grade: A/
Class Rank: 1

Publications:

Florian Wilfling^{#*}, **Chia-Wei Lee**[#], Philipp Erdmann^{*}, Yumei Zheng, Dawafuti Sherpa, Stefan Jentsch, Boris Pfander, Brenda Schulman, and Wolfgang Baumeister^{*}

A selective autophagy pathway for phase-separated endocytic protein deposits.

Mol. Cell **80**, 764–778

Shared first authors

Matteo Allegretti^{*}, Christian E. Zimmerli^{*}, Vasileios Rantos, Florian Wilfling, Paolo Ronchi, Herman K.H. Fung, **Chia-Wei Lee**, Wim Hagen, Beata Turonova, Kai Karius, Xiaojie Zhang, Christoph Müller, Yannick Schwab, Julia Mahamid, Boris Pfander[#], Jan Kosinski[#], and Martin Beck[#]

In-cell architecture of the nuclear pore complex and snapshots of its turnover.

Nature **586**, 796–800

Chia-Wei Lee[#], Florian Wilfling[#], Paolo Ronchi, Matteo Allegretti, Shyamal Mosalaganti, Stefan Jentsch, Martin Beck^{*} and Boris Pfander^{*} (2020).

Selective autophagy degrades nuclear pore complexes.

Nat. Cell Biol. **22**, 159–166

Shared first authors

Sahradha Albert, Wojciech Wietrzynski[#], **Chia-Wei Lee**[#], Miroslava Schaffer[#], Florian Beck, Jan M. Schuller, Patrice A. Salomé, Jürgen M. Plitzko, Wolfgang Baumeister^{1*}, and Benjamin D. Engel^{*} (2020).

Direct visualization of degradation microcompartments at the ER membrane.

Proc. Natl. Acad. Sci. USA **117**, 1069–1080.

Equal contribution

Chia-Wei Lee, Fu-Chia Yang, Hsin-Yun Chang, Hanyi Chou, Bertrand Chin-Ming Tan, and Sheng-Chung Lee^{*} (2014).

Interaction between salt-inducible kinase 2 and protein phosphatase 2A regulates the activity of calcium/calmodulin-dependent protein kinase I and protein phosphatase methylesterase-1.

J. Biol. Chem. **289**, 21108–21119.

C.M. Wen^{*}, **C.W. Lee**, C.S. Wang, Y.H. Cheng, H.Y. Huang (2008).

Development of two cell lines from *Epinephelus coioides* brain tissue for characterization of betanodavirus and megalocytivirus infectivity and propagation.

Aquaculture **278**, 14–21. * Corresponding author

Lebenslauf

Chia-Wei Lee

Hochschulbildung & Forschungserfahrung:

2014 – **Dissertation bei Prof. Wolfgang Baumeister und Prof. Stefan Jentsch (verstorben 10/2016).**

Das Programm der International Max Planck Research School of Life Science (IMPRS-LS), Max-Planck-Institut für Biochemie, Martinsried/München, Deutschland.

Abschluss am Fachbereich Chemie der Technischen Universität München, Deutschland.

Titel der Abschlussarbeit: Selektive Autophagie baut nukleare Porenkomplexe ab.

2013 – 2014 **Wissenschaftliche Mitarbeiterin bei Prof. Sheng-Chung Lee.**

Institut für Molekulare Medizin, College of Medicine, National Taiwan University (NTU), Taiwan.

2009 – 2012 **Masterarbeit bei Prof. Sheng-Chung Lee.**

MS. Institut für Molekulare Medizin, School of Medicine, National Taiwan University (NTU), Taiwan.

Titel der Abschlussarbeit: Funktionelle Interaktion zwischen SIK2 und PP2A

GPA: 4,0/ Kumulativer Durchschnitt: 90,48/ Briefqualität: A⁺

2005 – 2009 **Vordiplomarbeit bei Prof. Chiu-Ming Wen.**

BS. Department of Life Science, National University of Kaohsiung (NUK), Taiwan.

Major GPA: 3,92/ Kumulativer Durchschnitt: 85,14/ Letzter Grad: A/ Klassenrang: 1